TURUN
YLIOPISTO
UNIVERSITY
OF TURKU

EMPIRICAL MODELLING OF SOLAR ENERGETIC PARTICLES

Osku Raukunen

TURUN YLIOPISTON JULKAISUJA – ANNALES UNIVERSITATIS TURKUENSIS
SARJA – SER. AI OSA – TOM. 648 | ASTRONOMICA – CHEMICA – PHYSICA – MATHEMATICA | TURKU 2021

TURUN
YLIOPISTO
UNIVERSITY
OF TURKU

EMPIRICAL MODELLING OF SOLAR ENERGETIC PARTICLES

Osku Raukunen

TURUN YLIOPISTON JULKAISUJA – ANNALES UNIVERSITATIS TURKUENSIS
SARJA – SER. AI OSA – TOM. 648 | ASTRONOMICA – CHEMICA – PHYSICA – MATHEMATICA | TURKU 2021

University of Turku

Faculty of Science
Department of Physics and Astronomy
Physics
Doctoral Programme in Physical and Chemical Sciences

Supervised by

Professor Rami Vainio
Department of Physics and Astronomy
University of Turku
Turku, Finland

Docent Eino Valtonen
Department of Physics and Astronomy
University of Turku
Turku, Finland

Reviewed by

Doctor Stephen Kahler
Air Force Research Laboratory
Kirtland AFB
New Mexico, USA

Professor Pekka T. Verronen
Sodankylä Geophysical Observatory
Univerity of Oulu
Oulu, Finland

Opponent

Doctor Eamonn Daly
European Space Research and
Technology Centre
European Space Agency
Noordwijk, Netherlands

ISBN 978-951-29-8490-9 (PRINT)
ISBN 978-951-29-8491-6 (PDF)
ISSN 0082-7002 (PRINT)
ISSN 2343-3175 (ONLINE)
Painosalama, Turku, Finland, 2021

UNIVERSITY OF TURKU
Faculty of Science
Department of Physics and Astronomy
Physics
RAUKUNEN, OSKU: Empirical Modelling of Solar Energetic Particles
Doctoral dissertation, 142 pp.
Doctoral Programme in Physical and Chemical Sciences
June 2021

ABSTRACT

Solar energetic particles (SEPs) are an important component of space weather. They pose a serious radiation hazard to electronic equipment and biological organisms in space. They are produced in explosive events such as solar flares and coronal mass ejections, where particles can be accelerated up to several orders of magnitude above their thermal energy. During large SEP events, observed particle fluxes may increase by many orders of magnitude in timescales of minutes, and the increases may last several days. The occurrence of SEP events is approximately correlated with the overall activity of the Sun. The solar activity follows a nearly periodic cycle with the average period of approximately 11 years, and the amplitude of the cycle is modulated by longer variations. During the most recent solar cycle, activity has stayed at a very low level compared to previous cycles. The low activity has been interpreted as a result of long-term variability, and it is expected to continue at least for the recently started cycle 25.

This thesis presents research into two closely related topics, the first of which is the comparison of the properties of SEPs during the two recent solar cycles, namely cycles 23 and 24. We studied the heavy ion intensities and abundances, and found that the mean abundances of heavy ions were lower during cycle 24, and the overall number of SEP events with heavy ion enhancements was lower. These results reflect the reduced efficiency of SEP acceleration processes. We used shock acceleration theory and simulation results to show that the reduced efficiency can be explained by reduced average densities of coronal plasma and suprathermal seed particles.

Designers of space missions require accurate knowledge about the radiation environment their equipment or astronauts will be exposed to. As the processes behind SEPs are extremely complex, long-term forecasting is not possible according to current knowledge. Therefore, statistical models of previous SEPs events are the only option in estimating the particle radiation environment. The second topic of this thesis is the development of such models, with special emphasis on the high energy part of the SEP spectrum. We developed models for solar high energy proton fluences and peak fluxes. The models were based on space-borne and ground-based measurements over several solar cycles, and they provide improved estimations of the high energy radiation environment.

KEYWORDS: Space weather, solar energetic particles, particle radiation

TURUN YLIOPISTO
Matemaattis-luonnontieteellinen tiedekunta
Fysiikan ja tähtitieteen laitos
Fysiikka
RAUKUNEN, OSKU: Empirical Modelling of Solar Energetic Particles
Väitöskirja, 142 s.
Fysikaalisten ja kemiallisten tieteiden tohtoriohjelma
Kesäkuu 2021

TIIVISTELMÄ

Auringon suurienergiaiset hiukkaset ovat tärkeä osa avaruussäätä. Ne voivat aiheuttaa vakavan säteilyvaaran avaruuteen lähetettäville elektronisille laitteille ja eläville organismeille. Ne syntyvät Auringon räjähdysmäisissä soihduissa ja koronan massapurkauksissa, joissa hiukkaset voivat saavuttaa useita kertalukuja kaasun lämpöenergiaa suurempia energioita. Suurien Auringon hiukkaspurkausten aikana hiukkasvuot voivat kohota useita kertalukuja minuuteissa ja jäädä koholle useiden vuorokausien ajaksi. Auringon hiukkaspurkausten esiintymisen ja yleisen aktiivisuustason välillä on korrelaatio. Auringon aktiivisuus vaihtelee likimain jaksollisesti keskimäärin 11 vuoden jaksoissa. Auringon aktiivisuus vaihtelee likimain jaksollisesti keskimäärin 11 vuoden jaksoissa. Jaksojen voimakkuus vaihtelee lisäksi pidemmän ajan kuluessa. Viimeisimmän aktiivisuusjakson aikana Auringon aktiivisuus on pysynyt erittäin vähäisenä aiempiin jaksoihin verrattuna. Vähäisen aktiivisuuden odotetaan jatkuvan ainakin äskettäin alkaneen 25. jakson ajan.

Tässä väitöskirjassa esitetään tutkimustuloksia Auringon suurienergiaisten hiukkaspurkausten ominaisuuksien eroista Auringon 23. ja 24. aktiivisuusjakson aikana. Tutkimme raskasionien intensiteettejä ja runsaussuhteita, ja osoitimme, että raskasionien keskimääräiset runsaudet olivat vähäisempiä ja että kohonneita raskasionipitoisuuksia sisältävien hiukkaspurkausten määrä oli pienempi 24. jakson aikana. Tulokset viittaavat hiukkaskiihdytysprosessien heikentymiseen. Osoitimme shokkikiihdytysteorian ja simulaatioiden avulla, että hiukkaskiihdytyksen heikentyminen voidaan selittää koronan plasman ja supratermisten hiukkasten tiheyden pienenemisellä.

Avaruuslentojen suunnittelijat tarvitsevat tarkkaa tietoa säteily-ympäristöstä, jolle teknologia ja astronautit altistuvat. Koska Auringon suurienergiaisten hiukkasten syntyyn vaikuttavat prosessit ovat varsin monimutkaisia, pitkän ajan ennusteiden tekeminen on nykytiedolla mahdotonta. Aiempiin hiukkaspurkauksiin perustuvat tilastolliset mallit ovatkin ainoa tapa arvioida säteily-ympäristöä kvantitatiivisesti. Väitöskirjan toinen tutkimusaihe on tällaisten mallien kehittäminen, erityisesti suurienergiaisten hiukkasten osalta. Kehitimme tilastolliset mallit erittäin suurienergiaisten protonien hiukkasmäärälle ja huippuvuolle. Mallit pohjautuvat sekä satelliittien että maanpäällisten instrumenttien havaintoihin usean Auringon syklin ajalta. Kehitettyjen mallien avulla saadaan aiempaa selvästi parempia arvioita suurienergiaisesta säteily-ympäristöstä.

ASIASANAT: Avaruussää, auringon suurienergiaiset hiukkaset, hiukkassäteily

Acknowledgements

It seems difficult to comprehend that this project, having lasted so long, is finally finished. It has been a big part of my life throughout the years, and now, looking back on it, I realise how informative, interesting, and enjoyable it has been. I am truly grateful for having the possibility to work on, and complete, such a project.

First, I would like to express my sincere gratitude to my supervisors Eino Valtonen, who gave me the opportunity to start working on my doctoral research and provided invaluable support and guidance, especially during the early part of this project, and Rami Vainio, whose support, ideas, and endless enthusiasm helped me, especially in the later part of this project. Without their help, inexhaustible knowledge, patience, and dedicated support throughout the years I would not have been able to finish this dissertation.

I would like to extend my gratitude to Dr. Eamonn Daly for agreeing to be my opponent, and to Dr. Stephen Kahler and Prof. Pekka T. Verronen for their thorough pre-examination of this thesis and their informative reviews. I would also like to thank the Vilho, Yrjö and Kalle Väisälä Fund, The Finnish Cultural Foundation and the Doctoral Programme in Physical and Chemical Sciences for financial support during my doctoral research.

I also want to thank all the current and past members of the Space Research Laboratory that I have had the pleasure to meet. Special thanks go to my pre-COVID-19 office mates Miikka Paassilta and Matti Teittinen, with whom it has always been a pleasure to chat about various topics (such as programming, history, orienteering, education, comedy, Finnish grammar, English grammar, Latin grammar, food, etymology, philosophy, and deer species), and to Esa Riihonen, for always having time to listen to me complain about problems with IDL (and sharing his own similar experiences). And to all my dear friends outside of work, thank you for your friendship and support!

Finally, I am deeply grateful to my parents for their all their support, and always encouraging me in my studies and life in general. And Vaula, my love, you make my days happier and work easier. Thank you for your love, support, patience and understanding!

Turku, May 2021
Osku Raukunen

Table of contents

Acknowledgements **5**

Table of contents **6**

List of original publications **8**

Other published work **8**

Abbreviations **10**

1 Introduction **12**
1.1 Space weather 12
1.1.1 Origin and causes 12
1.1.2 Effects on Earth and society 14
1.1.3 Space climate 16
1.2 Solar energetic particles 17
1.2.1 Sources and acceleration mechanisms 17
1.2.2 Space weather effects 19

2 Particle environment modelling **21**
2.1 SEP models 21
2.2 Radiation belt models 24
2.3 GCR models 24

3 Solar activity **25**
3.1 Solar activity cycle 25
3.1.1 Sunspot number 25
3.1.2 Other measures of solar activity 27
3.1.3 Characteristics of solar cycles 29
3.1.4 Solar cycle prediction 32
3.2 Flare, CME and SEP activity 34

4 Comparison of solar cycles 23 and 24 . . . . . **39**
4.1 Observations 39

4.1.1 Flares and CMEs 40
4.1.2 Solar energetic particles 43
4.2 Statistical SEP model 49
4.2.1 Model details 50
4.2.2 Results 56

5 Conclusions and outlook 60

6 Summary of the original publications 62
6.1 Article I: Iron-rich solar particle events measured by SOHO/ERNE during two solar cycles 62
6.2 Article II: Why is solar cycle 24 an inefficient producer of high-energy particle events? 62
6.3 Article III: Two solar proton fluence models based on ground level enhancement observations 63
6.4 Article IV: Very high energy proton peak flux model 64

List of references 65

Original publications 85

List of Original Publications

This thesis consists of a review of the research subject and the following original publications:

I **Iron-rich solar particle events measured by SOHO/ERNE during two solar cycles**
O. Raukunen, E. Valtonen and R. Vainio
Astronomy & Astrophysics, 589, A138, 2016
doi:10.1051/0004-6361/201527462

II **Why is solar cycle 24 an inefficient producer of high-energy particle events?**
R. Vainio, O. Raukunen, A. J. Tylka, W. F. Dietrich and A. Afanasiev
Astronomy & Astrophysics, 604, A47, 2017
doi:10.1051/0004-6361/201730547

III **Two solar proton fluence models based on ground level enhancement observations**
O. Raukunen, R. Vainio, A. J. Tylka, W. F. Dietrich, P. Jiggens, D. Heynderickx, M. Dierckxsens, N. Crosby, U. Ganse and R. Siipola
Journal of Space Weather and Space Climate, 8, A04, 2018
doi:10.1051/swsc/2017031

IV **Very high energy proton peak flux model**
O. Raukunen, M. Paassilta, R. Vainio, J. V. Rodriguez, T. Eronen, N. Crosby, M. Dierckxsens, P. Jiggens, D. Heynderickx and I. Sandberg
Journal of Space Weather and Space Climate, 10, 24, 2020
doi:10.1051/swsc/2020024

Other Published Work

- **Catalogue of 55-80 MeV solar proton events extending through solar cycles 23 and 24**
  M. Paassilta, O. Raukunen, R. Vainio, E. Valtonen, A. Papaioannou, R. Siipola, E. Riihonen, M. Dierckxsens, N. Crosby, O. Malandraki, B. Heber and K.-L. Klein
  Journal of Space Weather and Space Climate, 7, A14, 2017
  doi:10.1051/swsc/2017013

- **Updated Model of the Solar Energetic Proton Environment in Space**
  P. Jiggens, D. Heynderickx, I. Sandberg, P. Truscott, O. Raukunen and R. Vainio
  Journal of Space Weather and Space Climate, 8, A31, 2018
  doi:10.1051/swsc/2018010

- **First Analysis of Ground-Level Enhancement (GLE) 72 on 10 September 2017: Spectral and Anisotropy Characteristics**
  A. Mishev, I. Usoskin, O. Raukunen, M. Paassilta, E. Valtonen, L. Kocharov and R. Vainio
  Solar Physics, 293, 136, 2018
  doi:10.1007/s11207-018-1354-x

- **New reconstruction of event-integrated spectra (spectral fluences) for major solar energetic particle events**
  S. Koldobskiy, O. Raukunen, R. Vainio, G. A. Kovaltsov and I. Usoskin
  Astronomy & Astrophysics, 647, A132, 2021
  doi:10.1051/0004-6361/202040058

Abbreviations

ACE	Advanced Composition Explorer
AR	active region
ARTEMIS	Automatic Recognition of Transient Events and Marseille Inventory from Synoptic maps
CDF	cumulative distribution function
CME	coronal mass ejection
CR	cosmic ray
CRAND	cosmic ray albedo neutron decay
CREME	Cosmic Ray Effects on MicroElectronics
EPS	Energetic Particle Sensor
ERNE	Energetic and Relativistic Nuclei and Electron experiment
ESA	European Space Agency
ESP	Emission of Solar Protons
FWHM	full width at half maximum
GCR	galactic cosmic ray
GIC	geomagnetically induced current
GLE	ground level enhancement
GOES	Geostationary Operational Environmental Satellite
GPS	Global Positioning System
HED	High Energy Detector
HEPAD	High Energy Proton and Alpha Detector

IMF	interplanetary magnetic field
IMP	Interplanetary Monitoring Platform
JPL	Jet Propulsion Laboratory
LASCO	Large Angle and Spectrometric Coronagraph experiment
LED	Low Energy Detector
MC	Monte Carlo
MSSREM	Mission Specific Solar Radiation Environment Model
MSU	Moscow State University
NM	neutron monitor
PDF	probability distribution function
PMF	polar magnetic field
PSYCHIC	Prediction of Solar particle Yields for CHaracterizing Integrated Circuits
R-ESC	Space Radiation Expert Service Centre
RDS	Reference Data Set
SAPPHIRE	Solar Accumulated and Peak Proton and Heavy Ion Radiation Environment
SDO	Solar Dynamics Observatory
SEE	single event effect
SEP	solar energetic particle
SEPEM	Solar Energetic Particle Environment Modelling
SIS	Solar Isotope Spectrometer
SOHO	Solar and Heliospheric Observatory
SSN	sunspot number
STEREO	Solar Terrestrial Relations Observatory
TSI	total solar irradiance
VESPER	Virtual Enhancements – Solar Proton Event Radiation

1 Introduction

1.1 Space weather

Space weather refers to time-varying conditions and phenomena within the heliosphere, especially in relation to their effects on geospace environment and the Earth. It includes processes in the whole solar-terrestrial chain, reaching from the convective zone of the Sun, through the corona, solar wind and Earth's magnetosphere, to the lower atmosphere and the surface of the Earth (e.g., Baker, 2000; Koskinen et al., 2017). The term space weather was introduced in the 1950s, and came to widespread use in the 1990s (Cade and Chan-Park, 2015, and references therein). As a subfield of solar-terrestrial physics, research into space weather related phenomena has been conducted for over a century, with main emphasis in pure science. However, interest in the applications and societal relevance of space weather research began to spread during the 1990s, and space weather research as it is known today began in earnest.

Nowadays space weather scientists constitute a large research community that has produced a vast number of scientific articles. Several books have been written about space weather (e.g., Song et al., 2001; Bothmer and Daglis, 2007; Koskinen, 2011), and several scientific journals and conference series are devoted partly or wholly to the topic. Various national and international space weather programs or committees have been founded, including the National Space Weather Program in the United States (Bonadonna et al., 2017), International Living With a Star program (Withbroe et al., 2005), the space weather office of the Space Situational Awareness programme (Luntama et al., 2010) of European Space Agency (ESA), and the space weather expert group of the United Nations Committee on the Peaceful Uses of Outer Space (Mann et al., 2018). Despite the significant progress in understanding the physical nature of the processes behind disturbances in space weather, we are still far from reliably forecasting them. To achieve that level, improved international collaboration and coordination in key areas in space weather research is needed (e.g., Schrijver et al., 2015; Mann et al., 2018).

1.1.1 Origin and causes

The Sun, as the main energy source in the solar system, is also the main source of space weather. The direct space weather effects are transported via the solar wind plasma, electromagnetic radiation, and energetic particles (e.g., Koskinen et al., 2017,

and references therein). The connection of magnetic storms (Gonzalez et al., 1994) with particles emanating from the Sun was made already in the early 1900s (Chapman, 1917, 1918). In the 1950s, theories began to form about transient emissions of ionised gas with embedded magnetic structures (Morrison, 1956; Parker, 1957; Gold, 1962; Fokker, 1963), which some of the early observations seemed to support (Fan et al., 1960; Bryant et al., 1962). A first theory of a constant stream of particles from the Sun was developed to explain the shape of the tails of comets (Biermann, 1951). Then, Parker (1958) formulated the first physics-based theory of the solar wind, and soon after, its existence was proved with in situ observations (Gringauz et al., 1960; Neugebauer and Snyder, 1962). Finally, the existence of the clouds of magnetised plasma emitted by the Sun, nowadays known as coronal mass ejections (CMEs), was proved by white light observations (Hansen et al., 1971; Tousey, 1973; Gosling et al., 1974). It is generally agreed that CMEs are initiated by a build-up of magnetic energy which is destabilised by an instability or magnetic reconnection (e.g., Forbes et al., 2006; Green et al., 2018). Nowadays they are known to be the main driver of large geomagnetic storms (e.g., Gosling et al., 1991), especially when the accompanying magnetic field has strong southward components (Kilpua et al., 2017).

The most space weather-relevant electromagnetic radiation occurs during solar flares, which are sudden releases of enormous amounts of energy; around 10^{25} J may be released in a timescale of hours (e.g., Shibata and Magara, 2011). The energy release is due to magnetic reconnection in the low solar corona (Priest and Forbes, 2002; Benz, 2017). Radiation is emitted on a wide range of wavelengths from kilometric radio waves (e.g., Dulk, 1985) to $<1 \cdot 10^{-15}$ m (>1 GeV) gamma rays (Chupp and Ryan, 2009). The first observation of a solar flare was made in September 1, 1859 (Carrington, 1859; Hodgson, 1859), and they have been observed regularily in the 656.3 nm Hα-line since the 1930s (Švestka, 1966) and in the soft X-rays since the 1970s (Fletcher et al., 2011).

The three main components of energetic particles in relation to space weather are solar energetic particles (SEPs), galactic cosmic rays (GCRs) and radiation belt particles. SEPs, sometimes also called solar cosmic rays, are ions and electrons that are accelerated mainly by flares and CMEs to energies ranging from keVs to GeVs (e.g., Klein and Dalla, 2017). As SEPs are the main topic of this thesis, their origin and effects are explained in more detail in Section 1.2.

According to current understanding, GCRs are accelerated in supernova remnants through diffusive shock acceleration (Blandford and Eichler, 1987). They are fully ionised high energy particles that arrive in the solar system with a fairly constant rate (e.g., Bazilevskaya et al., 2014). The lower energy part of the GCR spectrum, namely below some tens of GeVs, is modulated by the heliosphere, whose properties depend on the solar activity level (e.g., Parker, 1965; Jokipii, 1989; Potgieter, 2013, and references therein).

The Earth's radiation belts, which are often called Van Allen Belts since their

existence was first reported by van Allen (1959), consist of trapped electrons and protons with energies up to tens and hundreds of MeVs, respectively. Typically, the electrons occur in two belts, below $L < 2$ and between $L = 3$ and $L = 7$, while the protons are mostly confined below $L < 2$ (Hudson et al., 2008; Millan and Baker, 2012).[1] The dominant source for the highest energy protons is cosmic ray albedo neutron decay (CRAND) (Singer, 1958), while the lower energy protons are mostly trapped solar protons (Selesnick et al., 2007). The energetic electrons, however, are thought to originate from within the magnetosphere, accelerated via radial transport and resonant wave-particle interactions (e.g., Millan and Baker, 2012, and references therein).

1.1.2 Effects on Earth and society

Probably the earliest observed effects of space weather on technological systems are related to anomalous currents in the early electrical telegraph lines, coinciding with sightings of aurorae (Barlow, 1849). Another early example is the period of magnetic activity between August 28 and September 7, 1859 (Stewart, 1861), which disrupted telegraph operations around the world, producing currents strong enough to cause sparks to fly from the telegraph equipment and give electric shocks to operators (Boteler, 2006; Shea and Smart, 2006, and references therein). This period of solar activity has been widely held as the largest space weather event of the last 450 years (McCracken et al., 2001; Shea et al., 2006). Telephone lines have also been affected: for example, in the geomagnetic storm of March 24, 1940, the Bell Telephone Company experienced severe disturbances (McNish, 1940), and in February 10, 1958, the use of the first transatlantic telephone line was severely disrupted (Meloni et al., 1983).

The anomalous currents are produced when a potential difference is induced over an area of the Earth's surface by time variations in the geomagnetic field (e.g., Root, 1979; Lanzerotti, 2001). Largest field variations occur mostly in magnetic storms caused by large CMEs (Gosling et al., 1991; Koskinen and Huttunen, 2006). In addition to communication lines, these geomagnetically induced currents (GICs), or telluric currents, affect any other technological systems where long conductors are used, such as power grids and oil and gas pipelines. In power systems GICs cause saturation of transformers, which can lead to overheating and burn-out, and thus even system collapse (Boteler et al., 1998; Pirjola, 2000). The March 1940 and February 1958 magnetic storms both caused power system problems in several areas in the United States and Canada (Albertson et al., 1974), but the most striking example is the magnetic storm of March 13, 1989, when the entire province of

1 L-values denote the Earth's magnetic field lines that cross the equator at a distance of L Earth radii. In a dipole field the radial distance is given by $r = L\cos^2\lambda$ (McIlwain, 1961).

Quebec lost electicity for almost a day (e.g., Bolduc, 2002). In pipelines GICs can increase corrosion and interfere with corrosion protection systems (e.g., Boteler, 2000; Viljanen et al., 2006).

Space weather also affects technologies which utilise electromagnetic radiation, such as radiowaves or microwaves. Correlation of solar activity and anomalies with long distance radio communications was already observed in the 1920s (Marconi, 1928; Anderson, 1928), and most of the solar events which disturbed wired communication technologies had also an effect on wireless communication: for example, radio communication between North America and Europe was almost impossible during the March 1940 geomagnetic storm (McNish, 1940). As the ionosphere reflects the skyward-directed radiowaves, thus enabling over-the-horizon long-distance communication, changes in the ionosphere may disturb the reflection and prevent communication. The ionospheric properties are changed through Sun's ultraviolet and X-ray emissions, energetic particles and magnetic storms (Lanzerotti, 2007, and references therein). Ionospheric scintillation, caused by irregularities in the ionisation density, can also disrupt ground-to-satellite communications (e.g., Basu and Basu, 1981; Yeh and Liu, 1982; Kintner et al., 2007).

In addition to ionospheric effects, the Sun affects radio technologies by directly emitting solar radio noise and bursts. These emissions, originally discovered in the early 1940s (Reber, 1944; Southworth, 1945; Hey, 1946), interfere with communications, radar technology and Global Positioning System (GPS) communications (e.g., Lanzerotti, 2017). Especially noteworthy were the cases of radar jamming during the Second World War (Hey, 1946; Lovell, 1987) and the Cold War (Knipp et al., 2016), which luckily were quickly noticed to be the result of solar radio bursts rather than enemy activity. Timely discovery of the true source of the disruptions, especially in the latter case, was of paramount importance; if interpreted as deliberate surveillance jamming by the enemy, it could have resulted in an all-out war.

The energetic particle radiation environment in the near-Earth space encompasses trapped particles, SEPs and GCRs. Earth-orbiting satellites, as well as spacecraft and astronauts on interplanetary routes, are exposed to all of the three radiation fields to some extent. As ionising radiation, energetic particles are harmful for both electronic equipment and biological organisms. The type and severity of the radiation hazard depends on the energy of the particles and the amount of energy they transfer to the radiated medium. Large number of spacecraft anomalies, such as solar cell degradation, electronic errors and loss of control, have been reported to be caused by energetic particles (Baker et al., 1994; Barbieri and Mahmot, 2004; Iucci et al., 2005). Even complete loss of spacecraft have been attributed to particle radiation, such as the losses of communications satellites Telstar 1 in February 1963 (Lanzerotti, 2007, and references therein), Telstar-401 in January 1997 (Reeves et al., 1998), and Galaxy 4 in May 1998 (Baker et al., 1998). SEP events and GCRs contribute to the radiation dose received by astronauts and even aircraft crew (e.g.,

Facius and Reitz, 2007, and references therein); the large SEP event of August 1972, occurring between the Apollo missions 16 and 17, would have caused a potentially lethal radiation dose to an astronaut in a space suit (Wilson et al., 1999).

1.1.3 Space climate

Just like in the case of terrestrial weather and climate, space climate refers to the long-term variations in space weather (Mursula et al., 2007, 2013). Direct observations of the properties of solar wind plasma, energetic particles and interplanetary magnetic fields have been carried out routinely since the 1960s with increasing coverage and precision (Hapgood et al., 1991; Neugebauer, 1997), allowing for space climatological studies for the last five solar cycles. Cosmic ray observations began in the 1930s with ionisation chambers (Forbush, 1954), and have been made continuously with neutron monitors (NMs) since the 1950s (Shea and Smart, 2000; Simpson, 2000; Stoker et al., 2000). Solar radio flux at 10.7 cm (2.8 GHz) has been measured continuously since 1947 (Tapping, 2013), magnetic fields of the sunspots since 1917 (Howard, 1985; Pevtsov et al., 2019), and the geomagnetic *aa* index since 1868 (Mayaud, 1972). In addition, the daily sunspot number series extends until 1818 and monthly sunspot number series until 1749 (Clette et al., 2014). Although not all of the series measure single physical quantities, they provide crucial information on many differerent aspects of space climate. With careful intercorrelation, the longer observations can be used as proxies for the direct, physical quantities. Even longer time series can be attained by using cosmogenic isotopes such as ^{14}C in tree rings or ^{10}Be in ice cores as proxies for solar activity (Usoskin, 2017, and references therein).

The main topics of interest in space climate research are the long-term solar variability and its possible periodicities, the physical relationships between the various measures of solar activity and the Sun, and the effect of the solar activity on the Earth's climate (Mursula et al., 2007). These are directly related to the research presented in this thesis: as the level of solar activity during the recent solar cycle 24 was observed to be very low (e.g., McComas et al., 2013; Richardson, 2013; Richardson et al., 2017; Kakad et al., 2019), it has been suggested that the Sun is entering a grand minimum (Feynman and Ruzmaikin, 2011; Zolotova and Ponyavin, 2014), or returning to a lower level of activity after a grand maximum (de Jager et al., 2016). This long-term change would have consequences on future space endeavors: decreasing solar activity has resulted in diminished SEP acceleration (e.g., Gopalswamy et al., 2014; Mewaldt et al., 2015; Paassilta et al., 2017), but at the same time, GCRs have easier access into the inner heliosphere (e.g., Schwadron et al., 2017).

1.2 Solar energetic particles

SEPs consist of protons, electrons and heavier ions that are accelerated to high energies in processes occurring in the solar corona and in the interplanetary space. They occur in bursts, during which the observed fluxes may quickly increase by several orders of magnitude (e.g., Reames, 2013). These increases, known as SEP events, last from hours up to several days. Their energy spectra often resemble pure, broken, or double power laws (e.g. Ellison and Ramaty, 1985; Tylka et al., 2005; Mewaldt et al., 2012), with energies ranging from hundreds of keV up to tens of GeV (McCracken et al., 2012). Their occurrence rate is correlated with overall solar activity, although large events may occur even during solar minimum (Shea and Smart, 1990).

SEPs were first reported by Forbush (1946) who attributed three increases of cosmic rays (CRs) to solar flares that had occurred almost simultaneously. The early measurements of CRs were performed with ionisation chambers which required the primary particle to have an energy of ~4 GeV in order to generate muons that are able to reach ground level (Compton et al., 1934; Shea and Smart, 2000). The neutron monitor, developed in the early 1950s (Simpson et al., 1953; Simpson, 2000) and further optimised in the 1960s (Carmichael, 1968; Stoker et al., 2000), measures secondary particles generated when the primary particles interact with nuclei in the atmosphere. The SEP events observed with the ionisation chambers and NMs are the most energetic subset of SEP events, known as ground level enhancements (GLEs) (Poluianov et al., 2017). Space-borne observations of SEPs commenced in the early 1960s with instruments onboard Pioneer, Explorer and Mariner spacecraft (e.g., Fan et al., 1960; Bryant et al., 1962; van Allen and Krimigis, 1965). Regular observations have been conducted since the early 1970s with, e.g., Interplanetary Monitoring Platform (IMP) (McGuire et al., 1986), Geostationary Operational Environmental Satellite (GOES) (Onsager et al., 1996), Solar and Heliospheric Observatory (SOHO) (Domingo et al., 1995), Advanced Composition Explorer (ACE) (Stone et al., 1998) and Solar Terrestrial Relations Observatory (STEREO) (Kaiser et al., 2008).

1.2.1 Sources and acceleration mechanisms

Before the discovery of CMEs, flares were the only known major transient solar activity and thus, since the discovery of SEPs, it was generally agreed that they were caused by flares. Early evidence of particle acceleration in flares came from the close flare association of radio bursts (Wild et al., 1963), microwave bursts (Covington and Harvey, 1961) and X-rays (Chubb et al., 1957; Anderson and Winckler, 1962). However, the radio observations reviewed by Wild et al. (1963) suggested two different acceleration mechanisms: type III bursts were indicative of accelerated energetic electrons escaping from the Sun, whereas type II bursts suggested moving

shocks. More evidence of different mechanisms came from long duration X-ray events (Kreplin et al., 1962; Pallavicini et al., 1977), which were associated with CMEs (Sheeley et al., 1975).

Division of SEP events into two categories became firmly established in the 1980s (Cane et al., 1986; Reames and Stone, 1986; Cane and Reames, 1988; Reames, 1988). The first category, impulsive events, have lower intensities and they are short-duration, spatially compact and numerous (e.g., Reames, 2013, and references therein). They are distinguished by enhanced abundances of ^{3}He (Hsieh and Simpson, 1970; Serlemitsos and Balasubrahmanyan, 1975; Reames et al., 1985), heavy ions (Hurford et al., 1975; Gloeckler et al., 1975; Mason et al., 1986; Reames et al., 1994) and ultra-heavy ions (Mason et al., 2004). They are associated with type III radio bursts and impulsive, short-duration flares (Reames et al., 1985, 1988; Kahler et al., 1987). In addition, early measurements of charge states showed that impulsive events had high average ion charge states (Klecker et al., 1984; Luhn et al., 1987).

The second category, gradual events, have high intensities, long durations and are spatially extensive (e.g., Kahler, 1992; Desai and Giacalone, 2016). Their composition reflects that of the corona (Meyer, 1985; Reames, 1995), and they have lower ion charge states as compared to impulsive events (Hovestadt et al., 1981; Leske et al., 1995). Gradual events are associated with CMEs (Kahler et al., 1978, 1984) and type II and IV radio bursts (Kahler, 1982; Cane and Stone, 1984; Cliver et al., 1999). However, several studies of SEP events with both impulsive and gradual properties, as evidenced by particle composition (e.g., Mason et al., 1999; Kocharov and Torsti, 2002; Tylka et al., 2005; Cane et al., 2010) or flare/CME-associations (e.g., Kahler et al., 2001; McCracken et al., 2008; Cane et al., 2010), showed that the separation between the two categories is not clear, but rather, there exists a continuum of properties from impulsive to gradual.

Particle acceleration in flares has been attributed to resonant stochastic acceleration (Temerin and Roth, 1992; Miller, 1998; Petrosian, 2012) or magnetic reconnection (Drake and Swisdak, 2012). ^{3}He-enhancements in impulsive SEP events have been explained with oblique (Temerin and Roth, 1992; Roth and Temerin, 1997) and parallel propagating (Liu et al., 2004, 2006) Alfvén-ion-cyclotron waves. In addition, a model of particles undergoing multiple interactions with merging and contracting magnetic islands in a reconnection current sheet has been shown to reproduce the observed (Breneman and Stone, 1985) Q/A dependence of the ion abundance enhancements (Drake et al., 2009, 2013; Knizhnik et al., 2011).

Particle acceleration in the large gradual SEP events is associated with shocks driven by CMEs (e.g., Desai and Giacalone, 2016). Theory of particle acceleration in moving interplanetary shocks was developed by Lee (1983, 2005) based on diffusive shock acceleration theory (Bell, 1978). In this theory, accelerated ions streaming from the shock generate waves that in turn scatter subsequent ions back to the shock, resulting in multiple shock traversals and therefore more acceleration (Lee et al.,

2012). Shock acceleration has been shown to be able to accelerate particles to very high energies in realistic timescales (e.g., Ng and Reames, 2008; Afanasiev et al., 2018). The variability in the ion abundances in gradual events has been suggested to be caused by acceleration of seed populations from previous (impulsive) flares by quasi-perpendicular shocks (Tylka et al., 2005, 2006; Tylka and Lee, 2006; Sandroos and Vainio, 2007, 2009).

1.2.2 Space weather effects

For space missions outside the radiation belts and magnetosphere of the Earth, SEPs constitute the most serious radiation hazard (e.g., Vainio et al., 2009). In electronics, energetic particles cause both dose-related effects and transient, single event effects (SEEs). Dose-related effects are produced by ionisation or displacement damage, which cause the degradation and possible failure of semiconductor devices (Pease, 1996), as well as solar cell and sensor degradation (Crabb, 1994; Hopkinson et al., 1996). Another dose-related problem is internal charging, where high energy particles penetrate the shielding of the spacecraft and build up within dielectric materials, leading to electrostatic discharges which cause interference or damage to the electronics (Frederickson, 1996; Lai et al., 2018). SEEs occur when a high energy particle deposits energy or charge in a sensitive area of a component (McNulty, 1996). They can be either nondestructive (soft) errors, such as memory errors, logic state changes (Dodd and Massengill, 2003), or destructive, such as latchups, burnouts and gate ruptures (Sexton, 2003). SEEs also occur in sensors, causing background noise (e.g. Daly et al., 1996; Feynman and Gabriel, 2000).

Ionising radiation is harmful for humans and biological organisms in general. The radiation effects on humans are usually categorised as acute (or early) deterministic effects and chronic (or late) stochastic effects (Hellweg and Baumstark-Khan, 2007; Kennedy, 2014). SEPs contribute to both acute and chronic radiation effects, but are the dominant cause in the former due to their intermittent nature. Acute effects are caused after a sudden exposure to a large radiation dose; after a dose of >0.7 Sv, the symptoms include fatigue, nausea and decrease in bone marrow function. Higher acute doses lead to gastrointestinal syndrome, neurovascular syndrome and death from sepsis (Hellweg and Baumstark-Khan, 2007). The most significant chronic effects of radiation are various types of cancer, especially leukemia and thyroid cancer (Ron, 1998), and the development of cataracts (Lett et al., 1994).

In addition, SEPs, along with GCRs, can precipitate into the Earth's atmosphere, causing ionisation and chemical changes (Mironova et al., 2015). Ionisation by particles occurs throughout the atmosphere, but is the dominant source of ionisation in the middle and low atmosphere (Bazilevskaya et al., 2008). An important chemical change is the creation of odd hydrogen (HO_x) and nitrogen (NO_x) leading to destruction of ozone (e.g., Thorne, 1977), which may be substantial during large SEP

events (Seppälä et al., 2006; Verronen et al., 2006). The production of cosmogenic isotopes, although in very small quantities, is significant because they can be used in geochronology and studying long-term solar activity (Beer et al., 2012; Usoskin, 2017).

2 Particle environment modelling

Despite all the progress in understanding the processes that are driving space weather, long-term SEP event forecasts are not available. It has been suggested that SEP events and the processes behind them are a self-organised criticality phenomenon, preventing deterministic predictions (Lu and Hamilton, 1991; Xapsos et al., 2006). However, space mission designers need reliable estimates of the radiation environment their instruments will stay in. Therefore, statistical modelling, based on measurements of previous SEP events, is needed. The relevant quantities are the integrated flux, or fluence, which is related to dose-related particle radiation effects, and the peak flux, which is related to single-event effects. A number of different radiation environment models have been developed, most of them focusing on one component of the radiation environment: SEPs, radiation belt particles or GCRs. A short review of such models is presented here, with special emphasis on the SEP environment.

2.1 SEP models

The first widely used statistical SEP fluence model was developed by King (1974). The King model was based on IMP-4 and IMP-5 proton measurements >10 MeV to >100 MeV during solar cycle 20. The anomalously large event of August 1972 was modelled separately from the other, "ordinary", events, assuming that the fluences of "ordinary" events were distributed log-normally, and that all predicted "anomalous" events would have the spectrum of August 1972. The model used an extension of Poisson statistics to take into account the uncertainty in the parameter of the distribution. Using similar methodology, Feynman et al. (1990, 1993, 2002) developed the well-known Jet Propulsion Laboratory (JPL) model. The fluence database was extended to cover cycles 19–21, removing the need for separate treatment of any "anomalous" events. The first version of the JPL model gave cumulative fluence estimates for >10 MeV and >30 MeV protons, and the updated version was extended to >1 MeV at low energies and to >60 MeV at high energies. Further updates to the model were made by Rosenqvist et al. (2005) and Glover et al. (2008).

Another line of models is the Emission of Solar Protons (ESP) model (Xapsos et al., 1998b, 1999, 2000), which estimates the worst-case (peak) flux and fluence as well as the cumulative fluence. Maximum entropy principle (Jaynes, 1957) and results from extreme value theory (Xapsos et al., 1998a) were used to analytically

derive the functional form for flux and fluence distributions, resulting in truncated power law distribution for the worst case flux and fluence, and log-normal distribution for the cumulative fluence. The model is based on events observed in solar cycles 20–22 with IMP and GOES spacecraft and the results are given for peak fluxes at >10 MeV and fluences from >10 MeV to >100 MeV and up to >300 MeV with spectral extrapolation. An updated version of the cumulative ESP model, called Prediction of Solar particle Yields for CHaracterizing Integrated Circuits (PSYCHIC), used an improved integrated data set and extended the energy range to >327 MeV (Xapsos et al., 2004). The PSYCHIC model was later extended to cover all significant naturally occurring elements by using helium measurements from GOES, heavy ion measurements from ACE/Solar Isotope Spectrometer (SIS) and published abundance ratios (Xapsos et al., 2007). In addition, an interplanetary electron model was developed based on IMP-8 measurements between 0.2–10 MeV and the ESP modelling methodology (Taylor et al., 2011).

Using a somewhat similar methodology, Jiggens et al. (2012) developed a model for proton fluences and peak fluxes in ESA's Solar Energetic Particle Environment Modelling (SEPEM) project (Crosby et al., 2015). The model was based on a database of cross-calibrated IMP and GOES measurements from November 1973 to June 2009, rebinned into 10 logarithmically spaced energy bins from 5 MeV to 200 MeV (Reference Data Set (RDS) version 1). The fluence and peak flux distributions in each bin were modelled with cut-off power law functions. Instead of event frequency and Poisson distribution, the event occurrence was modelled with a "virtual timelines" method, which takes into account both the waiting times and the event durations. The model produced fluence and peak flux estimations for 0.5–7 year missions during solar maximum and for 0.5–4 year missions during solar minimum. The energy range of the results was extended downwards to 0.1 MeV and upwards to 1 GeV by using a double power law Band function (Band et al., 1993). The Solar Accumulated and Peak Proton and Heavy Ion Radiation Environment (SAPPHIRE) model (Jiggens et al., 2018a,b) brought an update to SEPEM, with significantly improved database, covering the time from July 1974 to May 2015 (RDS2). Other new aspects were the modelling of 1-in-X-year spectra (for X ranging from 10 to 10 000), and the addition of helium and heavier ions. Helium was modelled with the same method as protons, using GOES data, and the heavier ions were modelled using energy-dependent helium-heavy ion abundance ratios calculated with data from ACE/SIS.

A recent development is the Mission Specific Solar Radiation Environment Model (MSSREM) for peak fluxes by Robinson et al. (2020). It uses proton data from GOES, helium data from SEPEM RDS version 2 (which is also based on GOES) and heavy ion data from ACE. The ions that are not observed by ACE/SIS are scaled from the ACE measurements using coronal and photospheric abundances. They model the cumulative flux distributions of each ion and energy bin with piecewise

functions of three parts: power law for the lowest fluxes, logarithmic quadratic for the medium fluxes, and truncated power law for the highest fluxes. To account for different solar activity levels, they use a relationship between the number of SEP episodes and the sunspot number. The model provides peak flux estimations for all ions from $Z = 1$ to $Z = 92$ in energies from 1 MeV to 100 GeV. Usually the SEP event occurrence prevents model estimations for missions shorter than ~0.5 years, but in case of MSSREM, a unique sampling method allows for peak flux estimations for missions as short as few minutes.

The previous SEP models were similar in the sense that the fluxes and fluences were modelled separately at each energy. These models can be collectively called JPL-type models. In a Monte Carlo (MC) calculation this means that the spectra of the steps (or realisations) do not represent physical spectra. A different methodology was presented by Nymmik (1998, 1999a,b,c, 2007) of Moscow State University (MSU) (see also Kuznetsov et al., 2005). In the MSU model, the proton peak flux and fluence spectra are assumed to be described by power law functions of particle momentum where the power law index itself is a function of energy. The proton spectral parameters are functions of the event size, which is described by a cut off power law distribution for the >30 MeV fluence. In other words, the size of the event and the spectral shape are modelled parameters. Another feature of the MSU model is that the event frequency is related to the level of solar activity through dependence on the sunspot number. In addition, heavy ion peak fluxes and fluences are modelled through an averaged relation of the heavy ion spectra and proton spectra derived from the results of Mazur et al. (1992, 1993).

Recently, Aminalragia-Giamini et al. (2018) developed the Virtual Enhancements – Solar Proton Event Radiation (VESPER) model, using the SEPEM RDS2 and utilizing a new methodology by creation of "virtual time series" of differential proton fluxes. The methodology is based in the calculation of a time series of second moments of the flux energy spectrum in log-space, from which an event list is determined. Then, waiting times and event durations are sampled from their respective distributions (modelled with cut-off power law functions), forming a virtual timeline of specified length (mission duration). Using the demonstrated power law relationship with a Gaussian scatter between the event durations and "fluences", i.e., time integrals of the second moment over the event, the "fluences" for each event on the timeline are sampled. Then, a "seed" event is randomly sampled from the true events in the vicinity of the sampled "fluence". The final time series for the sampled virtual event is obtained by scaling the seed event so that its "fluence" matches that of the sampled event. The scaling is independent on energy and does not require any assumptions on the spectral shape, meaning that the virtual time series can be produced for the original channels although the scaling is calculated from the second moments. The model can produce results as probability of exceeding a fluence or a peak flux for the RDS2 channels during solar active and solar quiet times.

2.2 Radiation belt models

One of the most widely used models for radiation belt particles are the AE8/AP8 models (Vette, 1991). The electron model, AE8, is valid for L values of 1.2–11, divided into three parts: the inner zone, transition region and outer zone. It covers energies from 0.4 MeV to 5 MeV and handles solar minimum and solar maximum separately. The proton model, AP8, covers energies from 0.1 MeV to 400 MeV and L values 1.15–6.6. The updated versions AE9 and AP9 (Ginet et al., 2013) use a probabilistic approach and an improved dataset, and provide, e.g., confidence levels, error estimates and extended coverage in location and energy. Other radiation belt models include the Particle ONERA-LANL Environment model (POLE; Sicard-Piet et al., 2005) and International Geostationary Electron model (IGE-2006; Sicard-Piet et al., 2008), and the Slot Region Radiation Environment Model (SRREM; Sandberg et al., 2014).

2.3 GCR models

The first widely used GCR model was developed for the Cosmic Ray Effects on MicroElectronics (CREME) toolkit (Adams et al., 1981). Flux spectra were modelled with analytical functions and the solar cycle dependence of the GCRs was modelled with a simple sine curve. The effect of SEPs was included as a worst-case spectrum based on the August 1972 event. Tylka et al. (1997) described the updated version of the toolkit, CREME96. It had significant improvements in its radiation environment models, such as the adoption of a more advanced model for GCRs, developed by Nymmik et al. (1996). Recently, there has been another update to the toolkit (Adams et al., 2020), which implements the Badhwar-O'Neill model for GCRs (O'Neill et al., 2015) and the MSSREM model for SEPs (Robinson et al., 2020; see above).

The Badhwar-O'Neill model (Badhwar and O'Neill, 1992, 1996; O'Neill, 2006; O'Neill et al., 2015; Slaba and Whitman, 2020) is another well-known GCR model. It uses a numerical solution of the spherically symmetric, quasi-steady state Fokker-Planck-equation (Parker, 1965) and various satellite and balloon CR measurements to determine a GCR flux for all elements from $\mathrm{Z} = 1$ to $\mathrm{Z} = 28$. Other GCR models include the CRRES/SPACERAD Heavy Ion Model of the Environment (CHIME) model (Chenette et al., 1994) and the model by Matthiä et al. (2013).

3 Solar activity

3.1 Solar activity cycle

The level of solar activity follows a cycle with period of roughly 11 years (e.g., Balogh et al., 2014; Hathaway, 2015, and references therein). The 11-year solar cycle is also known as the Schwabe cycle, or the sunspot cycle, since it was discovered by Heinrich Schwabe using observations of sunspots and spotless days (Schwabe, 1844). The cause of the activity cycle is attributed to magnetic dynamo processes within the Sun, but the details of the processes are not known for certain (e.g., Ossendrijver, 2003; Charbonneau, 2020, and references therein). The magnetic nature of sunspots was originally discovered by Hale (1908), and after observations extending to the following solar cycle, they found that the sunspot groups in the northern hemisphere have opposite polarity to the corresponding groups in the southern hemisphere, and that the polarities are reversed in the following cycle (Hale et al., 1919; Hale and Nicholson, 1925). These findings, along with the discovery of the reversal of the polar magnetic field during solar cycles (Babcock, 1959, 1961), led to the concept of the 22-year magnetic cycle, also known as the Hale cycle. Although the average period of the sunspot cycle, as well as the period of many other variables of solar activity, is on average about 11 years as measured from minimum to minimum, the magnetic cycle itself is longer, beginning before and continuing after the apparent sunspot minima (e.g., Wilson et al., 1988; Cliver, 2014, and references therein).

Solar cycles have been numbered so that cycle number 1 starts in early 1755, and we are currently (January 2021) experiencing the very beginning of cycle 25. As the cycles are usually defined as the minima of the 13-month smoothed sunspot number, the exact date of cycle onset can be ascertained no less than 6 months after.

3.1.1 Sunspot number

Sunspots are regions of lower temperature and higher magnetic flux as compared to the surrounding areas in the Sun's photosphere. Because of the lower temperature, they appear darker than the surrounding regions. Earliest records of sunspots date back over 2000 years (Clark and Stephenson, 1978), but regular observations were commenced in the 1850s by Johann Rudolf Wolf (Friedli, 2016, and references therein). His "relative" sunspot number (SSN) series, also known as the International

Sunspot Number, Wolf Sunspot Number, or Zürich Sunspot Number, is defined as

$$R_{\mathrm{I}} = k(10N_{\mathrm{g}} + N_{\mathrm{s}}), \tag{1}$$

where k is the correction coefficient for the observer, N_{g} is the number of sunspot groups and N_{s} is the number of individual sunspots. Wolf extended the R_{I} record back to 1749, and it has been obtained daily in Zürich Observatory from 1849 to 1980 and in the Royal Observatory of Belgium in Brussels since 1981. Because of the length of the record, SSN is usually considered as the primary indicator of solar activity.

As the R_{I} series was compiled from a number of individual series of observations using partly incomplete data and different processing techniques, there was need for a revision of specific parts of the series as well as the complete series (e.g., Clette et al., 2014, and references therein). Using a large number of observations that were not included in the construction of R_{I}, especially in the time before the 1850s, Hoyt and Schatten (1998a,b) constructed the new Group Sunspot Number series, averaging the number of sunspot groups observed by different observers, i.e.,

$$R_{\mathrm{G}} = \frac{12.08}{N} \sum_{i=1}^{N} k_i N_{\mathrm{g},i}, \tag{2}$$

where N is the number of observers, k_i is the correction coefficient for the observer i, $N_{\mathrm{g},i}$ is the number of sunspot groups recorded by observer i and 12.08 is a scaling factor which made the averages of R_{G} and R_{I} equal for the time between 1874 and 1976. The new R_{G} series extended from 1610 to 1995 (although not completely uniformly in time), and was considered by many to be a more reliable record of solar activity. R_{G} agreed with R_{I} quite well between 1880 and 1995, but there was a significant disagreement before 1880, leading to some confusion in the community as having to choose between the two series. In addition, even after the significant effort of Hoyt and Schatten (1998a,b), need for new corrections and revisions were found (e.g., Leussu et al., 2013; Svalgaard, 2013), and more previously lost observations were uncovered (e.g., Vaquero et al., 2007; Arlt, 2008; Vaquero et al., 2011); a reliable revision of the sunspot number series was therefore needed. To answer this need, new versions of the International Sunspot Number (Clette et al., 2014; Clette and Lefèvre, 2016) and the Group Sunspot Number (Vaquero et al., 2016) were constructed in the framework of a series of Sunspot Number workshops (Clette et al., 2016).

The top panel in Figure 1 shows the daily values of the new International Sunspot Number, S_{N}[2], (in grey) and the smoothed values (in green) for the period between 1960 and 2020. Here, as well as in the other panels in Figure 1, the smoothing has

2 Data downloaded on 2020–11–16 from `http://sidc.be/silso/datafiles/`

been performed with a Gaussian filter with full width at half maximum (FWHM) of 13 months (more precisely, 395 days). In order to show the smoothed time series until the edges of data, each time series has been padded with constant values equal to the edgemost values in each end of the series.

Sunspot number series, as the longest directly observed measure of the solar activity, plays a very important role in understanding the evolution of Sun's magnetic processes and their influence on Earth and its climate, as well as the interplanetary space.

3.1.2 Other measures of solar activity

Along with the sunspot number, one of the most widely used indices of solar activity is the 10.7 cm solar radio flux ($F_{10.7}$) (Tapping and Detracey, 1990; Tapping, 2013). $F_{10.7}$ is measured over the whole solar disk in a 100 MHz band centered on 2.8 GHz (10.7 cm) and given in solar flux units (sfu), where $1\,\text{sfu} = 10 \cdot 10^{-22}\,\text{W}\,\text{m}^{-2}\,\text{Hz}^{-1}$. Daily $F_{10.7}$ measurements have been made since 1947 using ground-level facilities in Canada. $F_{10.7}$ consists of at least two sources of flux: thermal free-free emission from coronal plasma, and gyromagnetic emission from active regions. In addition to being an indicator of solar activity, it can be used as a proxy for other indices of solar activity. The second panel from the top in Figure 1 shows the time evolution of $F_{10.7}$[3]. Similarly to the sunspot number plot, daily values are shown in grey and 13-month Gaussian smoothed values in green. When the flux was measured more than once per day, the measurement closest to noon was selected. As can be seen, $F_{10.7}$ is highly correlated with the sunspot number, although their relationship is known to be slightly nonlinear (Holland and Vaughan, 1984; Tapping and Morgan, 2017).

Total solar irradiance (TSI) is the total solar radiative power per unit area. It has been measured continuously with various space-based instruments since late 1978, although with significantly differing absolute accuracy (e.g., Fröhlich, 2012). Three composites that are commonly used have been constructed from these measurements: ACRIM (Willson, 1997), PMOD (Fröhlich and Lean, 1998) and IRMB (Dewitte et al., 2004). Recently, to overcome the issues of different amplitudes and trends of these composites, there has been an effort to build a "Community Consensus" composite, using a traceable probabilistic approach (Dudok de Wit et al., 2017). In addition to being a measure of solar activity, total solar irradiance (TSI) is a measure of the total external radiative forcing of Earth's climate and thus an important parameter in climate studies (Solanki et al., 2013). The Community Consensus composite[4] and its 13-month Gaussian smoothed values are shown in the third panel from the top

3 Data downloaded on 2020–11–16 from `https://lasp.colorado.edu/lisird/data/penticton_radio_flux/`

4 Data downloaded on 2020–11–16 from `https://spot.colorado.edu/~koppg/TSI/`

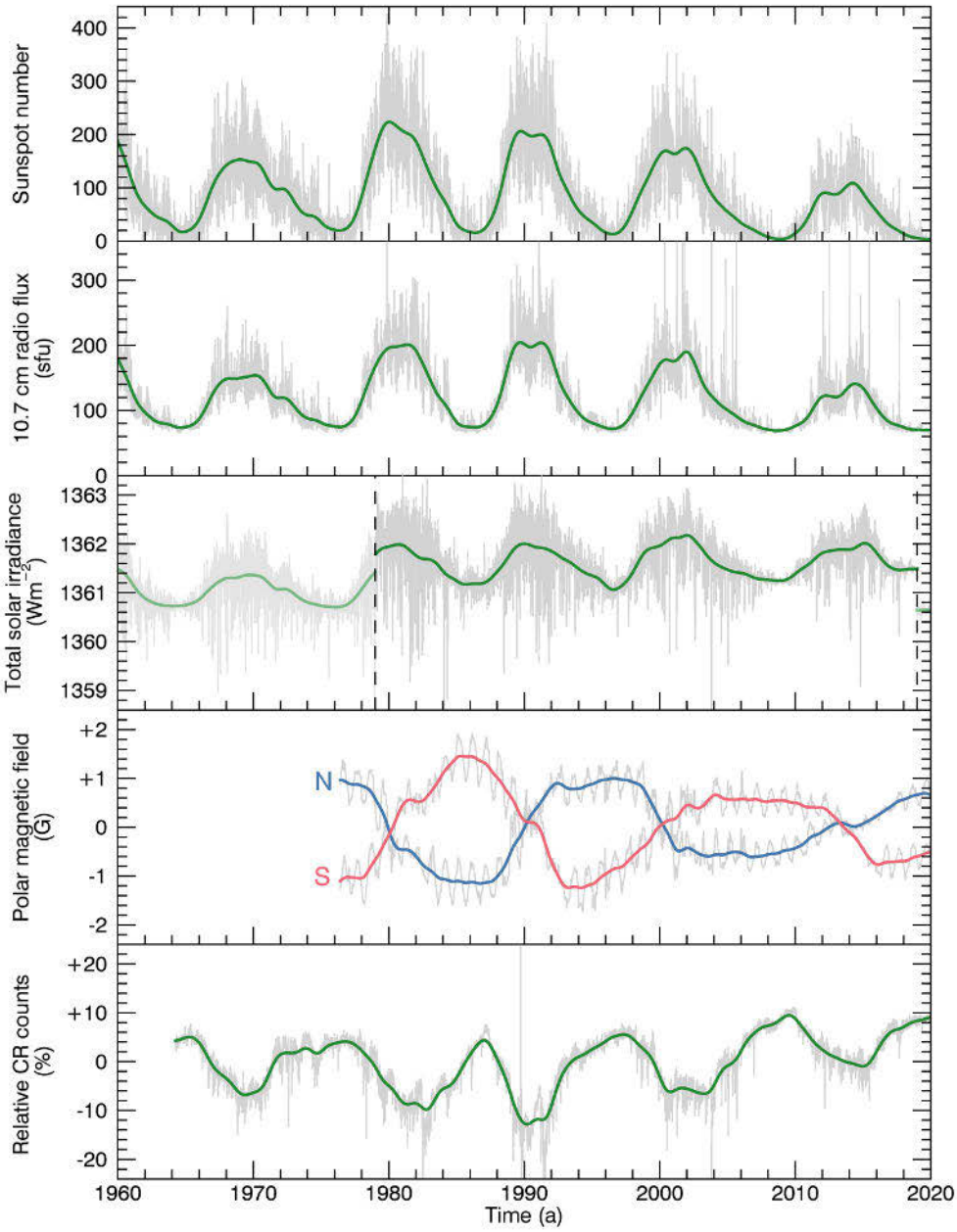

Figure 1. Various measures of solar activity. From top to bottom: international sunspot number S_N, 10.7 cm radio flux ($F_{10.7}$), total solar irradiance (TSI), polar magnetic field (PMF) strength and relative cosmic ray counts. In each panel except the PMF, grey line shows the daily values. In case of the PMF, the grey line shows the 30-day average for every 10 days. In all panels, the coloured line shows the 13-month Gaussian smoothed daily/30-day values. In the TSI panel the darker lines (between the dashed vertical lines) show the "Community Consensus" composite, and the lighter lines (outside the dashed lines) show the NRLTSI2 model. See the text for more details and the sources of data.

in Figure 1 for the time period between 1979–1–1 and 2018–12–31 (distinguished with the dashed vertical lines). Outside this time interval, shown in lighter colours, is the NRLTSI2[5] model (Coddington et al., 2016). Like $F_{10.7}$, TSI follows the general shape of the sunspot number time series, but with a slightly weaker correlation.

Solar polar fields have been found to have a dominant influence over the heliosphere and the solar cycle (e.g., Svalgaard et al., 1978). Most of the polar magnetic flux is open, and therefore it is the main source of the interplanetary magnetic field (IMF; Petrie et al., 2014; Petrie, 2015, and references therein). The open flux appears as coronal holes, which dominate the large-scale structure of the corona over a large part of the magnetic cycle. The bottom panel of Figure 1 shows the polar magnetic field (PMF) flux density[6] measured at the Wilcox Solar Observatory (Scherrer et al., 1977). Unlike in the other panels, here the grey lines show the 30-day averages every 10 days, and the coloured lines show their 13-month Gaussian smoothed values. The oscillation seen in the grey lines is caused by yearly projection effects, which disappear in the smoothed values. The absolute values of the PMFs are strongest around the solar activity minima, and their polarities change near the activity maxima.

The structure of the IMF is directly related to the modulation of GCRs. Since the 1950s, cosmic rays have been routinely observed using ground level NM (Shea and Smart, 2000). The bottom panel in Figure 1 shows the relative cosmic ray count rate of the Oulu NM[7], daily values in grey and 13-month Gaussian smoothed values in green. The solar modulation of GCRs is seen as anticorrelation of the NM count rate and sunspot numbers, i.e., fewer cosmic rays are able to reach the inner heliosphere when the solar activity is higher, and vice versa. Another clear feature that distinguishes CR counts from the previous solar activity indices is the alternation of flatter, plateau-like and sharper, peak-like maxima. This "even-odd" effect (referring to the cycle numbers; Webber and Lockwood, 1988; Van Allen, 2000; Usoskin et al., 2001) is caused by the drift effects of the cosmic rays (e.g., Jokipii et al., 1977; Ferreira and Potgieter, 2004) during the 22-year Hale cycle.

3.1.3 Characteristics of solar cycles

Solar cycles vary significantly in duration, shape, and amplitude. Figure 2 shows the 13-month Gaussian smoothed monthly sunspot number S_N[8] as a function of time after the cycle onset for all cycles 1–24, i.e., between 1755 and November 2020. The cycle onsets are defined as the center of the month of each minima in the smoothed

5 Data downloaded on 2020–11–16 from `https://lasp.colorado.edu/lisird/data/nrl2_tsi_P1D/`
6 Data downloaded on 2020–11–16 from `http://wso.stanford.edu/Polar.html`
7 Data downloaded on 2020–11–16 from `http://www01.nmdb.eu/nest/`
8 Data downloaded on 2020–11–16 from `http://sidc.be/silso/datafiles/`

sunspot numbers. Since the smoothing filter requires 17 datapoints on both sides of the centerpoint, it is impossible to have a definite determination of the end of cycle 24 (onset of cycle 25) until at least 17 months after the true minimum. The smoothed S_N time series of cycle 24 was continued until December 2019 by replicating the last value of the S_N series (October 2020), and cycle 24 was assumed to end in December 2019. The average duration of cycles 1–24 as defined using the Gaussian smoothed monthly S_N is 11.02 years, so the "11-year" cycle turns out to be a very precise definition. The range of variability in the cycle duration is almost 5 years, since the shortest cycle (3) lasted for only 8.9 years, and longest one (4) for 13.8 years.

The variability of the shape of the sunspot cycle is evident from Figure 2. Some cycles have a sharp peak, such as cycles 3 and 11, while some cycles are more plateau-like, such as cycles 7 and 14. Some cycles exhibit a double-peak structure, reported originally by Gnevyshev (1963) using observations of the coronal line at 5303 Å. This structure is seen most clearly in sunspot cycles 22–24. In most cycles the overall shape is skewed to the right, so that the rise time from cycle onset to the maximum is shorter than the decay time from the maximum to the next minimum. Clear exceptions to this are cycles 1, 5, and 7. Cycle 3 has the shortest rise time, 3.0 years, while cycle 7 has the longest, 6.8 years. There is a tendency for cycles with a short rise time to have a high maximum sunspot number, such as cycles 3, 4, 8, and 19, as well as for cycles with longer rise time to have a low maximum, such as cycles 5, 12, and 24; this inverse proportionality is known as the Waldmeier effect (Waldmeier, 1935). Another well-known property that can also be seen in the Figure is the Gnevyshev-Ohl-rule, which states that the sum (or the integral) of the sunspot numbers of an even-numbered cycle tends, with some exceptions, to be smaller than the sum of the sunspot numbers of the following odd-numbered cycle (Gnevyshev and Ohl, 1948; Mursula et al., 2001; Nagovitsyn et al., 2009).

Figure 3 shows the sunspot numbers of solar cycles 1–24 overlaid, with time normalised according to

$$t_s = 11 \cdot \frac{t - t_{onset}}{t_{end} - t_{onset}}, \tag{3}$$

to better illustrate the overall shape of the sunspot cycle. Individual cycles are marked with dashed lines, with blue representing even-numbered cycles and red representing odd-numbered cycles. In addition, the colours are tinted in such a way that the lines with the lightest colour show the oldest cycles, and vice versa. The average of all solar cycles is shown in black; it has a minimum S_N of 11 and a maximum of 158 at 3.94 years after the onset. The average curves for even and odd cycles are shown with the solid blue and red lines, respectively. The averages are different, but as the range of variability of individual cycles is so large, it should not be taken as evidence of difference between even and odd cycles. The average durations of even and odd cycles are 11.09 and 10.95, respectively.

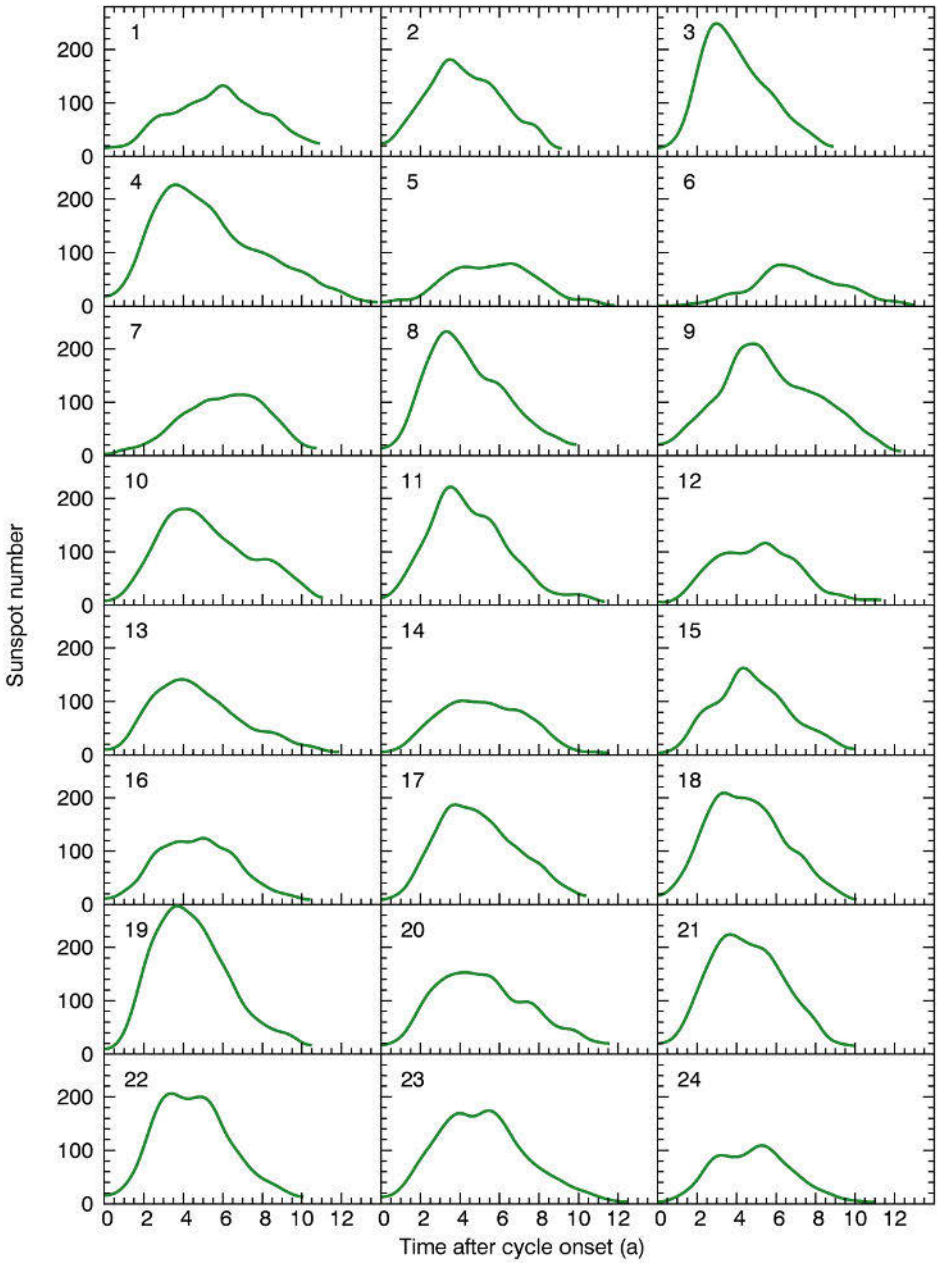

Figure 2. 13-month Gaussian smoothed monthly sunspot number as a function of time after the cycle minimum for solar cycles 1–24.

Solar activity also exhibits systematic variability on longer, multi-cycle timescales. The knowledge of historical solar activity can be extended beyond the sunspot record using indirect proxies such as tree ring records of radiocarbon ^{14}C (dendrochronology) or concentration of ^{10}Be in ice cores (Usoskin, 2017, and references therein). One of the defining aspects of long-term variability is the appearance of grand minima and maxima. A well-known example is the Maunder minimum, occurring in the latter half of the 17th century (Spörer, 1889; Maunder, 1890; Eddy, 1976), when sunspots were almost completely absent. Based on radiocarbon records and the increase of the long-term average of the sunspot numbers since the Maunder minimum, the 20th century has been often quoted as the so-called Modern maximum (e.g., Eddy, 1977; Usoskin et al., 2007); however, the increasing trend is considerably smaller in the recalibrated sunspot numbers (Clette et al., 2014). In addition to the 11-year Schwabe and 22-year Hale cycles, several periodicities have been suggested in the sunspot and proxy records, such as the Gleissberg cycle, with period around 80 years (Gleissberg, 1939), the ~210 years Suess (or de Vries) cycle (Suess, 1980), the Millenial (or Eddy) cycle (e.g., Sonett and Finney, 1990), and the 2400-year Hallstatt cycle (e.g., Damon and Linick, 1986). However, many studies indicate that the solar activity is not determined by a deterministic, multi-periodic process, but rather by stochastic or chaotic processes (e.g., Feynman and Gabriel, 1990; Usoskin et al., 2007; Käpylä et al., 2016).

3.1.4 Solar cycle prediction

Accurate knowledge about the level of solar activity would be extremely valuable for planning long-term space missions (Petrovay, 2020). Predictions of sunspot cycles were made already before the space age (e.g., Kimura, 1913; Waldmeier, 1936; Stewart and Eggleston, 1939; McNish and Lincoln, 1949). The early predictions were based purely on statistical properties of sunspot number cycles themselves, but during the 1960s and 1970s, prediction techniques based on precursors, such as geomagnetic conditions (Ohl, 1966; Ohl and Ohl, 1979), and polar magnetic conditions (Schatten et al., 1978; Schatten and Hedin, 1984), were developed. Precursor methods were found to outperform the statistical prediction methods (e.g., Sargent, 1978; Withbroe, 1989), and have been used extensively ever since (e.g., Thompson, 1993; Joselyn et al., 1997; Wang and Sheeley, 2009; Muñoz-Jaramillo et al., 2013).

Prediction methods based on the physics-based models of solar dynamo form another major category of solar cycle predictions. The first such studies were made by Dikpati et al. (2006) and Choudhuri et al. (2007), with predictions for maximum of cycle 24 differing by almost a factor of two; in retrospect, the result of Dikpati et al. proved to be far too high, whereas the result of Choudhuri et al. proved to be only slightly low. Further development in the modelling techniques have been achieved by, e.g., Yeates and Muñoz-Jaramillo (2013); Cameron and Schüssler (2017); Labonville

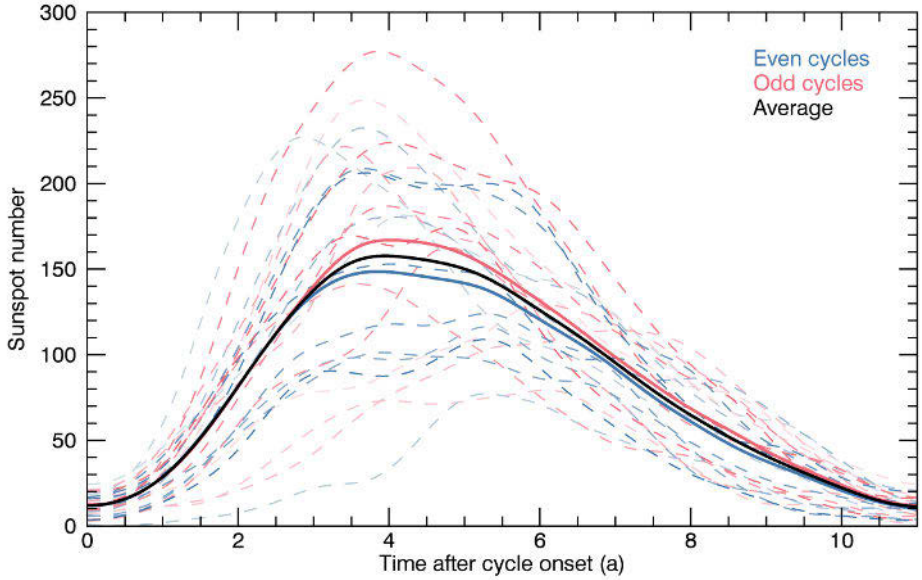

Figure 3. 13-month Gaussian smoothed monthly sunspot number as a function of time after the cycle minimum. Each cycle is normalised to have a duration of 11 years (see text for details). Individual cycles are shown with dashed lines; even-numbered cycles in blue, and odd-numbered in red. The tint of the colours change as a function of cycle number, with lightest red line showing cycle 1 and darkest blue line showing cycle 24. The averages of even-numbered, odd-numbered and all cycles are shown in solid blue, red and black, respectively.

et al. (2019), but the accuracy of their predictive cababilities cannot be established before the maximum of cycle 25 has been passed. The predictive power of dynamo models has, however, been criticised by, e.g., Bushby and Tobias (2007), who claim that due to the chaotic nature of the solar dynamo, it is impossible to get meaningful predictions even of the following solar cycle. In any case, whichever method is used, making predictions of a cycle before the previous cycle is near its end, is extremely difficult.

Since we have most probably passed the end of solar cycle 24, it is interesting to look at predictions of cycle 24 in retrospect. Pesnell (2008, 2012) made a comprehensive summary study of predictions for cycle 24, dividing them into categories according to the prediction technique. The average value of all 75 predictions for the maximum of smoothed sunspot number listed in his study is 113 ± 32, while the true value was 109, as taken from the Gaussian filtered series, or 116, as taken from the 13-month-smoothed series[9]. Perhaps surprisingly, the prediction technique category whose average value was closest to the Gaussian filtered true value was

9 Data downloaded on 2020–11–16 from `http://sidc.be/silso/datafiles/`

"climatology", i.e., the statistical techniques. The range of predictions in this category, however, was the largest in the study (40–185). Of the individual predictions that were very close to the Gaussian filtered true value, three were statistical, two were classified as spectral, which also would fall in the statistical category in the sense that they do not use precursors or physical modelling, one was based on neural networks and one on precursors. The maximum sunspot value was reached in March 2014, 2–4 years later than majority of the timing predictions; only three individual predictions were able to arrive within ~1 year of the true time. The wide range of different predicted amplitudes and the inaccurate predictions of time of maximum show that despite the sunspot time series covering centuries, direct observations of physical properties of the Sun covering several full solar cycles, and modern computing resources capable of data processing and detailed modelling, we are still unable to accurately predict the overall activity of the sun.

3.2 Flare, CME and SEP activity

Solar flares and CMEs, which together can be referred to as solar eruptions, are the main drivers of solar energetic particle events (e.g., Reames, 2013; Klein and Dalla, 2017). These eruptions originate from complex centers of magnetic activity known as active regions (AR; van Driel-Gesztelyi and Green, 2015; Toriumi and Wang, 2019), where the highest concentration of magnetic fields are seen as sunspots. Therefore, the occurrence rates of solar eruptions and SEP events follow the overall level of the sunspot cycle (e.g., Webb and Howard, 1994; Bazilevskaya et al., 2014; Hathaway, 2015), but major events may still occur near or during the solar minimum (e.g., Garcia and Dryer, 1987; Shea and Smart, 1990; Hudson, 2007).

The occurrence of flares, CMEs and solar energetic particle events during the last four solar cycles is shown in the top three panels of Figure 4, respectively. As an indicator of the overall solar activity level, the bottom panel shows the monthly sunspot number S_N for the same time period. In the top panel the blue histogram shows the monthly number of ≥C-class[10] X-ray flares observed in the 0.1–0.8 nm band by the GOES sensors[11] (Garcia, 1994), and the red histogram shows the monthly number of ≥M-class flares. The darker blue and red lines show the Gaussian smoothing with FWHM of 13 months. Flare activity shows large variation during the course of the solar cycles, with the difference in the number of flares during successive months as

10 X-ray flares are traditionally assigned a class according to the order of magnitude of their peak flux as measured in $\mathrm{W\,m^{-2}}$, as follows: A ($\leq 10^{-7}$), B (10^{-7}), C (10^{-6}), M (10^{-5}), and X ($\geq 10^{-4}$). For a more precise notation, significance can be given with the class; for example, an M5.2 flare corresponds to a flare with peak flux of $5.2 \cdot 10^{-5}\,\mathrm{W\,m^{-2}}$.

11 Data downloaded on 2020–11–16 from `https://www.ngdc.noaa.gov/stp/space-weather/solar-data/solar-features/solar-flares/x-rays/goes/xrs/`

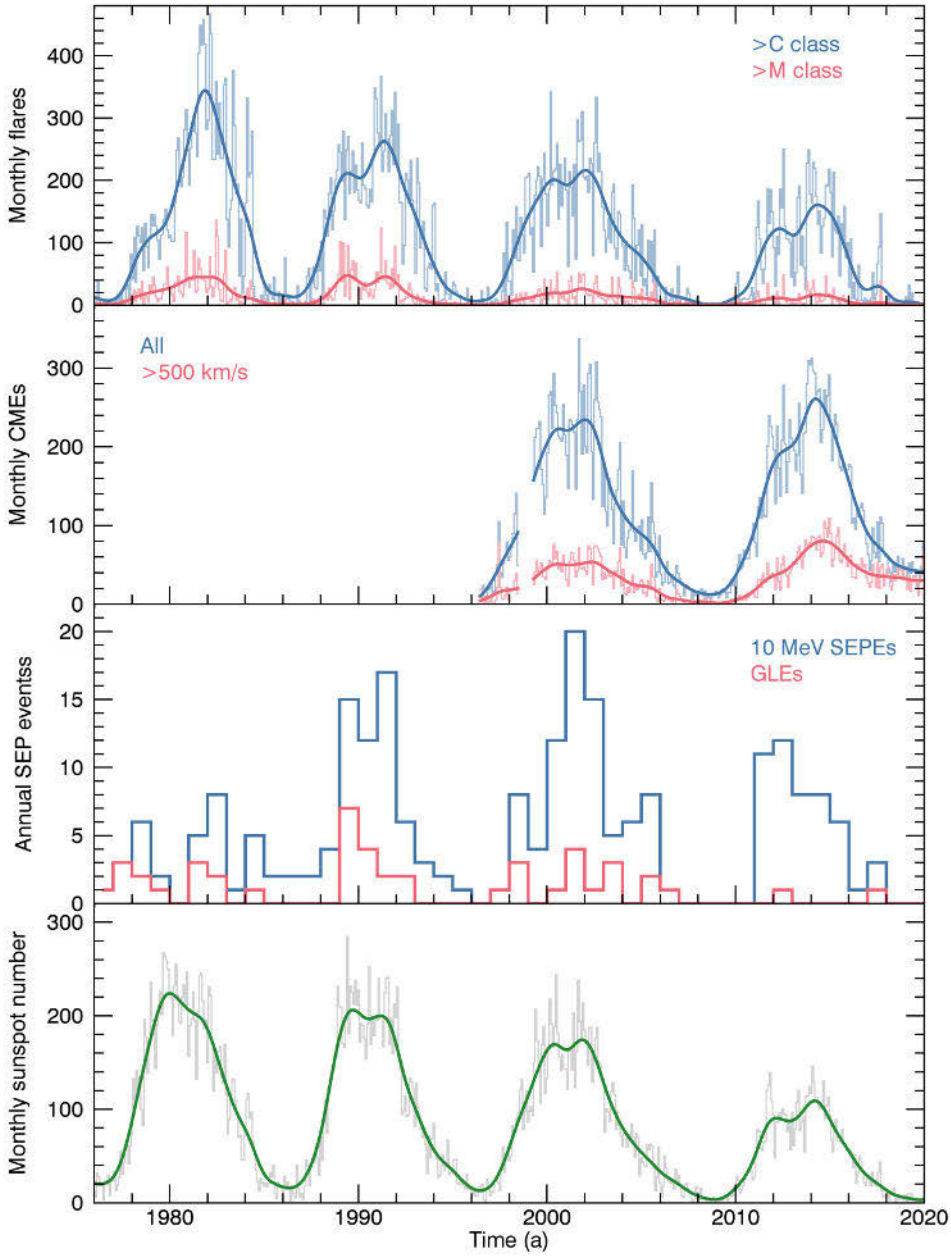

Figure 4. From top to bottom: monthly number of ≥C-class flares (blue) and ≥M-class flares (red), monthly number of all CMEs (blue) and fast CMEs (red), annual number of SEP events (blue) and GLEs (red), and the monthly sunspot number, for years 1976–2019. For flares, CMEs and sunspot number, the darker coloured lines show the 13-month Gaussian smoothing. See text for data sources and other details.

large as 207. The double-peaked structure of the cycles is visible in the smoothed dataset, even more clearly than in the S_N series. However, in case of the flares, the second peak is higher in all four cycles, whereas for the S_N the second peak is higher only in the last two cycles. Similarly to the S_N series, an overall pattern of declining cycle amplitudes is seen. However, the total number of flares per cycle does not decrease, since cycle 23 had a slightly larger number of flares than cycle 22.

The second panel in Figure 4 shows the monthly number of CMEs in the Automatic Recognition of Transient Events and Marseille Inventory from Synoptic maps (ARTEMIS) catalogue[12] (Boursier et al., 2009; Floyd et al., 2013), based on observations by the Large Angle and Spectrometric Coronagraph experiment (LASCO) (Brueckner et al., 1995) onboard the SOHO. The blue histogram and smoothed line show all CMEs with a velocity estimate in the ARTEMIS catalogue (herafter simply referred to as all CMEs), and red histogram and smoothed line show the CMEs with a velocity estimate greater than $500\,\mathrm{km\,s^{-1}}$. Note the gap in observations in the latter half of 1998 due to loss of contact with SOHO. Similarly to flares, the CME occurrence shows large month-to-month variation, especially near the cycle maxima. The two-peak structure is also visible in the CMEs, again with the later peak being higher in both cycles. Perhaps the most interesting feature of the CME occurrence is that unlike flares, large solar particle events, sunspot numbers and other measures of solar activity (see also Figure 1), cycle 24 does not show significantly lower numbers compared to the previous cycles. The smoothed monthly CME occurrence even peaks slightly higher during cycle 24. This apparent overabundance of CMEs, as well as other peculiarities of cycle 24, will be examined in more detail in Section 4.1.

The annual number of solar energetic particle events during 1976–2019 is shown in the third panel in Figure 4. The SEP events, shown in blue, have been defined using the proton channel 2 (7.23–10.46 MeV) of the SEPEM RDS version 3.0 [13]. The event criterion was the same as in Jiggens et al. (2012, 2018a), i.e., the channel flux had to exceed $0.01\,\mathrm{cm^{-2}\,sr^{-1}\,s^{-1}\,MeV^{-1}}$ continuously for at least 24 hours, the maximum flux during the event had to exceed $0.5\,\mathrm{cm^{-2}\,sr^{-1}\,s^{-1}\,MeV^{-1}}$, and events starting within 24 hours after the end of the preceding event were combined. In addition, the annual number of GLE events is shown in red. The SEP event rate is highly variable, but follows the overall shape of the solar cycle. Noteworthy features of SEP occurrence are the low number of events during cycle 21 compared to the number of flares, presence of events during the cycle 21–22 minima (around 1985–1986), and the pronounced additional "peak" during the descending phase of cycle 23 in 2004–2005. However, it should be noted that the event definition cannot

12 Data downloaded on 2020–11–16 from `http://idoc-lasco.ias.u-psud.fr/sitools/client-user/index.html?project=ARTEMIS_Catalog`

13 Data received on 2020–12–01 from D. Heynderickx.

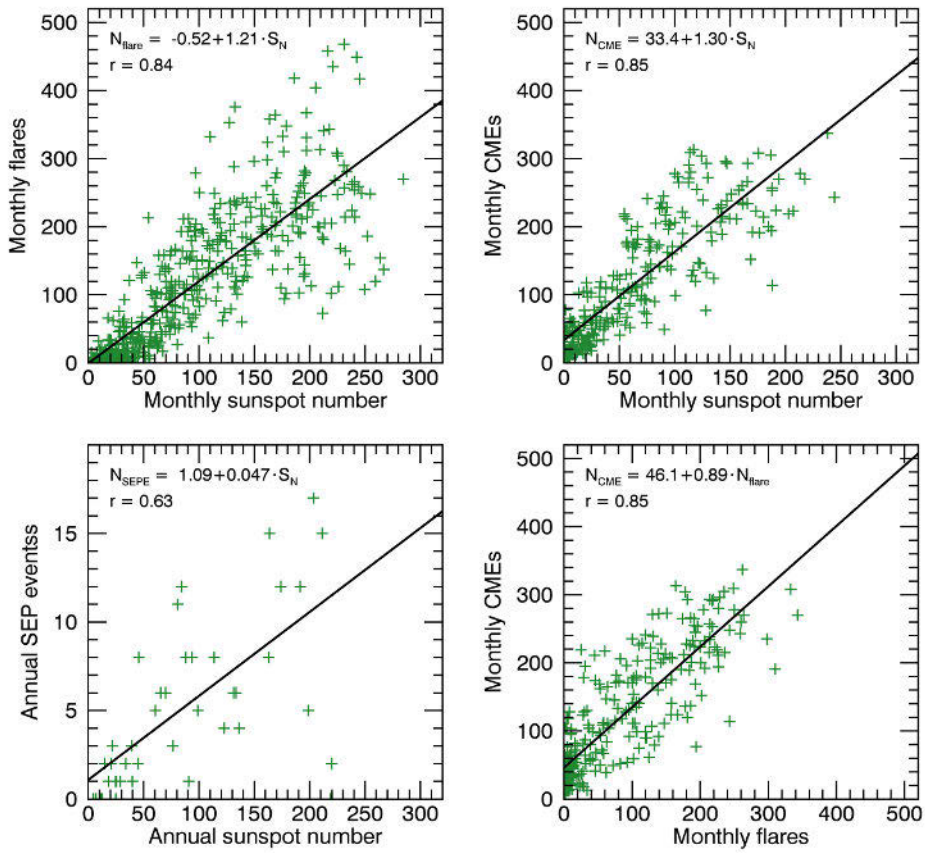

Figure 5. Correlations of the occurrence of flares, CMEs, SEP events and the sunspot number. Top left: monthly number of flares vs. monthly sunspot number; top right: monthly number of CMEs vs. monthly sunspot number; bottom left: annual number of SEP events vs. annual sunspot number; bottom right: monthly number of CMEs vs. monthly number of flares. The regression lines and equations, as well as the Pearson correlation coefficients are given in each panel.

separate consecutive events if the flux does not drop below the threshold between them; therefore, the number of events may be too low for time periods when there have been active regions capable of producing multiple eruptions.

Figure 5 shows the correlation of the occurrence of flares (top left), CMEs (top right) and SEP events (bottom left) with the sunspot number, and the correlation of the occurrence of CMEs with the occurrence of flares (bottom right). Linear regression lines, their equations, and Pearson correlation coefficients are given in each panel. In each panel, the correlations are significant ($p < 0.05$), which is not surprising given the physical connections between the phenomena. However, even with significant correlations, there is very large scatter around the linear relationships,

especially for flares and SEP events vs. the sunspot number. Therefore, it is not possible to accurately predict one quantity using only it's linear relationship to another quantity.

4 Comparison of solar cycles 23 and 24

The recent apparent change in the level of solar activity has been a subject of intensive research since the end of solar cycle 23. Numerous studies have contrasted the extremely deep activity minimum and the reduced activity of cycle 24 with the previous cycle(s) (e.g., McComas et al., 2008, 2013; Clette and Lefèvre, 2012; Richardson and Cane, 2012; Mewaldt et al., 2015; Paassilta et al., 2017; Article I; Article II). In Section 4.1 we present an overview of flare, CME and SEP observations, revisiting and confirming some of the main results of Articles I and II with updated data covering the full cycle 24. Then, in Section 4.2, we use the methods presented in Articles III and IV to develop statistical SEP models individually for the two cycles, and compare the cycles using their results.

4.1 Observations

As seen in the previous Chapter, the level of solar activity varies significantly from cycle to cycle. In general, the recent few solar cycles have shown a trend of decreasing activity, culminating in the quiet solar cycle 24 after a peculiarly deep and extended activity minimum of 2008–2009. During the minimum, sunspot numbers fell to the lowest level in about 100 years: the 13-month Gaussian smoothed S_N was 3.4 in December 2008, and the previous time when the smoothed S_N dropped below 5 was during the cycle 14–15 minimum in May 1913. The number of spotless days was also the highest since that same period (Clette and Lefèvre, 2012). Polar magnetic fields were weaker by 40 % in the 23–24 minimum than in the three previous minima (Wang et al., 2009), and a consistent weakening was seen in the interplanetary magnetic field (Smith and Balogh, 2008; Lee et al., 2009). The fast solar wind was less dense and had lower temperature and less mass flux and momentum flux than during the previous minimum (McComas et al., 2008). Geomagnetic storm activity was at the lowest level since at least 1932 (Richardson and Cane, 2012). In addition, galactic cosmic rays were at highest levels measured during the space age (Mewaldt et al., 2010; Oh et al., 2013).

Following the extremely quiet minimum, solar cycle 24 also turned out to be very quiet in most aspects. As can be seen from Figure 1, sunspot numbers and 10.7 cm radio flux have stayed at low levels throughout cycle 24, and cosmic ray count rates have stayed high troughout the cycle. Solar wind properties, such as temperature,

thermal pressure and mass, momentum and energy fluxes, as well as the magnitude of the IMF were also still significantly lower during the active phase than in previous cycles (McComas et al., 2013; Zerbo and Richardson, 2015). Geomagnetic activity was extremely quiet during the ascending and early descending parts of cycle 24 (Richardson, 2013; Rawat et al., 2018); however, the number of CMEs, which are the main origin of large geomagnetic disturbances (e.g., Gonzalez et al., 1999; Richardson et al., 2001), has not been lower during solar cycle 24 (Gopalswamy et al., 2014; Compagnino et al., 2017; Lamy et al., 2019). The number of SEP events has been lower in cycle 24 as compared to previous cycles, and the difference is even larger in higher energies (Mewaldt et al., 2015; Richardson et al., 2017; Paassilta et al., 2017). In this section we take a look into some of these observed changes between the cycles, especially in their relation to solar energetic particles and space weather.

4.1.1 Flares and CMEs

The top panel in Figure 6 presents a comparison of the number of ≥C-class flares and the sunspot number during cycles 23 and 24. The figure is based on the same GOES X-ray dataset as Figures 4 and 5. Here, blue and red histograms show the monthly number of flares, and the grey filled area shows the monthly average sunspot number. The cumulative values of the number of flares in cycles 23 and 24 and the monthly sunspot number have been divided by 1000, and are shown with the blue, red and grey curves, respectively. Onset times of the cycles are defined as the middle of the month of minimum in Gaussian smoothed S_N and are given in Table 1 for cycles 21–25. Flares have similar behaviour to the sunspot number: the cycle 24 to 23 ratio is 0.59 for the total number of flares and 0.53 for the total number of S_N. The total numbers of flares in cycles 21 and 22 are indicated in the figure with grey markers and are 12 % above and 0.5 % below the cycle 23 totals, respectively.

The bottom panels in Figure 6 show the correlations of the monthly number of ≥C-class flares (left) and ≥M-class flares (right) vs. the monthly average sunspot number. Again, solar cycle 23 is shown in blue and cycle 24 in red, and the correlation coefficients and linear regression lines along with their equations are shown in the figure. For both ≥C-class and ≥M-class flares, the linear relationship with S_N is steeper for cycle 24, and the difference in slopes is significant for ≥C-class flares but not significant for ≥M-class flares. In addition, the linear fits to cycle 21 and 22 data are shown with grey dashed and continuous lines. For ≥C-class flares their slopes are slightly less steep than that of cycle 23, but for ≥M-class flares they are significantly steeper than that of cycle 24. Correlations are statistically significant for both ≥C-class and ≥M-class flares, and in case of ≥C-class flares, slightly higher for both cycles 23 and 24 separately than for cycles 21–24 combined (Figure 5).

Curiously, CME occurrence has been nearly at the same level during cycles 23

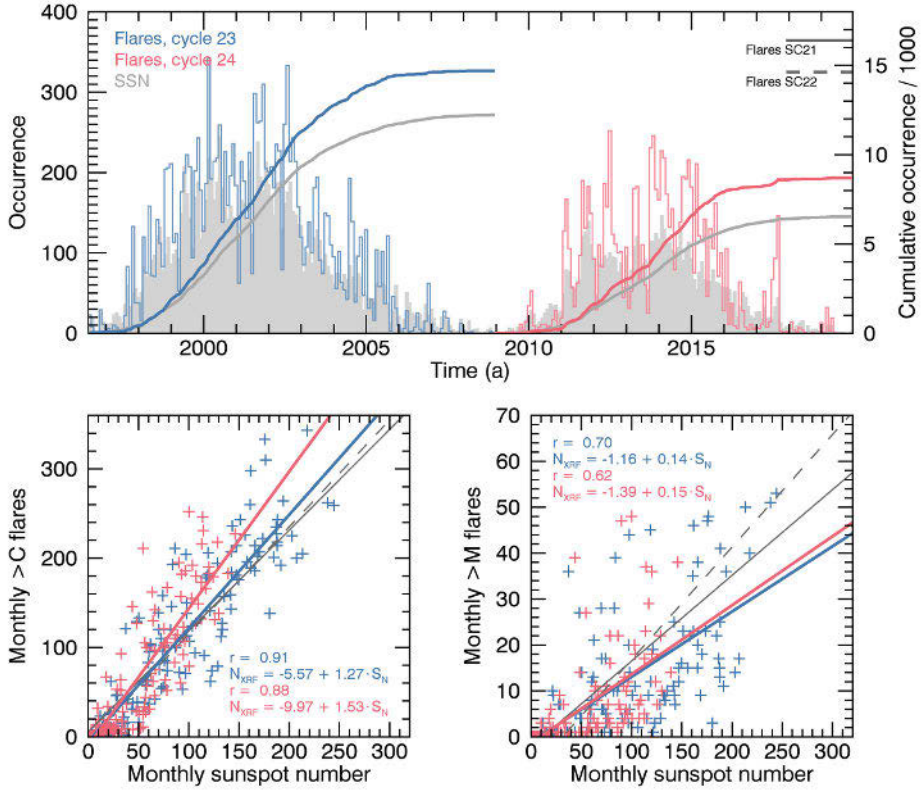

Figure 6. Top panel: monthly number ≥C-class flares during solar cycles 23 and 24 (blue and red histograms, respectively) and the cumulative number of ≥C-class flares during solar cycles 23 and 24 (blue and red curves, respectively). The monthly average sunspot number and its cumulative value are shown in grey for comparison. All cumulative values have been divided with 1000. Bottom panels: correlation of the monthly number ≥C-class (left) and ≥M-class (right) with the monthly average sunspot number. Blue and red lines show the linear fits to cycles 23 and 24, respectively. Linear fits to cycles 21 and 22 are shown with solid and dashed grey lines, respectively.

and 24, as seen in Figure 7. The formatting of the figure is similar to the previous figure. In the top panel, the number of CMEs during the data gap caused by the loss of communications with SOHO has been estimated using the linear relationship between monthly CMEs and montly sunspot number given in Figure 5. Similar apparent overabundance of CMEs during cycle 24, as compared to other solar activity, has been reported by, e.g., Petrie (2013); Gopalswamy et al. (2015a); Lamy et al. (2019), although there has been discussion on whether or not some of it could be explained by inhomogenities in the detection method or observational cadence (Wang and Colaninno, 2014; Hess and Colaninno, 2017; Michalek et al., 2019). However, CME data in Figures 5 and 7 are based on the ARTEMIS catalogue, which does not suffer from these effects because it is based on synoptic maps constructed from resampled

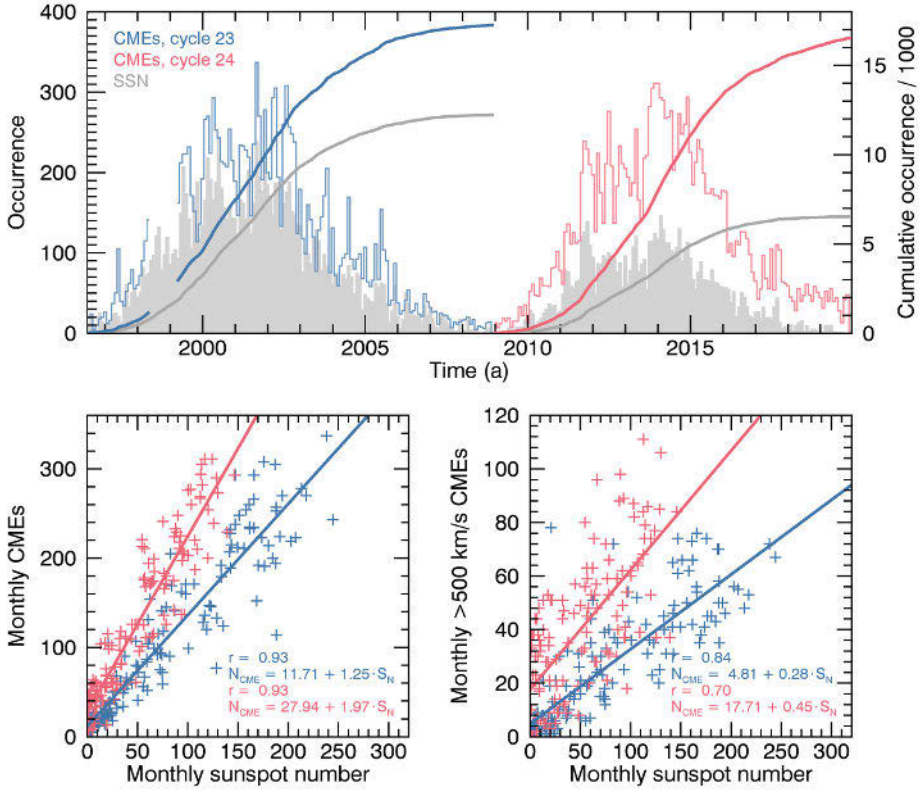

Figure 7. Top panel: monthly number of CMEs during solar cycles 23 and 24 (blue and red histograms, respectively) and the cumulative number of CMEs during solar cycles 23 and 24 (blue and red curves, respectively). The monthly average sunspot number and its cumulative value are shown in grey for comparison. All cumulative values have been divided with 1000. Bottom panels: correlation of the monthly number of all CMEs (left) and $>500\,\mathrm{km\,s^{-1}}$ CMEs (right) with the monthly average sunspot number. Blue and red lines show the linear fits to cycles 23 and 24, respectively.

uniform time series (Floyd et al., 2013). Lamy et al. (2019) reported a cycle 24 to 23 ratio of 0.94 for CMEs in cycle 24, including all CMEs before 28 September 2018, whereas in Figure 7 the ratio is 0.97, including all CMEs with a mass estimate until the end of 2019. However, they noted that the CME mass rate is in better agreement with S_N and other activity indices during both cycles than the occurrence rate.

The relationship of CMEs and S_N is much more different between cycles 23 and 24 than that of flares and S_N, as can be seen in the bottom panels in Figure 7. The difference in slopes is significant for all CMEs and $>500\,\mathrm{km\,s^{-1}}$ CMEs, and the higher offset of cycle 24 makes the populations even more distinct. Again, the correlations are slightly higher for the cycles separately than combined. Anomalous behaviour of CMEs during cycle 24 has been discussed by Gopalswamy et al. (2014,

Table 1. Onset time, sunspot number at onset, time of cycle maximum and sunspot number at maximum for cycles 21–25, based on the 13-month Gaussian smoothed monthly average sunspot numbers.

Cycle	Onset time	S_N at onset	Time of maximum	Maximum S_N
21	1976–05	20.0	1980–01	223.9
22	1986–05	15.9	1989–10	206.2
23	1996–06	13.1	2001–11	174.3
24	2008–12	3.4	2014–03	108.9
25	2019–12	3.3		

2015a,b) and Dagnew et al. (2020), who reported that CMEs have been significantly wider, resulting in increased fraction of halo CMEs as compared to cycle 23. They account their findings to reduced total pressure near the Sun, which allows for easier expansion of the CMEs. The increased expansion causes the magnetic fields of the CMEs to dilute, which would explain the reduced geoeffectiveness (Gopalswamy et al., 2014).

4.1.2 Solar energetic particles

Figure 8 compares the number of SEP events and the sunspot number during cycles 23 and 24. The dark blue and red histograms in the top panel show the annual number of the 7.23–10.46 MeV SEP events for cycles 23 and 24, based on the SEPEM RDS3, similarly to the third panel in Figure 4. In addition, the light blue and yellow histograms show the annual number of 55–80 MeV SEP events measured by the Energetic and Relativistic Nuclei and Electron experiment (ERNE) instrument (Torsti et al., 1995) onboard the SOHO satellite. The event list is described in full detail in (Vainio et al., 2013; Paassilta et al., 2017)[14], and has since been extended until the end of 2019. Although the energy at which the events have been defined is higher than for the SEPEM RDS3 events, the SOHO/ERNE list contains more events, for two main reasons: ERNE's High Energy Detector (HED) is considerably larger than the GOES/Energetic Particle Sensor (EPS) on which the SEPEM RDS3 data is based, allowing the detection of smaller events, and rather than using a threshold criterion, the events are defined with a Poisson-CUSUM method that detects event onsets from a variable background level (Huttunen-Heikinmaa et al., 2005). Both datasets show that cycle 24 produced a smaller number of SEP events than cycle 23: the ratio of cycle 24 to 23 was 0.61 for 7.23–10.46 MeV (80 events during cycle 23

14 The event list has been released as part of the UTU/SRL tool package at the Space Radiation Expert Service Centre (R-ESC) under ESA's Space Weather Service Network. The full event catalogue can be found online at `https://swe.ssa.esa.int/utu-srl-federated`.

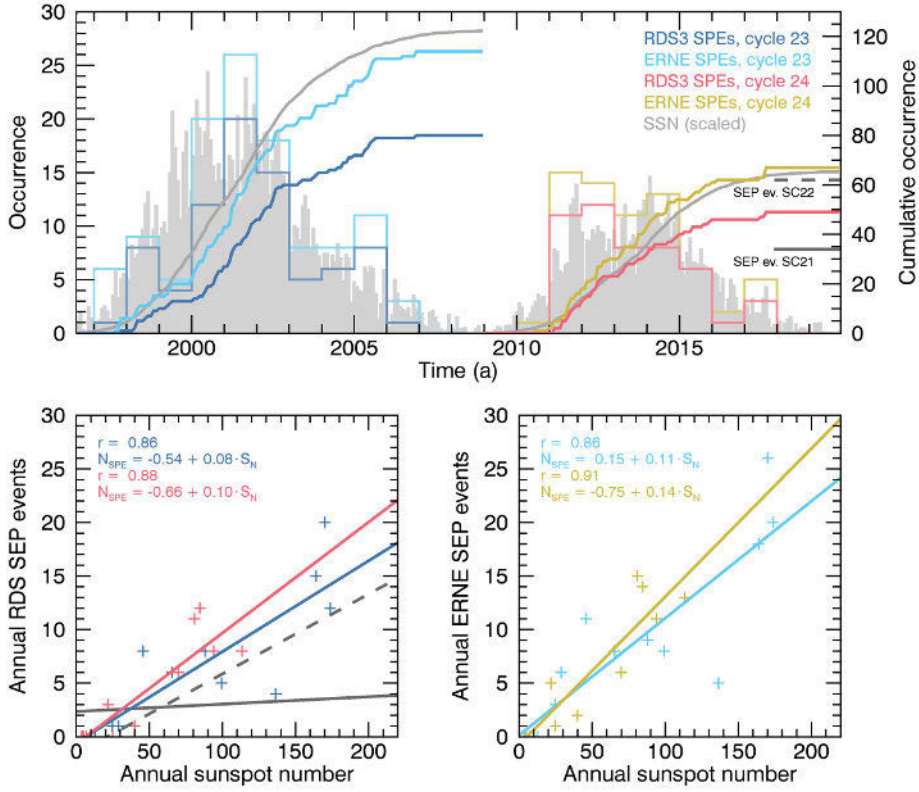

Figure 8. Top panel: Annual number of SEP events during solar cycles 23 (dark blue and light blue histograms for RDS3 events and ERNE events, respectively) and 24 (red and yellow histograms for RDS3 and ERNE events, respectively) and the corresponding cumulative values. The monthly average sunspot number (divided by 10) and its cumulative value (divided by 100) are shown in grey for comparison. Bottom panels: correlation of annual SEP events in RDS3 (left) and ERNE (right) with the annual average sunspot number. The linear fits for cycles 23 and 24 are shown with lines with the same colours as in the top panel. In addition, the linear fits for cycles 21 and 22 are shown in the left panel with solid and dashed grey lines, respectively.

and 49 during cycle 24) and 0.59 for 55–80 MeV (114, and 67 events, respectively). However, as shown by the grey markers in Figure 8, the total number of RDS3 events in cycles 21 and 22 were both below cycle 23, and cycle 21 was even below cycle 24, so in regard to the low energy SEP event occurrence, cycle 24 was perhaps not especially unique during the space era. On the other hand, only two GLEs occurred during cycle 24, whereas there were 12, 15 and 16 GLEs in cycles 21, 22 and 23, respectively (e.g., Bazilevskaya et al., 2014; Miroshnichenko, 2018), so the activity at higher energies clearly seems to be suppressed.

The bottom panels in Figure 8 show the relationship of the annual number of 7.23–10.46 MeV SEP events (left) and 55–80 MeV SEP events (right) with the an-

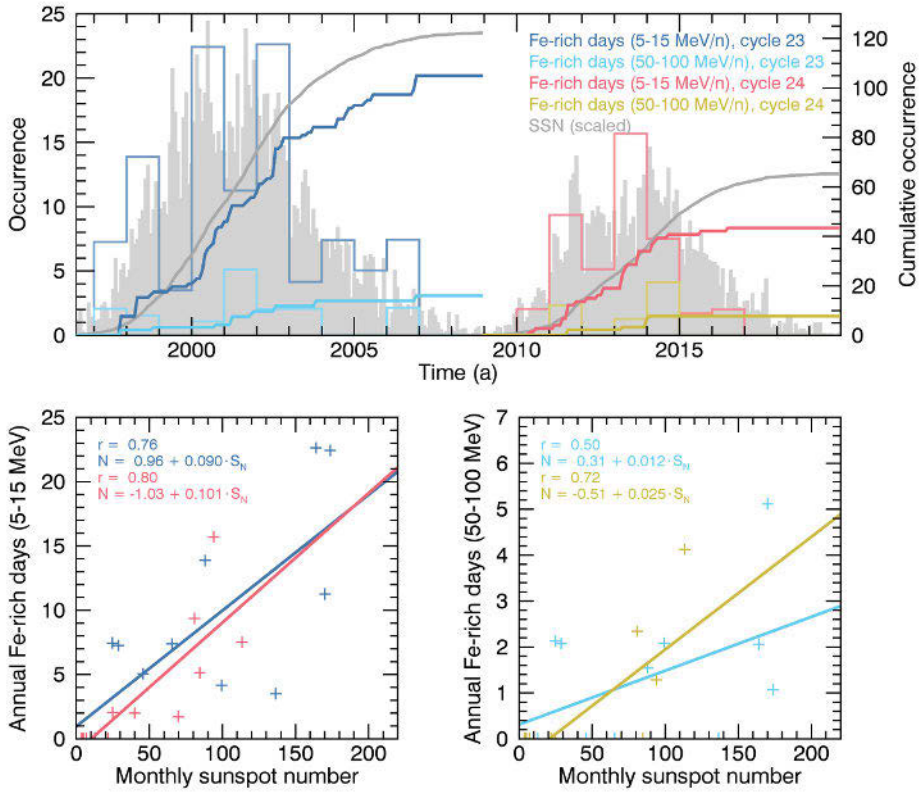

Figure 9. Top panel: annual number of Fe-rich days during solar cycles 23 (dark blue and light blue histograms for 5–15 MeV n^{-1} and 50–100 MeV n^{-1}, respectively) and 24 (red and yellow histograms for 5–15 MeV n^{-1} and 50–100 MeV n^{-1}, respectively), and the corresponding cumulative values. The monthly average sunspot number (divided by 10) and its cumulative value (divided by 100) are shown in grey for comparison. Bottom panels: correlation of annual Fe-rich days in 5–15 MeV n^{-1} (left) and 50–100 MeV n^{-1} (right) with the annual average sunspot number. The linear fits for cycles 23 and 24 are shown with lines with the same colours as in the top panel.

nual average sunspot number. Cycles 23 and 24 are shown in the left panel in dark blue and red, respectively, and in the right panel in light blue and yellow, respectively. Correlation coefficients and linear fits along with their equations are also shown. For the 7.23–10.46 MeV events, the linear fits for cycles 21 and 22 are also shown with the solid and dashed lines, respectively. For both energies, the correlations are statistically significant. Again, the slope for cycle 24 is steeper for both energies, although the differences are not statistically significant. A noteworthy feature is the almost flat slope for cycle 21, showing nearly no dependence between event rate and sunspot number.

Figure 9 shows the annual number of Fe-rich days observed by SOHO/ERNE with the Low Energy Detector (LED) instrument at 5–15 MeV n^{-1} during cycles 23

and 24 (dark blue and red histograms, respectively), extending the data shown in Figure 4 of Article I until the end of 2019. All values are multiplied with a correction factor to account for the time ERNE detectors have been offline. Here Fe-rich means that the daily Fe/(C+O)-ratio is higher than 0.183, i.e., at least twice the value in gradual solar energetic particle events reported by Reames (1995). A minimum of 2 daily counts of each ion species C, O and Fe is required; this ensures that the relative statistical error of the ratio is not too large, as well as serves as a threshold for excluding days where no SEP activity is detected above the GCR background. In addition, the annual number of Fe-rich days observed at 50–100 MeV n^{-1} is shown with light blue and yellow histograms for cycles 23 and 24, respectively. The threshold for the Fe/(C+O)-ratio is the same as for 5–15 MeV n^{-1}, but since the higher energies are observed with ERNE's considerably larger HED, the requirement for daily counts for each ion species is increased to 8, which again provides a reasonable background threshold.

As the peak of cycle 24 was already covered in the dataset of Article I, only two additional Fe-rich days were found. In total, 96 Fe-rich days were observed in cycle 23 and 32 in cycle 24 in the 5–15 MeV n^{-1} energy range, resulting in cycle 24 to 23 ratio of 0.41 when the correction for the measurement time is taken into account. In the 50–100 MeV n^{-1} energy range the total number of observed Fe-rich days during the two cycles were 15 and 7, resulting in 24/23 ratio of 0.48. Although the ratio is slightly higher at higher energy, the statistical uncertainties are too high to draw any conclusions about energy differences between cycles. These ratios are smaller, but still comparable to the 24/23 ratio of sunspots, 0.53, meaning that the heavy ion acceleration efficiency has decreased about similarly to the overall activity level. Like in the previous figures, the bottom panels in Figure 9 show the relationship of the annual number of Fe-rich days with the annual average sunspot number. In the 5–15 MeV n^{-1} range (left panel) there is no discernible difference between the solar cycles. In the 50–100 MeV n^{-1} range the slopes for the two cycles are different, but again, the number of events is too low to make any definite conclusions.

The two Fe-rich days that occurred after the end of the period studied in Article I were related to rather small SEP events. The first one, occurring on 2015–09–20, was observed by ERNE with proton energies above 55 MeV and associated with a M2.1 flare at S20W24 and a 1239 km s^{-1} halo CME (Paassilta et al., 2017). The second one occurred on 2016–07–20 and was only observed at the low energy proton channels of ERNE but not above 55 MeV, and thus was not included in Paassilta et al. (2017). The most probable solar event associations are a C4.6 flare at N05W41 and a 426 km s^{-1} CME of 52° width. Their event-integrated 5–15 MeV n^{-1} Fe/C-ratios are 0.29 ± 0.16 and 1.68 ± 0.72, respectively. Figure 6 in Article I shows the Fe/C ratios of all events in the study as functions of flare longitude, flare peak flux, CME speed and CME width; the former of the new events would fit along well with the other cycle 24 events, but the latter one, with its rather high Fe/C, weak flare and

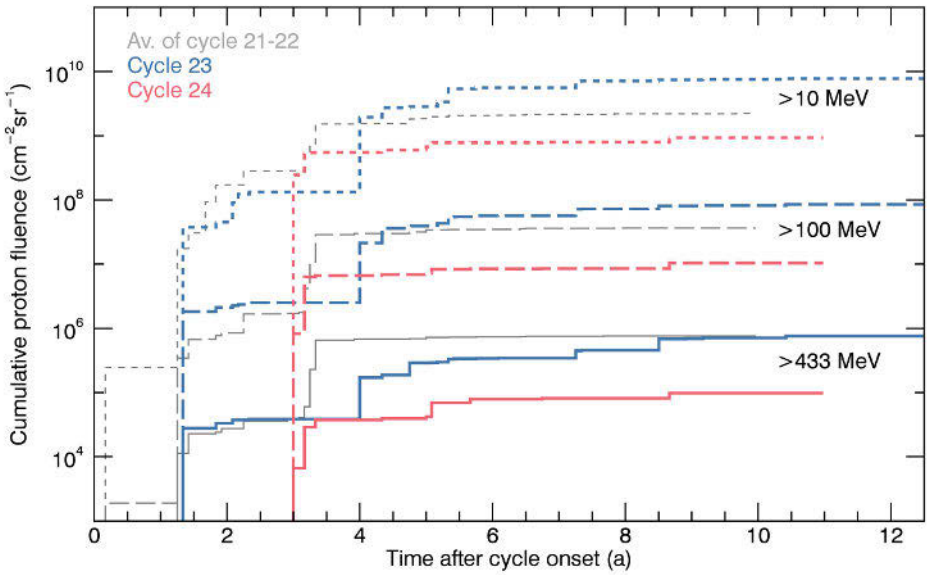

Figure 10. Cumulative integral solar energetic proton fluences as functions of time after cycle onset at three energies: >10 MeV (short-dashed lines), >100 MeV (long-dashed lines) and >433 MeV (solid lines). Blue lines show solar cycle 23, red lines show cycle 24, and grey lines show the average of cycles 21 and 22.

slow and narrow CME, would be an outlier among other cycle 24 events. One of the conclusions of Article I was that events with impulsive characteristics were almost completely absent from cycle 24, but the latter one of the new events would fall into that category. However, one impulsive-like event does not change the conclusion that there has been a significant lack of impulsive-like events during cycle 24. In total, the cycle 24 to 23 ratios in the number of SEP events with enhanced abundances of Fe are 0.35 at 5–15 MeV n^{-1} and 0.50 at 50–100 MeV n^{-1}. The general conclusion of Article I that the efficiency of particle accerelation processes was significantly weakened during cycle 24 can be thus confirmed with measurements covering the cycle completely.

Figure 10 shows the cumulative integral SEP fluences at >10 MeV (short-dashed lines), >100 MeV (long-dashed lines) and >433 MeV (solid lines) as functions of time after cycle onset. Solar cycle 23 is shown in blue, cycle 24 in red and the average of cycles 21 and 22 in grey. The fluences are calculated using a dataset of sub-GLE and GLE fluences observed with IMP-8 (McGuire et al., 1986) and GOES (Onsager et al., 1996) as well as ground-based neutron monitors (e.g., Shea and Smart, 2000; Mavromichalaki et al., 2011), and fitted with double power law Band functions (Band et al., 1993). The analysis method and fitting are explained in Tylka and Dietrich (2009) and Article III. Here sub-GLE means SEP events with particles

accelerated to energies of hundreds of MeVs, which are observed with space-borne instruments, but do not cause statistically significant signal in ground level neutron monitors[15]. The events and their spectral parameters are listed in Tables A.1 and A.2 of Article II and Tables 2 and 3 of Article III. To get the spectral parameters for GLE 72, occurring on September 10, 2017 (Mishev et al., 2018), we integrated the differential fluence spectrum given in Jiggens et al. (2019), and made a Band fit to the integrated spectrum.

Figure 3 of Article II shows a fluence comparison of cycle 23 and the first 8 years of cycle 24 at >1 GV rigitidy, which for protons equals 433 MeV. Figure 10 extends the comparison to cover the whole of both cycles and shows two additional energies. The only event added after the 8 years covered in Article II was GLE 72, which did not have a huge effect in the total cycle fluence. The cycle 24 to 23 ratios for integral fluences at the three energies >10 MeV, >100 MeV and >433 MeV are 0.12, 0.12 and 0.13, respectively. Mewaldt et al. (2015) showed a similar comparison (their Figure 2), based on integral GOES observations. For the first 5.8 years of the cycles, they reported cycle 24 to 23 ratios of 0.23 and 0.16 for >10 MeV and >100 MeV energies, respectively, whereas our corresponding ratios after 5.8 years were 0.14 and 0.15. In an updated study, Mewaldt et al. (2017) reported cycle 24 to 23 ratios of 0.17 and 0.11 at >10 MeV and >100 MeV, respectively, 8 years after the cycle onsets. Our corresponding ratios after 8 years were 0.11 and 0.12. Our results differ from those of Mewaldt et al. (2015, 2017) more at >10 MeV, which may result from event selection: some events may have high observed fluence at low energies but no discernible signal at higher energies, and thus would not be observed as a (sub-)GLE. The same reason may be why the cycle difference is not larger at higher energies in our study, although an energy dependence would be expected from, e.g., the much larger decrease in the number of GLEs compared to SEP events in lower energies (Cohen and Mewaldt, 2018; Miroshnichenko, 2018).

Figure 11 shows the 5 minute peak fluxes for SEP events occurring during solar cycles 22–24 for two energies: 7.23–10.46 MeV RDS3 channel with nominal energy 8.7 MeV in the top panel, and 500 MeV GOES/High Energy Proton and Alpha Detector (HEPAD) data in the bottom panel. The latter values have been calculated by means of bow-tie analysis (originally named such by Van Allen et al. (1974)) of the nominal HEPAD channels. In general, the bow-tie analysis means integrating the product of the channel response function and a realistic range of SEP spectral functions over energy; the result is a family of energy-dependent curves for $G\Delta E$ (geometric factor times the channel width) which form a bow-tie shape. The optimal values for $G\Delta E$ and the effective channel energy are found where the curves converge,

15 This follows Atwell et al. (2015, 2016), Article II and Article III, i.e., relaxes the requirement of statistically significant signals in two high elevation NMs, which is given in the sub-GLE definition of Poluianov et al. (2017).

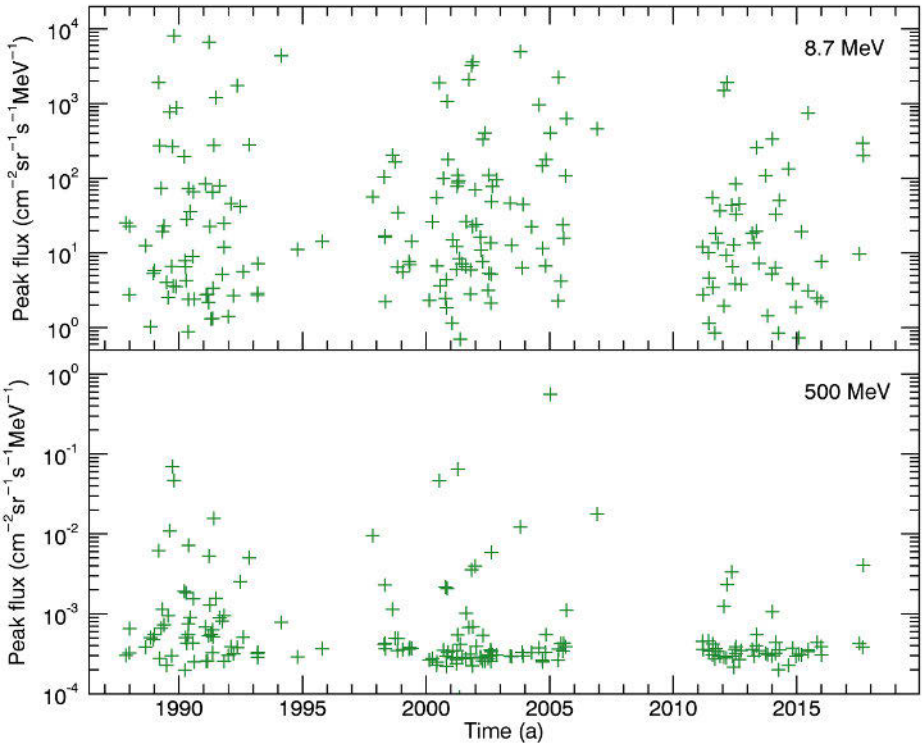

Figure 11. Peak fluxes for SEP events during solar cycles 22–24. Top panel shows the 7.23–10.46 MeV RDS3 channel and the bottom panel shows the bow-tie processed GOES/HEPAD P9 channel interpolated to 500 MeV. See text for details about the HEPAD processing and Section 3.2 for details about the event definition.

i.e., the knot of the bow-tie. Article IV gives full details about the processing of the HEPAD data. The events shown in Figure 11 are defined using the 7.23–10.46 MeV RDS3 channel as explained in Section 3.2. In the lower energy, the highest peak fluxes have a slight declining trend, but the difference between the cycles do not seem extreme. In the higher energy, on the other hand, the weakness of cycle 24 is apparent: in cycles 22 and 23 there are 8 and 7 events, respectively, with higher peak fluxes than the highest in cycle 24, and the highest peak fluxes in cycles 22 and 23 are over 17 and 137 times higher, respectively, than the highest peak flux of cycle 24.

4.2 Statistical SEP model

The differences between solar cycles 23 and 24 regarding solar energetic particles can also be examined via SEP environment modelling. For this purpose we develop an MSU-type statistical SEP model, following the methodology presented in Article

III. Two versions of the model are built, one based on data observed during cycle 23, and the other on data observed during cycle 24. Compared to many other SEP models, the statistics based on only one solar cycle are low, and therefore, results above confidence levels[16] $\geq 95\%$ should be considered as extrapolations. This way of comparing two solar cycles can also illustrate the downside of models which are based on several solar cycles of data: the results reflect averaged properties of cycles with different levels of activity. Using a model built on previous cycles with higher activity during a cycle with lower activity can result in overestimation of the particle radiation environment, and ultimately in costly overdesign of radiation protection for space missions.

4.2.1 Model details

Event definition and timing

The model[17] is built upon the same set of GLE and sub-GLE spectral fits as Figure 10. The total number of events in the dataset is 48; 36 occurred during solar cycle 23 and 12 during cycle 24. Onset times were taken, in order of preference, from Paassilta et al. (2017), Papaioannou et al. (2016), or estimated from GOES particle data. Following the approach of Article III, consecutive events produced by the same active region have been combined into episodes, which allows for treating them as statistically independent occurrences. The waiting time distributions of the episodes are shown in Figure 12 as complementary cumulative distributions, separately for solar cycles 23 and 24 (blue and red, respectively). Although the distributions are not perfectly linear in lin-log space, there is no clear indication of any other functional form. Therefore, because of simplicity and convenience, the distributions are fitted with exponential functions (linear in lin-log-space). Since the exponential distribution describes the waiting times of a Poisson process, and the complementary cumulative distribution function (CDF) of exponential distribution is the exponential function $e^{-\lambda \cdot t}$, the event occurrence can be assumed to be a memoryless Poisson process. The fit parameters, i.e., the rate of the Poisson processes, are given in the figure.

Each combined episode consists of one to four GLEs or sub-GLEs, with averages of $\mu_{n_{\mathrm{ev},23}} = 1.5$ and $\mu_{n_{\mathrm{ev},24}} = 1.2$ events per episode for cycles 23 and 24, respectively. Although the properties of the consecutive events produced by the same active region may be somehow correlated, the dataset is far too small to verify or model this in

16 A model result at confidence level P means the level of the estimated quantity that is exceeded with probability of $100 - P$.

17 A similar model based on GLEs and sub-GLEs observed since 1973, has been released as part of the UTU/SRL tool package at the R-ESC under ESA's Space Weather Service Network. The model can be found as an interactive tool at `https://swe.ssa.esa.int/utu-srl-federated`.

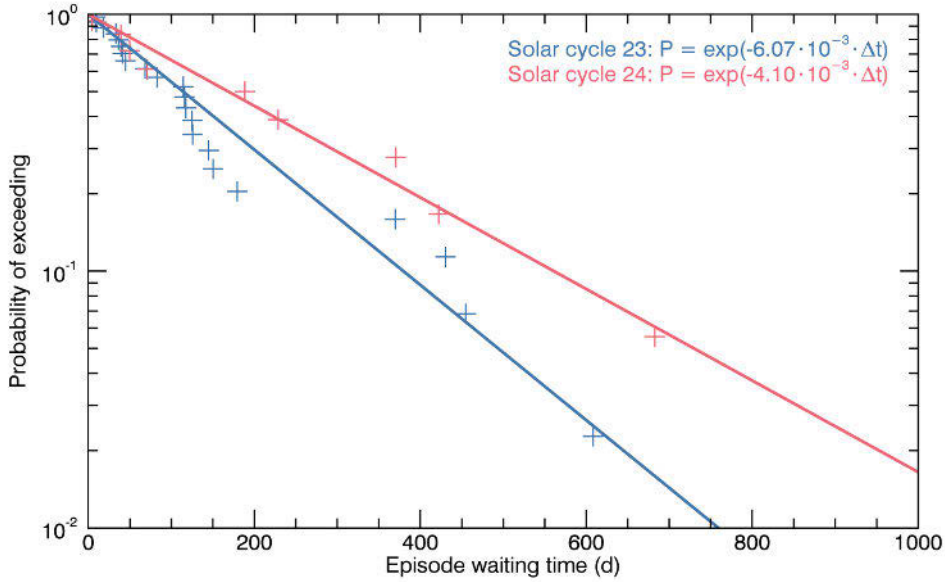

Figure 12. Waiting time distribution of episodes of GLEs and sub-GLEs occurring during solar cycles 23 (blue) and 24 (red), along with exponential function fits.

any meaningful way. Therefore, all events, whether they occur alone or as a part of a multi-event episode, are modelled similarly. Figure 13 shows the distribution of number of events per episode for both solar cycles. The number of events per episodes are modelled with geometric distributions, which are also shown in the figure along with their parameters, p_g. The probability distribution function (PDF) of geometric distribution is calculated from $(1-p_g)^{k-1}p_g$, where the parameter p_g is related to the mean (expected value) μ by $p_g = 1/\mu$.

Event fluence spectra

The fluence modelling is based on Band function fits to fluence spectra in rigidity. Band function (Band et al., 1993) is a four parameter, double power law function with an exponential rollover between the power laws, given by

$$J(>R) = \begin{cases} J_0 R^{-\gamma_1} \exp\left(-\frac{R}{R_0}\right), & R < (\gamma_2 - \gamma_1) R_0 \equiv R_1 \\ J_0 R_1^{\gamma_2 - \gamma_1} \exp\left(-\frac{R_1}{R_0}\right) R^{-\gamma_2}, & R \geq R_1, \end{cases} \quad (4)$$

where J_0 is an overall fluence coefficient, γ_1 is the low rigidity power law index, γ_2 is the high rigidity power law index and R_0 is the rollover rigidity. The Band function and its first derivative are continuous. It has been commonly used in representing SEP spectra (e.g., Mewaldt et al., 2005; Tylka and Dietrich, 2009; Zhao et al., 2016;

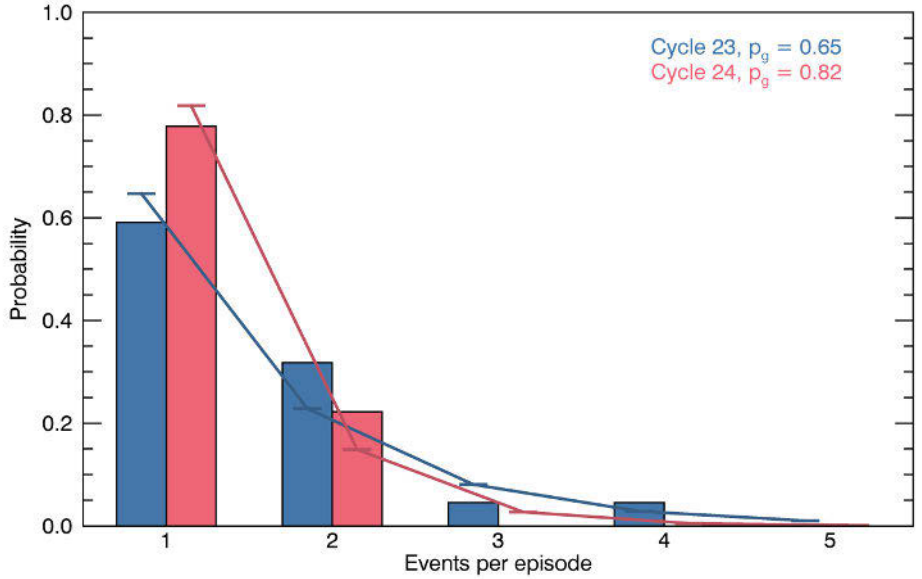

Figure 13. Number of events per episode for solar cycles 23 (blue bars) and 24 (red bars), along with geometric distrubutions and their parameters.

Jiggens et al., 2018a). The fit parameters can be found in Tables A.1 and A.2 of Article II for all events except GLE 72, for which we integrated the differential spectrum given in Jiggens et al. (2019) and fitted the Band function. Some events had also a separately fitted energetic storm particle component, whose fit parameters are also listed in the tables. Figure 14 shows the interdependence of the fit parameters as well as their distributions (the histograms in the topmost panels of each column). Parameters J_0 and R_0 are shown as log-transforms. The Pearson correlation coefficients are also given for all parameter pairs. Significant correlation can be seen between J_0 and γ_1, J_0 and R_0, as well as γ_1 and R_0. γ_2, on the other hand, is not correlated with any other parameter. Again following Article III, we take $\log_{10}(J_0)$ and γ_2 to be independent variables, and assume that γ_1 and $\log_{10}(R_0)$ depend linearly on $\log_{10}(J_0)$; the linear relations are shown in the corresponding panels, and are given by the following equations:

$$\gamma_{1_{23}} = 6.598 - 0.634 \cdot \log_{10}(J_{0_{23}}) \tag{5a}$$
$$\gamma_{1_{24}} = 8.124 - 0.842 \cdot \log_{10}(J_{0_{24}}) \tag{5b}$$
$$\log_{10}(R_{0_{23}}) = 0.437 - 0.158 \cdot \log_{10}(J_{0_{23}}) \tag{5c}$$
$$\log_{10}(R_{0_{24}}) = 0.691 - 0.199 \cdot \log_{10}(J_{0_{24}}). \tag{5d}$$

The topmost panels in Figure 14 also show normal distributions calculated with

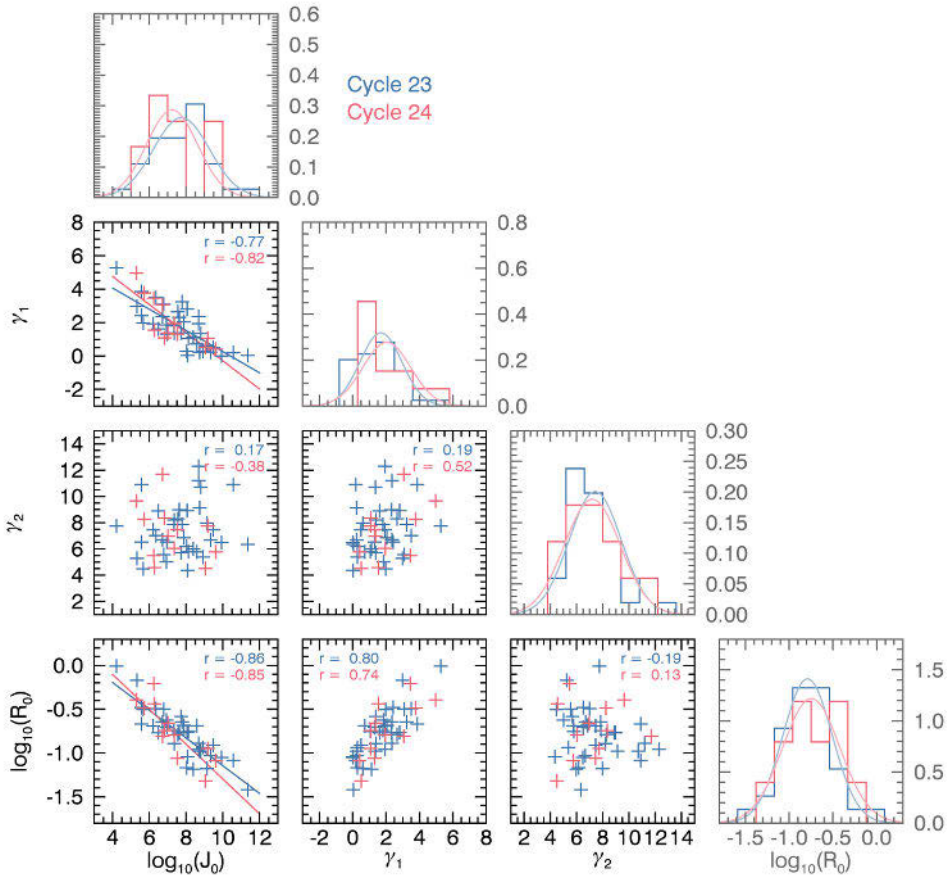

Figure 14. Relationships of Band fit parameters of GLEs, sub-GLEs and energetic storm particle components. Blue crosses represent solar cycle 23, and red crosses cycle 24. The histograms in the topmost panel of each column show the distribution of each parameter, whereas the smooth curves show normal distributions calculated with the mean and standard deviation of the data in the histograms.

the mean and standard deviation of each set of parameters. These are used to model the independent parameters $\log_{10}(J_0)$ and γ_2. The $\log_{10}(J_0)$-dependence is subtracted from the dependent parameters γ_1 and $\log_{10}(R_0)$, and the "residual" parameters are modelled with normal distributions.

There are two possible downsides to this approach. Firstly, the error estimates of the Band parameters are not taken into account in any way. Secondly, the distribution of γ_2 is positively skewed for both solar cycles, and the normal distribution overestimates the number of small values of γ_2, which can result in overestimation of fluences at high energies. To address these points, we take a second approach to the fluence modelling: we create a MC ensemble of simulated Band parameters by sampling 10^4 points from a normal distribution $N(\mu_{p_{i,j,k}}, \sigma^2_{p_{i,j,k}})$ for each parameter

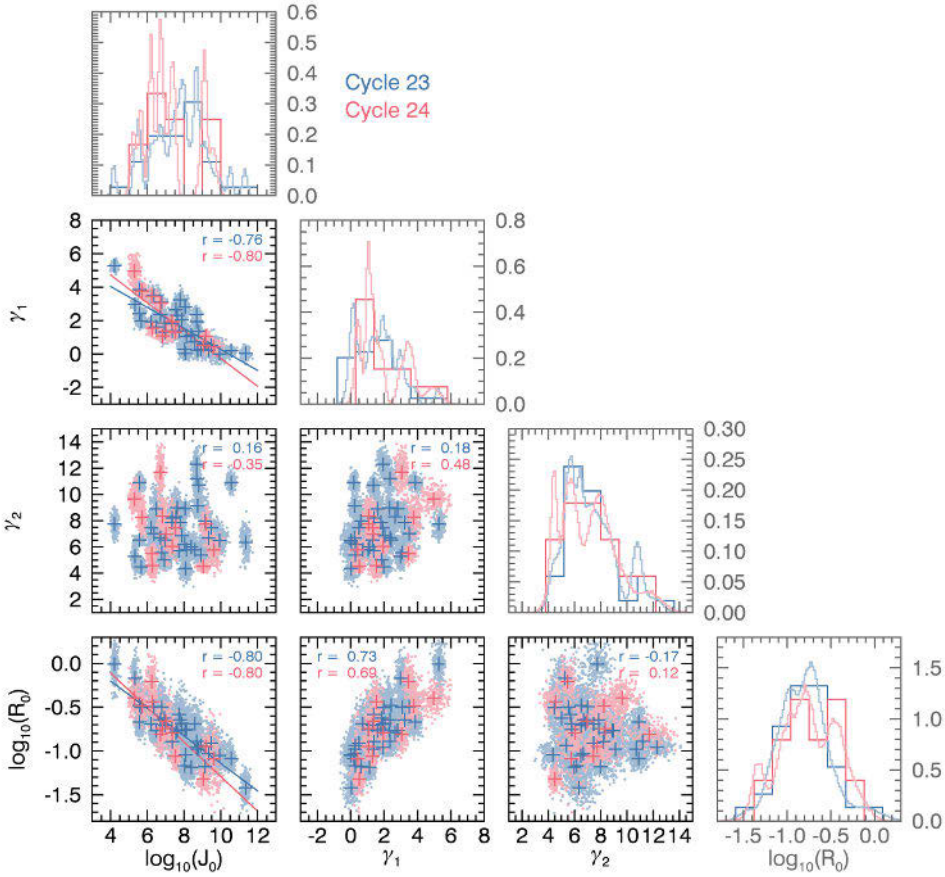

Figure 15. Same as the previous figure, but with a Monte Carlo-generated ensemble for each datapoint (see text for details). Empirical distribution of the total ensemble is shown in the topmost panels instead of the normal distribution.

$p_{i,j,k}$, where i refers to the event number, j to the Band parameter and k to solar cycle. Thus, we have ensembles of $N_{23} \cdot 10000 = 360000$ points for cycle 23 and $N_{24} \cdot 10000 = 120000$ points for cycle 24, for each four parameters. A subset of these ensembles is shown in Figure 15, with formatting similar to Figure 14. The linear relations are now calculated from the complete ensembles, and are given by the following equations:

$$\gamma_{1_{23}} = 6.550 - 0.629 \cdot \log_{10}(J_{0_{23}}) \tag{6a}$$

$$\gamma_{1_{24}} = 8.055 - 0.832 \cdot \log_{10}(J_{0_{24}}) \tag{6b}$$

$$\log_{10}(R_{0_{23}}) = 0.426 - 0.157 \cdot \log_{10}(J_{0_{23}}) \tag{6c}$$

$$\log_{10}(R_{0_{24}}) = 0.677 - 0.197 \cdot \log_{10}(J_{0_{24}}). \tag{6d}$$

Instead of normal distributions, the topmost panels in Figure 15 show the probability distributions of the total ensembles. The parameters can be modelled using these distributions by inverse transform sampling from the empirical CDFs.

Modelling method

The modelling follows a simple Monte Carlo procedure which can be described by the following steps:

1. User inputs the duration of mission to be modelled, t (in years)
2. The number of episodes is drawn from the Poisson distribution with parameters $\lambda_{23} = t \cdot 6.07 \cdot 10^{-3}$ and $\lambda_{24} = t \cdot 4.10 \cdot 10^{-3}$
3. For each episode, the number of events is drawn from the geometric distribution with parameters $p_{\mathrm{g},23} = 0.65$ and $p_{\mathrm{g},24} = 0.82$
4. For each event, the indepedent parameters ($\log_{10}(J_0)$ and γ_2) are drawn from $N(\mu_{j,k}, \sigma^2_{j,k})$
5. For each event, the dependent parameters (γ_1 and $\log_{10}(R_0)$) are drawn from $N(\mu_{j,k}, \sigma^2_{j,k}) + a_{j,k} + b_{j,k} \cdot \log_{10}(J_0)$, where $a_{j,k}$ and $b_{j,k}$ are the corresponding linear parameters from equations 5
6. If the simulated parameter set does not produce a physically meaningful spectrum[18], two previous steps are repeated
7. For each event, the integral fluence spectrum is calculated on a pre-determined rigidity grid using the Band function
8. For each episode, the fluence spectrum is calculated by summing the event fluence spectra
9. The cumulative fluence spectrum is calculated by summing the episode fluence spectra, and the worst case fluence spectrum is taken as the highest episode fluences at each rigidity

In case of the "ensemble" version of the model, the normal distributions in steps 4 and 5 are replaced with the empirical CDFs, and the linear parameters in step 5 are taken from equations 6 instead of 5. For both model versions, steps 2 – 9 are repeated for a total of $5 \cdot 10^5$ times. The fluence percentages and their relative change at each rigidity value are calculated after each 10^4 repeats to check the convergence of the calculation.

18 The conditions are, again following Article III: $\gamma_1 < \gamma_2$, and in case γ_1 has a negative value, $-\gamma_1 R_0 < 0.137$GV.

4.2.2 Results

Figures 16 and 17 show the model outputs as probability of exceeding a fluence for 0.5-year and 7-year missions for >10 MeV and >1000 MeV energies, respectively. Again, blue colour refers to solar cycle 23 and red to cycle 24. As can be seen from Figure 16, the two model versions produce quite similar results in the low energy region. The only notable difference is that the solar cycle difference is smaller for the ensemble-version at higher confidences. But looking at Figure 17, the difference between the model versions is more apparent. The difference between the solar cycles in the ensemble version starts to decrease quickly below 3 % and 30 % for the 0.5 and 7-year periods, respectively. The cycle difference even changes sign below 5 % in the 7-year fluence estimate for the ensemble model. Overall, the model based on normal distributions provides higher fluence estimates at high energies at high confidence levels, which was indeed expected. Note, however, that for solar cycle 23, results below ~5 % (95 % confidence level) and for cycle 24, results below ~10 % (90 % confidence level) start to be based on extrapolation because of the low statistics.

Figures 18 and 19 show the model output cumulative and worst-cast differential fluence spectra, respectively, at 50 % and 95 % confidences for a 1-year mission, with results from the SAPPHIRE model (Jiggens et al., 2018a) shown for comparison. The colours and formatting are similar to the previous figures. Corresponding spectral comparisons for a 7-year mission are shown in Figures 20 and 21. At 50 % confidence, SAPPHIRE results are generally between the cycle 23 and 24 results of our models for cumulative and worst-case models and both mission durations. Above ~100 MeV SAPPHIRE drops below our results for cycle 24 in all modelled cases.

The results presented in Figures 16 through 21 show that although the difference in SEP activity between the solar cycles is clearly reflected in the model results, the modelling method, i.e., in this case the construction of the fluence distributions, may have a large effect, especially at higher confidences. The results, along with the comparisons with the SAPPHIRE model, also demonstrate the effect of different solar activity level in input data to the model results: estimating the SEP environment during a period of reduced activity with a model constructed with data from periods of higher activity may lead to overestimation.

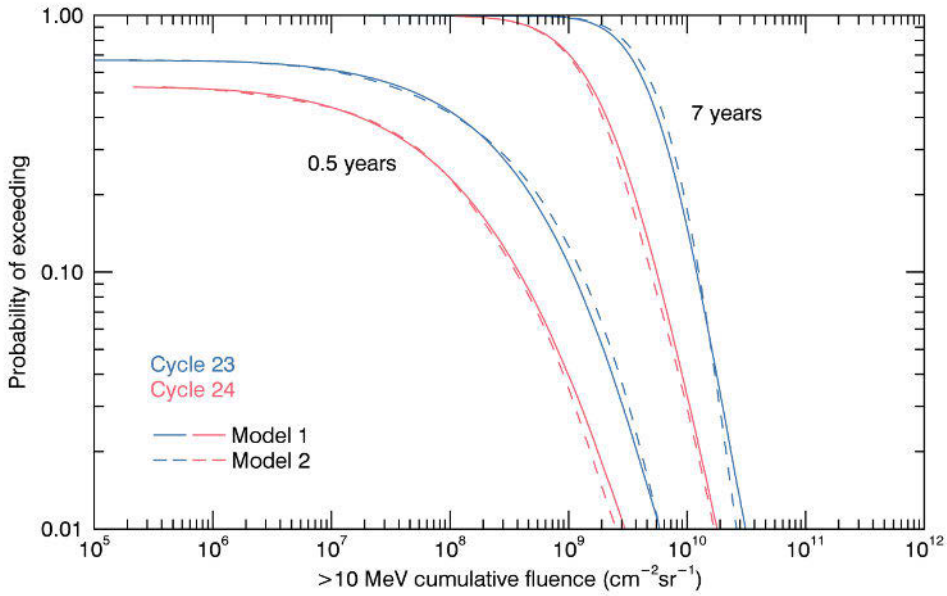

Figure 16. Probability of exceeding a fluence at >10 MeV for 0.5 and 7-year missions. Solid lines show the normal distribution-version of the model, and dashed lines show the ensemble-version. Blue colour indicates solar cycle 23 and red indicates cycle 24.

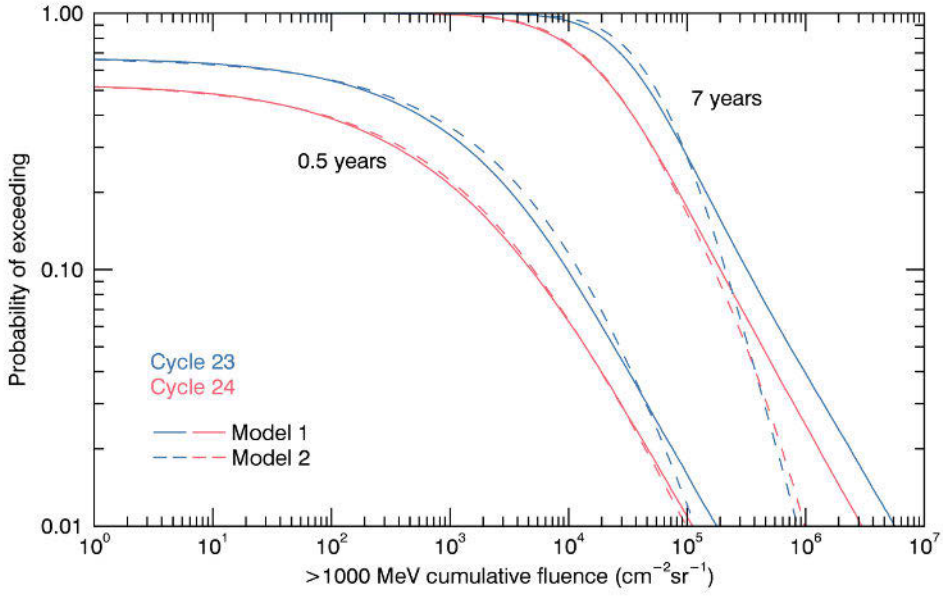

Figure 17. Similar to the previous figure, but for >1000 MeV fluence.

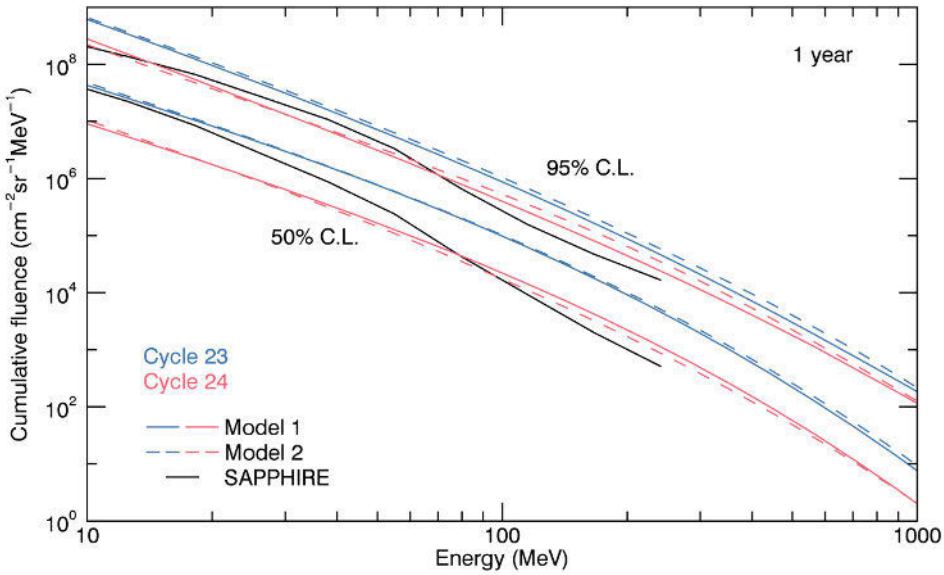

Figure 18. Cumulative fluence spectra for a 1 year mission at 50 % and 95 % confidence levels, along with corresponding results from the SAPPHIRE model. Line colours and styles are similar to the previous figures.

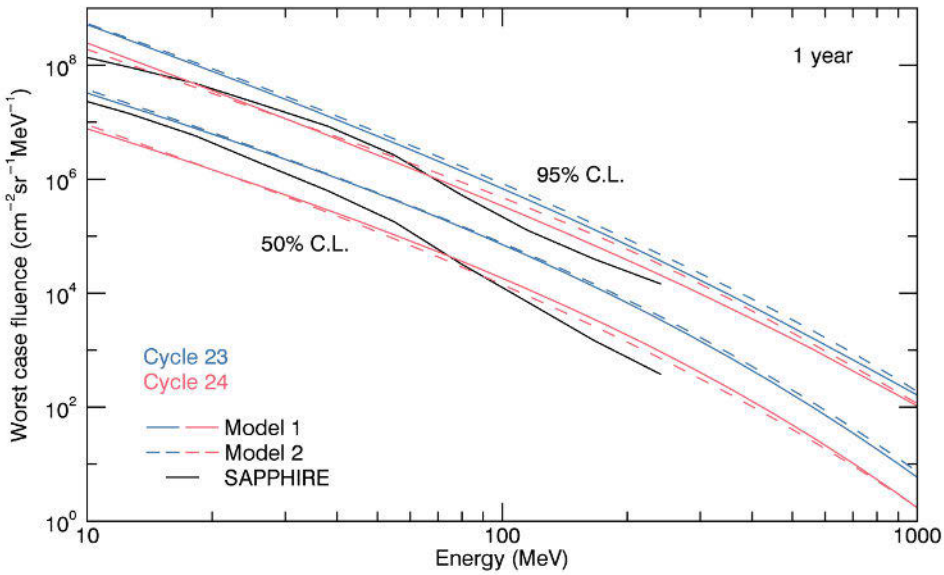

Figure 19. Similar to the previous figure, but for worst-case fluences.

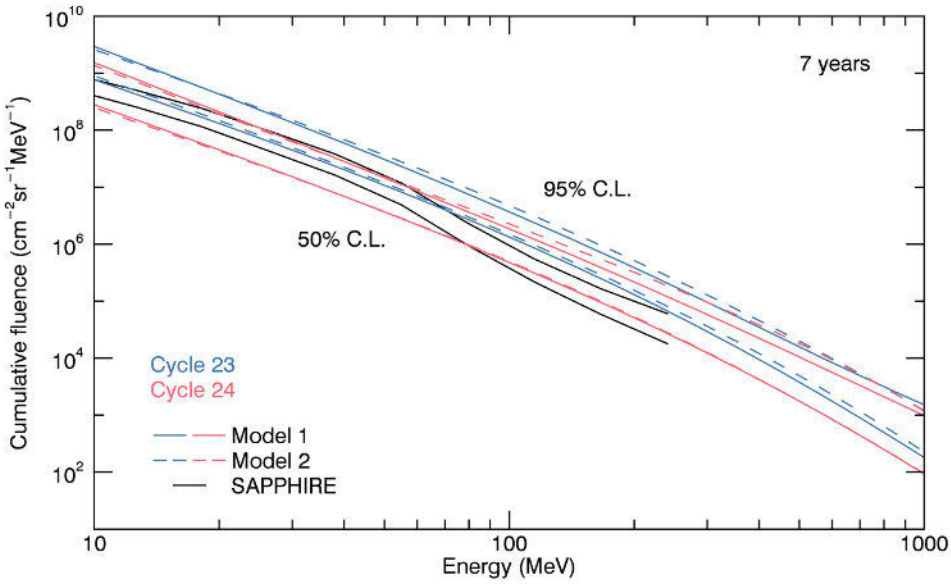

Figure 20. Similar to Figure 18, but for a 7 year mission.

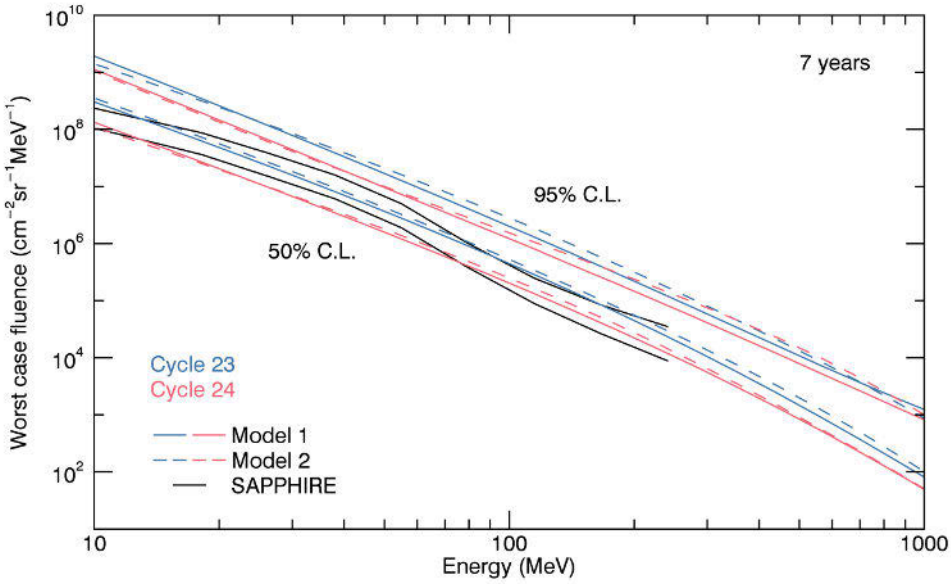

Figure 21. Similar to Figure 19, but for a 7 year mission.

5 Conclusions and outlook

The research presented in this thesis consists of two different, but closely related topics. The first one was studying the differences in SEP activity between solar cycles 23 and 24. By using observations from space-borne and ground-based instruments, as well as results from particle acceleration theory and simulations, we showed that cycle 24 was significantly different: the SEP activity in cycle 24 was significantly reduced, and the reduction could be explained by reduced plasma and suprathermal densities (Article I and Article II). The second topic was developing probabilistic high energy SEP fluence and peak flux models for the space weather community (Article III and Article IV). These models provide improved estimates of the high energy radiation environment encountered in future space missions, and are essential for achieving cost-effective shielding designs for spacecraft. In Chapter 4 of this thesis we showed that the results of Article I remain unchanged after the completion of cycle 24, and presented a new comparison of cycles 23 and 24 based on the modelling methodology of Article III.

The deep minimum between cycles 23 and 24 and the low level of activity during cycle 24 has been suggested to result from a beginning of a modern grand minimum of the Gleissberg cycle (Feynman and Ruzmaikin, 2011; Zolotova and Ponyavin, 2014; Gao, 2016). On the other hand, the high solar activity of the (mid)-20th century can be considered as modern grand maximum, and the lower activity of cycle 24 as a return to "regular" level of activity (de Jager et al., 2016). Either way, the low activity level is expected to continue at least in cycle 25; majority of the early predictions for cycle 25 favour a cycle comparable to cycle 24 (e.g., Pesnell and Schatten, 2018; Upton and Hathaway, 2018; Labonville et al., 2019; Kitiashvili, 2020), although there are differing opinions as well (McIntosh et al., 2020). The change in solar activity has been of great research interest for purely scientific reasons as well as because of its possible implications for applications and, ultimately, for technology and society. The most fundamental scientific interest is perhaps related to understanding of the solar dynamo: the changing activity conditions, coinciding with the increase in observational cababilities provided by, e.g., SOHO (Domingo et al., 1995), STEREO (Kaiser et al., 2008) and Solar Dynamics Observatory (SDO) (Pesnell et al., 2012), enable unprecedented accuracy in defining parameters and constraints to the dynamo models.

The direct space weather consequences to Earth and human technologies are

clear. Weakening solar activity results in fewer SEP events, and on average, reduced intensities especially at higher energies (Articles I and II). This means less radiation-induced problems in space-borne electronics. On the other hand, weakening pressure and magnetic fields result in increasing GCR fluxes, which might result in shorter allowable durations for manned missions (Schwadron et al., 2017). Modern GCR models take the solar activity level into account in their estimations, but most state-of-the-art SEP models do not. This provides an opportunity for important future work on the subject: to include the dependence on solar activity in our SEP models (Articles III and IV). This could be achieved by adding a sunspot number (or some other activity index) dependency to the event frequency in the models, like in the MSU and MSSREM models (Nymmik, 1999a; Robinson et al., 2020) or perhaps by some scaling of the model outputs. The solar cycle dependence would be of special importance in the New Space-paradigm, which relies on affordable, commercial components and quick development and launch cycles. The designers of such missions would certainly benefit from radiation models which could give reliable estimates for a certain solar activity range, which can be reasonably well predicted for a few years in advance, at least some time after a cycle onset.

6 Summary of the original publications

6.1 Article I: Iron-rich solar particle events measured by SOHO/ERNE during two solar cycles

In this article we studied the differences of solar cycles 23 and 24 in heavy ion composition of solar energetic particles. Using SOHO/ERNE observations between 1996 and 2015 we calculated daily intensities of carbon, oxygen and iron in the energy range of 5–15 $\mathrm{MeV\,n^{-1}}$. Using the daily intensities, we identified all SEP events with at least one day of enhanced abundance of iron, i.e., Fe/(C+O) > 0.183, and found most probable solar flare and CME associations for the events.

We found that during solar cycle 24 there were fewer days with increased intensities of C, O and Fe, and fewer days with enhanced abundances of iron, as compared to solar cycle 23. The total rate of occurrence of SEP events with at least one day of enhanced Fe abundance was lower during solar cycle 24, and the rate of SEP events with impulsive characteristics was greatly reduced. In general, the abundances of heavy ions were lower during solar cycle 24, implicating reduced efficiency of SEP acceleration processes.

Author's contribution

The author contributed to the research topic and approach of the paper, performed the data analysis, prepared all of the figures and wrote most of the manuscript.

6.2 Article II: Why is solar cycle 24 an inefficient producer of high-energy particle events?

In this article we studied the reduced production of high energy solar energetic particle events during solar cycle 24. The study was based on scaling of particle spectra, which was derived from diffusive shock acceleration theory and simulation results. In deriving the scaling laws, we assumed that the particle transport in coronal shocks is dominated by self-generated turbulence.

We scaled the cumulative >1 GV fluence of the GLEs and sub-GLEs in cycle 23 according to observed plasma and suprathermal proton densities and found that if the seed population consists of 40 % suprathermals, the scaled fluence is close to the

observed fluence of cycle 24. Using the same proportion of suprathermals in the seed population, we scaled the heavy ion abundances, and found that the scaled abundance ratios have a similar charge-to-mass dependence to what has been observed. Overall, the study showed that the reduced average plasma and suprathermal proton densities of solar cycle 24 can explain the reduced number of highest energy SEP events as well as the reduced amount of low charge-to-mass ions.

Author's contribution

Using the spectral function parameters from previous studies, the author performed the fluence calculations, prepared most of the figures and contributed to parts of the manuscript.

6.3 Article III: Two solar proton fluence models based on ground level enhancement observations

This study presents two statistical models of solar energetic particle radiation. Both models are based on integral proton fluence spectra, measured by neutron monitor and space-borne instruments during GLEs, which have been fitted with Band functions. The first model version is a JPL-type model, where we calculated the fluences at certain energies from the spectral fits, and modelled their distributions with exponentially cut-off power law distributions. In the second version, we modelled the distributions and interdependence of the spectral fit parameters, thus producing a physical spectrum with each iteration of the model. In both model versions, the event occurrence is modelled as a Poisson process, either with one event rate, only for the active part of the solar cycle, or with two event rates, separately for the active and quiet parts of the solar cycle.

Since the model was based on fits on integral spectra, the results can be given in either differential or integral units, at any energies within the measurement range. We compared the results of the models with each other as well as with other, well-known SEP models (JPL, ESP and SEPEM). We showed that our models were in decent agreement with SEPEM in the common energy range, but were clearly below both JPL and ESP, especially at higher energies and confidence levels. However, our models were based on longer set of observations (nearly six solar cycles), and had a much greater energy range than the other models, which were based only on space-borne observations.

Author's contribution

The author performed the statistical analysis of the event timing, fluence distributions, and spectral parameter distributions. The author also wrote the code for the statistical

modelling and performed the model calculations. In addition, the author prepared most of the figures and wrote most of the manuscript.

6.4 Article IV: Very high energy proton peak flux model

In this study we constructed a statistical high energy proton peak flux model based on the whole available GOES/HEPAD measurement series, i.e., from 1986 to 2017. The HEPAD channel responses were analysed using a "bow-tie" method to find more realistic geometric factors and effective energies. The statistical modelling was done in the JPL-style, using an event list derived from the processed channels with a statistical event criterion. Event occurrence was modelled as a Poisson process and peak fluxes were modelled with exponentially cut-off power law distributions.

Model results were given for the three bow-tie-processed differential channels. Given the low statistics of high-energy SEP events during solar quiet time, the results only apply for the active part of the cycle. For comparison, we ran an updated version of the SEPEM data through the same modelling method, i.e., same event list, same distributions etc. In addition, we compared the results with the SAPPHIRE model, which is based on the SEPEM dataset. At low energies, our model agrees very well with both the modelled SEPEM data and the SAPPHIRE model, but at higher energies our model gives significantly higher results.

Author's contribution

The author contributed to the research topic and approach of the paper. The author did a large part of the data analysis, wrote the code for the statistical modelling and performed the model calculations. In addition, the author prepared most of the figures and wrote most of the manuscript.

List of references

Adams, J. H., Robinson, Z. D., Nonnast, J. H., Fisher, J. H., Hope, D. M., Lane, Z. B., Reed, R. A., Fisher, J. Z., Warren, K. M., Sierawski, B. D. The SIRE2 Toolkit. *Space Weather*, 18(7):e02364, 2020. doi:10.1029/2019SW002364

Adams, J. H., Silberberg, R., Tsao, C. H. Cosmic Ray Effects on Microelectronics, Part I: The Near-Earth Particle Environment. Technical Report NRL Memorandum Report 4506, Washington, D.C., 1981

Afanasiev, A., Vainio, R., Rouillard, A. P., Battarbee, M., Aran, A., Zucca, P. Modelling of proton acceleration in application to a ground level enhancement. *Astronomy & Astrophysics*, 614:A4, 2018. doi:10.1051/0004-6361/201731343

Albertson, V., Thorson, J., Miske, S. The Effects of Geomagnetic Storms on Electrical Power Systems. *IEEE Transactions on Power Apparatus and Systems*, 93(4):1031–1044, 1974. doi:10.1109/TPAS.1974.294047

Aminalragia-Giamini, S., Sandberg, I., Papadimitriou, C., Daglis, I. A., Jiggens, P. The virtual enhancements - solar proton event radiation (VESPER) model. *Journal of Space Weather and Space Climate*, 8:A06, 2018. doi:10.1051/swsc/2017040

Anderson, C. N. Correlation of long wave transatlantic radio transmission with other factors affected by solar activity. *Proceedings of the Institute of Radio Engineers*, 16(3):297–347, 1928. doi:10.1109/JRPROC.1928.221400

Anderson, K. A., Winckler, J. R. Solar Flare X-Ray Burst on September 28, 1961. *Journal of Geophysical Research*, 67(11):4103–4117, 1962. doi:10.1029/JZ067i011p04103

Arlt, R. Digitization of Sunspot Drawings by Staudacher in 1749–1796. *Solar Physics*, 247(2):399–410, 2008. doi:10.1007/s11207-007-9113-4

Atwell, W., Tylka, A. J., Dietrich, W. F., Rojdev, K., Matzkind, C. Sub-GLE Solar Particle Events and the Implications for Lightly-Shielded Systems Flown During an Era of Low Solar Activity. In *Proceedings of the 45th International Conference on Environmental Systems*. Bellevue, WA, USA, 2015

Atwell, W., Tylka, A. J., Dietrich, W. F., Rojdev, K., Matzkind, C. Probability Estimates of Solar Proton Doses During Periods of Low Sunspot Number for Short Duration Missions. In *Proceedings of the 46th International Conference on Environmental Systems*. Vienna, Austria, 2016

Babcock, H. D. The Sun's Polar Magnetic Field. *Astrophysical Journal*, 130:364, 1959. doi:10.1086/146726

Babcock, H. W. The Topology of the Sun's Magnetic Field and the 22-Year Cycle. *Astrophysical Journal*, 133:572, 1961. doi:10.1086/147060

Badhwar, G. D., O'Neill, P. M. An improved model of galactic cosmic radiation for space exploration missions. *International Journal of Radiation Applications and Instrumentation. Part D. Nuclear Tracks and Radiation Measurements*, 20(3):403–410, 1992. ISSN 1359-0189. doi:10.1016/1359-0189(92)90024-P

Badhwar, G. D., O'Neill, P. M. Galactic cosmic radiation model and its applications. *Advances in Space Research*, 17(2):7–17, 1996. doi:10.1016/0273-1177(95)00507-B

Baker, D. N. Effects of the Sun on the Earth's environment. *Journal of Atmospheric and Solar-Terrestrial Physics*, 62(17-18):1669–1681, 2000. doi:10.1016/S1364-6826(00)00119-X

Baker, D. N., Allen, J. H., Kanekal, S. G., Reeves, G. D. Disturbed space environment may have been related to pager satellite failure. *EOS Transactions of the American Geophysical Union*, 79(40):477–477, 1998. doi:10.1029/98EO00359

Baker, D. N., Kanekal, S., Blake, J. B., Klecker, B., Rostoker, G. Satellite anomalies linked to electron increase in the magnetosphere. *EOS Transactions of the American Geophysical Union*, 75(35):401–405, 1994. doi:10.1029/94EO01038

Balogh, A., Hudson, H. S., Petrovay, K., von Steiger, R. Introduction to the Solar Activity Cycle: Overview of Causes and Consequences. *Space Science Reviews*, 186:1–15, 2014. doi:10.1007/s11214-014-0125-8

Band, D., Matteson, J., Ford, L., Schaefer, B., Palmer, D., Teegarden, B., Cline, T., Briggs, M., Paciesas, W., Pendleton, G., Fishman, G., Kouveliotou, C., Meegan, C., Wilson, R., Lestrade, P. BATSE observations of gamma-ray burst spectra. I - Spectral diversity. *Astrophysical Journal*, 413:281–292, 1993. doi:10.1086/172995

Barbieri, L. P., Mahmot, R. E. October-November 2003's space weather and operations lessons learned. *Space Weather*, 2(9):S09002, 2004. doi:10.1029/2004SW000064

Barlow, W. H. On the Spontaneous Electrical Currents Observed in the Wires of the Electric Telegraph. *Philosophical Transactions of the Royal Society of London Series I*, 139:61–72, 1849

Basu, S., Basu, S. Equatorial scintillations - A review. *Journal of Atmospheric and Solar-Terrestrial Physics*, 43:473–489, 1981. doi:10.1016/0021-9169(81)90110-0

Bazilevskaya, G. A., Cliver, E. W., Kovaltsov, G. A., Ling, A. G., Shea, M. A., Smart, D. F., Usoskin, I. G. Solar Cycle in the Heliosphere and Cosmic Rays. *Space Science Reviews*, 186(1-4):409–435, 2014. doi:10.1007/s11214-014-0084-0

Bazilevskaya, G. A., Usoskin, I. G., Flückiger, E. O., Harrison, R. G., Desorgher, L., Bütikofer, R., Krainev, M. B., Makhmutov, V. S., Stozhkov, Y. I., Svirzhevskaya, A. K., Svirzhevsky, N. S., Kovaltsov, G. A. Cosmic Ray Induced Ion Production in the Atmosphere. *Space Science Reviews*, 137(1-4):149–173, 2008. doi:10.1007/s11214-008-9339-y

Beer, J., McCracken, K., von Steiger, R. *Cosmogenic Radionuclides*. 2012. doi:10.1007/978-3-642-14651-0

Bell, A. R. The acceleration of cosmic rays in shock fronts - I. *Monthly Notices of the Royal Astronomical Society*, 182:147–156, 1978. doi:10.1093/mnras/182.2.147

Benz, A. O. Flare Observations. *Living Reviews in Solar Physics*, 14(1):2, 2017. doi:10.1007/s41116-016-0004-3

Biermann, L. Kometenschweife und solare Korpuskularstrahlung. *Zeitschrift für Astrophysik*, 29:274, 1951

Blandford, R., Eichler, D. Particle acceleration at astrophysical shocks: A theory of cosmic ray origin. *Physics Reports*, 154(1):1–75, 1987. doi:10.1016/0370-1573(87)90134-7

Bolduc, L. GIC observations and studies in the Hydro-Québec power system. *Journal of Atmospheric and Solar-Terrestrial Physics*, 64(16):1793–1802, 2002. doi:10.1016/S1364-6826(02)00128-1

Bonadonna, M., Lanzerotti, L., Stailey, J. The National Space Weather Program: Two decades of interagency partnership and accomplishments. *Space Weather*, 15(1):14–25, 2017. doi:10.1002/2016SW001523

Boteler, D. H. Geomagnetic Effects on the Pipe-To-Soil Potentials of A Continental Pipeline. *Advances in Space Research*, 26(1):15–20, 2000. doi:10.1016/S0273-1177(99)01020-0

Boteler, D. H. The super storms of August/September 1859 and their effects on the telegraph system. *Advances in Space Research*, 38(2):159–172, 2006. doi:10.1016/j.asr.2006.01.013

Boteler, D. H., Pirjola, R. J., Nevanlinna, H. The effects of geomagnetic disturbances on electrical systems at the earth's surface. *Advances in Space Research*, 22(1):17–27, 1998. doi:10.1016/S0273-1177(97)01096-X

Bothmer, V., Daglis, I. A. *Space Weather: Physics and Effects*. Springer Berlin Heidelberg, Berlin, Germany, 2007. ISBN 978-3-540-34578-7

Boursier, Y., Lamy, P., Llebaria, A., Goudail, F., Robelus, S. The ARTEMIS Catalog of LASCO Coronal Mass Ejections. Automatic Recognition of Transient Events and Marseille Inventory from Synoptic maps. *Solar Physics*, 257(1):125–147, 2009. doi:10.1007/s11207-009-9370-5

Breneman, H. H., Stone, E. C. Solar coronal and photospheric abundances from solar energetic particle measurements. *Astrophysical Journal, Letters*, 299:L57–L61, 1985. doi:10.1086/184580

Brueckner, G. E., Howard, R. A., Koomen, M. J., Korendyke, C. M., Michels, D. J., Moses, J. D., Socker, D. G., Dere, K. P., Lamy, P. L., Llebaria, A., Bout, M. V., Schwenn, R., Simnett, G. M., Bedford, D. K., Eyles, C. J. The Large Angle Spectroscopic Coronagraph (LASCO). *Solar Physics*, 162(1-2):357–402, 1995. doi:10.1007/BF00733434

Bryant, D. A., Cline, T. L., Desai, U. D., McDonald, F. B. Explorer 12 Observations of Solar Cosmic Rays and Energetic Storm Particles after the Solar Flare of September 28, 1961. *Journal of Geophysical Research*, 67(13):4983–5000, 1962. doi:10.1029/JZ067i013p04983

Bushby, P. J., Tobias, S. M. On Predicting the Solar Cycle Using Mean-Field Models. *Astrophysical Journal*, 661(2):1289–1296, 2007. doi:10.1086/516628

Cade, W. B., Chan-Park, C. The Origin of "Space Weather". *Space Weather*, 13(2):99–103, 2015. doi:10.1002/2014SW001141

Cameron, R. H., Schüssler, M. An update of Leighton's solar dynamo model. *Astronomy & Astrophysics*, 599:A52, 2017. doi:10.1051/0004-6361/201629746

Cane, H. V., McGuire, R. E., von Rosenvinge, T. T. Two Classes of Solar Energetic Particle Events Associated with Impulsive and Long-Duration Soft X-Ray Flares. *Astrophysical Journal*, 301:448, 1986. doi:10.1086/163913

Cane, H. V., Reames, D. V. Soft X-Ray Emissions, Meter-Wavelength Radio Bursts, and Particle Acceleration in Solar Flares. *Astrophysical Journal*, 325:895, 1988. doi:10.1086/166060

Cane, H. V., Richardson, I. G., von Rosenvinge, T. T. A study of solar energetic particle events of 1997-2006: Their composition and associations. *Journal of Geophysical Research*, 115:A08101, 2010. doi:10.1029/2009JA014848

Cane, H. V., Stone, R. G. Type II solar radio bursts, interplanetary shocks, and energetic particle events. *Astrophysical Journal*, 282:339–344, 1984. doi:10.1086/162207

Carmichael, H. Cosmic Ray Measurements. In *Annals of the IQSY*. MIT Press, Cambridge, MA, USA, 1968

Carrington, R. C. Description of a Singular Appearance seen in the Sun on September 1, 1859. *Monthly Notices of the Royal Astronomical Society*, 20:13–15, 1859. doi:10.1093/mnras/20.1.13

Chapman, S. On the Times of Sudden Commencement of Magnetic Storms. *Proceedings of the Physical Society of London*, 30(1):205–214, 1917. doi:10.1088/1478-7814/30/1/317

Chapman, S. An Outline of a Theory of Magnetic Storms. *Proceedings of the Royal Society of London Series A*, 95(666):61–83, 1918. doi:10.1098/rspa.1918.0049

Charbonneau, P. Dynamo models of the solar cycle. *Living Reviews in Solar Physics*, 17(1):4, 2020. doi:10.1007/s41116-020-00025-6

Chenette, D. L., Chen, J., Clayton, E., Guzik, T. G., Wefel, J. P., Garcia-Munoz, M., Lopate, C., Pyle, K. R., Ray, K. P., Mullen, E. G., Hardy, D. A. The CRRES/SPACERAD heavy ion model of the environment (CHIME) for cosmic ray and solar particle effects on electronic and biological systems in space. *IEEE Transactions on Nuclear Science*, 41(6):2332–2339, 1994. doi:10.1109/23.340584

Choudhuri, A. R., Chatterjee, P., Jiang, J. Predicting Solar Cycle 24 With a Solar Dynamo Model. *Physical Review Letters*, 98(13):131103, 2007. doi:10.1103/PhysRevLett.98.131103

Chubb, T. A., Friedman, H., Kreplin, R. W., Kupperian, J., J. E. Lyman Alpha and X-Ray Emissions during a Small Solar Flare. *Journal of Geophysical Research*, 62(3):389–398, 1957. doi:10.1029/JZ062i003p00389

Chupp, E. L., Ryan, J. M. High energy neutron and pion-decay gamma-ray emissions from solar flares. *Research in Astronomy and Astrophysics*, 9(1):11–40, 2009. doi:10.1088/1674-4527/9/1/003

Clark, D. H., Stephenson, F. R. An Interpretation of the Pre-Telescopic Sunspot Records from the Orient. *Quarterly Journal of the Royal Astronomical Society*, 19:387, 1978

Clette, F., Cliver, E. W., Lefèvre, L., Svalgaard, L., Vaquero, J. M., Leibacher, J. W. Preface to Topical Issue: Recalibration of the Sunspot Number. *Solar Physics*, 291(9-10):2479–2486, 2016. doi:10.1007/s11207-016-1017-8

Clette, F., Lefèvre, L. Are the sunspots really vanishing? Anomalies in solar cycle 23 and implications for long-term models and proxies. *Journal of Space Weather and Space Climate*, 2:A06, 2012. doi:10.1051/swsc/2012007

Clette, F., Lefèvre, L. The New Sunspot Number: Assembling All Corrections. *Solar Physics*, 291(9-10):2629–2651, 2016. doi:10.1007/s11207-016-1014-y

Clette, F., Svalgaard, L., Vaquero, J. M., Cliver, E. W. Revisiting the Sunspot Number. A 400-Year Perspective on the Solar Cycle. *Space Science Reviews*, 186(1-4):35–103, 2014. doi:10.1007/s11214-014-0074-2

Cliver, E. W. The Extended Cycle of Solar Activity and the Sun's 22-Year Magnetic Cycle. *Space Science Reviews*, 186(1-4):169–189, 2014. doi:10.1007/s11214-014-0093-z

Cliver, E. W., Webb, D. F., Howard, R. A. On the origin of solar metric type II bursts. *Solar Physics*, 187:89–114, 1999. doi:10.1023/A:1005115119661

Coddington, O., Lean, J. L., Pilewskie, P., Snow, M., Lindholm, D. A Solar Irradiance Climate Data Record. *Bulletin of the American Meteorological Society*, 97(7):1265, 2016. doi:10.1175/BAMS-D-14-00265.1

Cohen, C. M. S., Mewaldt, R. A. The Ground-Level Enhancement Event of September 2017 and Other Large Solar Energetic Particle Events of Cycle 24. *Space Weather*, 16(10):1616–1623, 2018. doi:10.1029/2018SW002006

Compagnino, A., Romano, P., Zuccarello, F. A Statistical Study of CME Properties and of the Correlation Between Flares and CMEs over Solar Cycles 23 and 24. *Solar Physics*, 292(1):5, 2017. doi:10.1007/s11207-016-1029-4

Compton, A. H., Wollan, E. O., Bennett, R. D. A Precision Recording Cosmic-Ray Meter. *Review of Scientific Instruments*, 5(12):415–422, 1934. doi:10.1063/1.1751765

Covington, A. E., Harvey, G. A. Coincidence of the Explosive Phase of Solar Flares with 10.7-cm. Solar Noise Bursts. *Nature*, 192(4798):152–153, 1961. doi:10.1038/192152a0

Crabb, R. L. Solar cell radiation damage. *Radiation Physics and Chemistry*, 43(1):93–103, 1994. ISSN 0969-806X. doi:10.1016/0969-806X(94)90204-6

Crosby, N., Heynderickx, D., Jiggens, P., Aran, A., Sanahuja, B., Truscott, P., Lei, F., Jacobs, C., Poedts, S., Gabriel, S., Sandberg, I., Glover, A., Hilgers, A. SEPEM: A tool for statistical modeling the solar energetic particle environment. *Space Weather*, 13(7):406–426, 2015. doi:10.1002/2013SW001008

Dagnew, F. K., Gopalswamy, N., Tessema, S. B., Akiyama, S., Yashiro, S., Tesfu, T. Y. Intercycle and Intracycle Variation of Halo CME Rate Obtained from SOHO/LASCO Observations. *Astrophysical Journal*, 903(2):118, 2020. doi:10.3847/1538-4357/abb887

Daly, E. J., Drolshagen, G., Hilgers, A., Evans, H. D. R. Space Environment Analysis: Experience and Trends. In T. D. Guyenne, A. Hilgers (editors), *Environment Modeling for Space-Based Applications*, volume 392 of *ESA Special Publication*, page 15. 1996

Damon, P. E., Linick, T. W. Geomagnetic-Heliomagnetic Modulation of Atmospheric Radiocarbon Production. *Radiocarbon*, 28(2A):266–278, 1986. doi:10.1017/S0033822200007360

de Jager, C., Akasofu, S. I., Duhau, S., Livingston, W. C., Nieuwenhuijzen, H., Potgieter, M. S. A Remarkable Recent Transition in the Solar Dynamo. *Space Science Reviews*, 201(1-4):109–145, 2016. doi:10.1007/s11214-016-0293-9

Desai, M., Giacalone, J. Large gradual solar energetic particle events. *Living Reviews in Solar Physics*, 13(1):3, 2016. doi:10.1007/s41116-016-0002-5

Dewitte, S., Crommelynck, D., Mekaoui, S., Joukoff, A. Measurement and Uncertainty of the Long-Term Total Solar Irradiance Trend. *Solar Physics*, 224(1-2):209–216, 2004. doi:10.1007/s11207-005-5698-7

Dikpati, M., de Toma, G., Gilman, P. A. Predicting the strength of solar cycle 24 using a flux-transport dynamo-based tool. *Geophysical Research Letters*, 33(5):L05102, 2006. doi:10.1029/2005GL025221

Dodd, P. E., Massengill, L. W. Basic mechanisms and modeling of single-event upset in digital microelectronics. *IEEE Transactions on Nuclear Science*, 50(3):583–602, 2003. ISSN 0018-9499. doi:10.1109/TNS.2003.813129

Domingo, V., Fleck, B., Poland, A. I. The SOHO Mission: an Overview. *Solar Physics*, 162(1-2):1–37, 1995. doi:10.1007/BF00733425

Drake, J. F., Cassak, P. A., Shay, M. A., Swisdak, M., Quataert, E. A Magnetic Reconnection Mechanism for Ion Acceleration and Abundance Enhancements in Impulsive Flares. *Astrophysical Journal, Letters*, 700:L16–L20, 2009. doi:10.1088/0004-637X/700/1/L16

Drake, J. F., Swisdak, M. Ion Heating and Acceleration During Magnetic Reconnection Relevant to the Corona. *Space Science Reviews*, 172(1-4):227–240, 2012. doi:10.1007/s11214-012-9903-3

Drake, J. F., Swisdak, M., Fermo, R. The Power-law Spectra of Energetic Particles during Multi-island Magnetic Reconnection. *Astrophysical Journal, Letters*, 763(1):L5, 2013. doi:10.1088/2041-8205/763/1/L5

Dudok de Wit, T., Kopp, G., Fröhlich, C., Schöll, M. Methodology to create a new total solar irradiance record: Making a composite out of multiple data records. *Geophysical Research Letters*, 44(3):1196–1203, 2017. doi:10.1002/2016GL071866

Dulk, G. A. Radio emission from the sun and stars. *Annual Review of Astronomy and Astrophysics*, 23:169–224, 1985. doi:10.1146/annurev.aa.23.090185.001125

Eddy, J. A. The Maunder Minimum. *Science*, 192(4245):1189–1202, 1976. doi:10.1126/science.192.4245.1189

Eddy, J. A. Climate and the changing sun. *Climatic Change*, 1(2):173–190, 1977. doi:10.1007/BF01884410

Ellison, D. C., Ramaty, R. Shock acceleration of electrons and ions in solar flares. *Astrophysical Journal*, 298:400–408, 1985. doi:10.1086/163623

Facius, R., Reitz, G. *Space weather impacts on space radiation protection*, pages 289–352. In Bothmer and Daglis (2007), 2007

Fan, C. Y., Meyer, P., Simpson, J. A. Rapid Reduction of Cosmic-Radiation Intensity Measured in Interplanetary Space. *Physical Review Letters*, 5(6):269–271, 1960. doi:10.1103/PhysRevLett.5.269

Ferreira, S. E. S., Potgieter, M. S. Long-Term Cosmic-Ray Modulation in the Heliosphere. *Astrophysical Journal*, 603(2):744–752, 2004. doi:10.1086/381649

Feynman, J., Armstrong, T. P., Dao-Gibner, L., Silverman, S. New interplanetary proton fluence model. *Journal of Spacecraft and Rockets*, 27:403–410, 1990. doi:10.2514/3.26157

Feynman, J., Gabriel, S. B. Period and phase of the 88-year solar cycle and the Maunder minimum: Evidence for a chaotic sun. *Solar Physics*, 127(2):393–403, 1990. doi:10.1007/BF00152176

Feynman, J., Gabriel, S. B. On space weather consequences and predictions. *Journal of Geophysical Research*, 105(A5):10543–10564, 2000. doi:10.1029/1999JA000141

Feynman, J., Ruzmaikin, A. The Sun's Strange Behavior: Maunder Minimum or Gleissberg Cycle? *Solar Physics*, 272(2):351–363, 2011. doi:10.1007/s11207-011-9828-0

Feynman, J., Ruzmaikin, A., Berdichevsky, V. The JPL proton fluence model: an update. *Journal of Atmospheric and Solar-Terrestrial Physics*, 64(16):1679–1686, 2002. ISSN 1364-6826. doi:10.1016/S1364-6826(02)00118-9

Feynman, J., Spitale, G., Wang, J., Gabriel, S. Interplanetary proton fluence model - JPL 1991. *Journal of Geophysical Research*, 98:13, 1993. doi:10.1029/92JA02670

Fletcher, L., Dennis, B. R., Hudson, H. S., Krucker, S., Phillips, K., Veronig, A., Battaglia, M., Bone, L., Caspi, A., Chen, Q., Gallagher, P., Grigis, P. T., Ji, H., Liu, W., Milligan, R. O., Temmer, M. An Observational Overview of Solar Flares. *Space Science Reviews*, 159(1-4):19–106, 2011. doi:10.1007/s11214-010-9701-8

Floyd, O., Lamy, P., Boursier, Y., Llebaria, A. ARTEMIS II: A Second-Generation Catalog of LASCO Coronal Mass Ejections Including Mass and Kinetic Energy. *Solar Physics*, 288(1):269–289, 2013. doi:10.1007/s11207-013-0281-0

Fokker, A. D. Type IV Solar Radio Emission. *Space Science Reviews*, 2(1):70–90, 1963. doi:10.1007/BF00174028

Forbes, T. G., Linker, J. A., Chen, J., Cid, C., Kóta, J., Lee, M. A., Mann, G., Mikić, Z., Potgieter, M. S., Schmidt, J. M., Siscoe, G. L., Vainio, R., Antiochos, S. K., Riley, P. CME Theory and Models. *Space Science Reviews*, 123(1-3):251–302, 2006. doi:10.1007/s11214-006-9019-8

Forbush, S. E. Three Unusual Cosmic-Ray Increases Possibly Due to Charged Particles from the Sun. *Physical Review*, 70:771–772, 1946. doi:10.1103/PhysRev.70.771

Forbush, S. E. World-Wide Cosmic-Ray Variations, 1937-1952. *Journal of Geophysical Research*, 59(4):525–542, 1954. doi:10.1029/JZ059i004p00525

Frederickson, A. R. Upsets related to spacecraft charging. *IEEE Transactions on Nuclear Science*, 43(2):426–441, 1996. ISSN 0018-9499. doi:10.1109/23.490891

Friedli, T. K. Sunspot Observations of Rudolf Wolf from 1849–1893. *Solar Physics*, 291(9-10):2505–2517, 2016. doi:10.1007/s11207-016-0907-0

Fröhlich, C. Total Solar Irradiance Observations. *Surveys in Geophysics*, 33(3-4):453–473, 2012. doi:10.1007/s10712-011-9168-5

Fröhlich, C., Lean, J. The Sun's total irradiance: Cycles, trends and related climate change uncertainties since 1976. *Geophysical Research Letters*, 25(23):4377–4380, 1998. doi:10.1029/1998GL900157

Gao, P. X. Long-term Trend of Sunspot Numbers. *Astrophysical Journal*, 830(2):140, 2016. doi:10.3847/0004-637X/830/2/140

Garcia, H. A. Temperature and Emission Measure from GOES Soft X-Ray Measurements. *Solar Physics*, 154(2):275–308, 1994. doi:10.1007/BF00681100

Garcia, H. A., Dryer, M. The solar flares of February 1986 and the ensuing intense geomagnetic storm. *Solar Physics*, 109(1):119–137, 1987. doi:10.1007/BF00167403

Ginet, G. P., O'Brien, T. P., Huston, S. L., Johnston, W. R., Guild, T. B., Friedel, R., Lindstrom, C. D., Roth, C. J., Whelan, P., Quinn, R. A., Madden, D., Morley, S., Su, Y.-J. AE9, AP9 and SPM: New Models for Specifying the Trapped Energetic Particle and Space Plasma Environment. *Space Science Reviews*, 179(1-4):579–615, 2013. doi:10.1007/s11214-013-9964-y

Gleissberg, W. A long-periodic fluctuation of the sun-spot numbers. *The Observatory*, 62:158–159, 1939

Gloeckler, G., Hovestadt, D., Vollmer, O., Fan, C. Y. Unusual emission of iron nuclei from the sun. *Astrophysical Journal, Letters*, 200:L45–L48, 1975. doi:10.1086/181893

Glover, A., Hilgers, A., Rosenqvist, L., Bourdarie, S. Interplanetary proton cumulated fluence model update. *Advances in Space Research*, 42:1564–1568, 2008. doi:10.1016/j.asr.2007.08.023

Gnevyshev, M. N. The Corona and the 11-Year Cycle of Solar Activity. *Soviet Astronomy*, 7:311, 1963

Gnevyshev, M. N., Ohl, A. I. On 22-year cycle of the solar activity. *Astronomicheskii Zhurnal*, 25:18–20, 1948

Gold, T. Magnetic Storms. *Space Science Reviews*, 1(1):100–114, 1962. doi:10.1007/BF00174637

Gonzalez, W. D., Joselyn, J. A., Kamide, Y., Kroehl, H. W., Rostoker, G., Tsurutani, B. T., Vasyliunas, V. M. What is a geomagnetic storm? *Journal of Geophysical Research*, 99(A4):5771–5792, 1994. doi:10.1029/93JA02867

Gonzalez, W. D., Tsurutani, B. T., Clúa de Gonzalez, A. L. Interplanetary origin of geomagnetic storms. *Space Science Reviews*, 88:529–562, 1999. doi:10.1023/A:1005160129098

Gopalswamy, N., Akiyama, S., Yashiro, S., Xie, H., Mäkelä, P., Michalek, G. Anomalous expansion of coronal mass ejections during solar cycle 24 and its space weather implications. *Geophysical Research Letters*, 41:2673–2680, 2014. doi:10.1002/2014GL059858

Gopalswamy, N., Tsurutani, B., Yan, Y. Short-term variability of the Sun-Earth system: an overview of progress made during the CAWSES-II period. *Progress in Earth and Planetary Science*, 2:13, 2015a. doi:10.1186/s40645-015-0043-8

Gopalswamy, N., Xie, H., Akiyama, S., Mäkelä, P., Yashiro, S., Michalek, G. The Peculiar Behavior of Halo Coronal Mass Ejections in Solar Cycle 24. *Astrophysical Journal, Letters*, 804:L23, 2015b. doi:10.1088/2041-8205/804/1/L23

Gosling, J. T., Hildner, E., MacQueen, R. M., Munro, R. H., Poland, A. I., Ross, C. L. Mass ejections from the Sun: A view from Skylab. *Journal of Geophysical Research*, 79(31):4581, 1974. doi:10.1029/JA079i031p04581

Gosling, J. T., McComas, D. J., Phillips, J. L., Bame, S. J. Geomagnetic activity associated with earth passage of interplanetary shock disturbances and coronal mass ejections. *Journal of Geophysical Research*, 96(A5):7831–7839, 1991. doi:10.1029/91JA00316

Green, L. M., Török, T., Vršnak, B., Manchester, W., Veronig, A. The Origin, Early Evolution and Predictability of Solar Eruptions. *Space Science Reviews*, 214(1):46, 2018. doi:10.1007/s11214-017-0462-5

Gringauz, K. I., Bezrokikh, V. V., Ozerov, V. D., Rybchinskii, R. E. A Study of the Interplanetary Ionized Gas, High-Energy Electrons and Corpuscular Radiation from the Sun by Means of the Three-Electrode Trap for Charged Particles on the Second Soviet Cosmic Rocket. *Soviet Physics Doklady*, 5:361, 1960

Hale, G. E. On the Probable Existence of a Magnetic Field in Sun-Spots. *Astrophysical Journal*, 28:315, 1908. doi:10.1086/141602

Hale, G.-E., Ellerman, F., Nicholson, S. B., Joy, A. H. The Magnetic Polarity of Sun-Spots. *Astrophysical Journal*, 49:153, 1919. doi:10.1086/142452

Hale, G. E., Nicholson, S. B. The Law of Sun-Spot Polarity. *Astrophysical Journal*, 62:270, 1925. doi:10.1086/142933

Hansen, R. T., Garcia, C. J., Grognard, R. J. M., Sheridan, K. V. A coronal disturbance observed simultaneously with a white-light corona-meter and the 80 MHz Culgoora radioheliograph. *Proceedings of the Astronomical Society of Australia*, 2:57, 1971

Hapgood, M. A., Lockwood, M., Bowe, G. A., Willis, D. M., Tulunay, Y. K. Variability of the interplanetary medium at 1 a.u. over 24 years: 1963-1986. *Planetary and Space Science*, 39(3):411–423, 1991. doi:10.1016/0032-0633(91)90003-S

Hathaway, D. H. The Solar Cycle. *Living Reviews in Solar Physics*, 12:4, 2015. doi:10.1007/lrsp-2015-4

Hellweg, C. E., Baumstark-Khan, C. Getting ready for the manned mission to Mars: the astronauts' risk from space radiation. *Naturwissenschaften*, 94(7):517–526, 2007. doi:10.1007/s00114-006-0204-0

Hess, P., Colaninno, R. C. Comparing Automatic CME Detections in Multiple LASCO and SECCHI Catalogs. *Astrophysical Journal*, 836(1):134, 2017. doi:10.3847/1538-4357/aa5b85

Hey, J. S. Solar Radiations in the 4-6 Metre Radio Wave-Length Band. *Nature*, 157(3976):47–48, 1946. doi:10.1038/157047b0

Hodgson, R. On a curious Appearance seen in the Sun. *Monthly Notices of the Royal Astronomical Society*, 20:15–16, 1859. doi:10.1093/mnras/20.1.15

Holland, R. L., Vaughan, W. W. Lagrangian least-squares prediction of solar flux ($F_{10.7}$). *Journal of Geophysical Research*, 89(A1):11–16, 1984. doi:10.1029/JA089iA01p00011

Hopkinson, G. R., Dale, C. J., Marshall, P. W. Proton effects in charge-coupled devices. *IEEE Transactions on Nuclear Science*, 43(2):614–627, 1996. doi:10.1109/23.490905

Hovestadt, D., Gloeckler, G., Höfner, H., Klecker, B., Fan, C. Y., Fisk, L. A., Ipavich, F. M., O'Gallagher, J. J., Scholar, M. Direct observation of charge state abundances of energetic He, C, O, and Fe emitted in solar flares. *Advances in Space Research*, 1(3):61–64, 1981. doi:10.1016/0273-1177(81)90017-X

Howard, R. Eight Decades of Solar Research at Mount-Wilson. *Solar Physics*, 100:171, 1985. doi:10.1007/BF00158427

Hoyt, D. V., Schatten, K. H. Group Sunspot Numbers: A New Solar Activity Reconstruction. *Solar Physics*, 179(1):189–219, 1998a. doi:10.1023/A:1005007527816

Hoyt, D. V., Schatten, K. H. Group Sunspot Numbers: A New Solar Activity Reconstruction. *Solar Physics*, 181(2):491–512, 1998b. doi:10.1023/A:1005056326158

Hsieh, K. C., Simpson, J. A. The Relative Abundances and Energy Spectra of ^{3}He and ^{3}He from Solar Flares. *Astrophysical Journal, Letters*, 162:L191, 1970. doi:10.1086/180652

Hudson, H. S. The Unpredictability of the Most Energetic Solar Events. *Astrophysical Journal, Letters*, 663(1):L45–L48, 2007. doi:10.1086/519923

Hudson, M. K., Kress, B. T., Mueller, H.-R., Zastrow, J. A., Blake, J. B. Relationship of the Van Allen radiation belts to solar wind drivers. *Journal of Atmospheric and Solar-Terrestrial Physics*, 70(5):708–729, 2008. doi:10.1016/j.jastp.2007.11.003

Hurford, G. J., Mewaldt, R. A., Stone, E. C., Vogt, R. E. Enrichment of heavy nuclei in ^{3}He-rich flares. *Astrophysical Journal, Letters*, 201:L95–L97, 1975. doi:10.1086/181950

Huttunen-Heikinmaa, K., Valtonen, E., Laitinen, T. Proton and helium release times in SEP events observed with SOHO/ERNE. *Astronomy & Astrophysics*, 442:673–685, 2005. doi:10.1051/0004-6361:20042620

Iucci, N., Levitin, A. E., Belov, A. V., Eroshenko, E. A., Ptitsyna, N. G., Villoresi, G., Chizhenkov, G. V., Dorman, L. I., Gromova, L. I., Parisi, M. Space weather conditions and spacecraft anomalies in different orbits. *Space Weather*, 3(1):S01001, 2005. doi:10.1002/2003SW000056

Jaynes, E. T. Information Theory and Statistical Mechanics. *Physical Review*, 106(4):620–630, 1957. doi:10.1103/PhysRev.106.620

Jiggens, P., Clavie, C., Evans, H., O'Brien, T. P., Witasse, O., Mishev, A. L., Nieminen, P., Daly, E., Kalegaev, V., Vlasova, N., Borisov, S., Benck, S., Poivey, C., Cyamukungu, M., Mazur, J., Heynderickx, D., Sandberg, I., Berger, T., Usoskin, I. G., Paassilta, M., Vainio, R., Straube, U., Müller, D., Sánchez-Cano, B., Hassler, D., Praks, J., Niemelä, P., Leppinen, H., Punkkinen, A., Aminalragia-Giamini, S., Nagatsuma, T. In Situ Data and Effect Correlation During September 2017 Solar Particle Event. *Space Weather*, 17(1):99–117, 2019. doi:10.1029/2018SW001936

Jiggens, P., Heynderickx, D., Sandberg, I., Truscott, P., Raukunen, O., Vainio, R. Updated Model of the Solar Energetic Proton Environment in Space. *Journal of Space Weather and Space Climate*, 8:A31, 2018a. doi:10.1051/swsc/2018010

Jiggens, P., Varotsou, A., Truscott, P., Heynderickx, D., Lei, F., Evans, H., Daly, E. The Solar Accumulated and Peak Proton and Heavy Ion Radiation Environment (SAPPHIRE) Model. *IEEE Transactions on Nuclear Science*, 65(2):698–711, 2018b. doi:10.1109/TNS.2017.2786581

Jiggens, P. T. A., Gabriel, S. B., Heynderickx, D., Crosby, N., Glover, A., Hilgers, A. ESA SEPEM Project: Peak Flux and Fluence Model. *IEEE Transactions on Nuclear Science*, 59(4):1066–1077, 2012. ISSN 0018-9499. doi:10.1109/TNS.2012.2198242

Jokipii, J. R. The physics of cosmic-ray modulation. *Advances in Space Research*, 9(12):105–119, 1989. doi:10.1016/0273-1177(89)90317-7

Jokipii, J. R., Levy, E. H., Hubbard, W. B. Effects of particle drift on cosmic-ray transport. I. General properties, application to solar modulation. *Astrophysical Journal*, 213:861–868, 1977. doi:10.1086/155218

Joselyn, J. A., Anderson, J. B., Coffey, H., Harvey, K., Hathaway, D., Heckman, G., Hildner, E., Mende, W., Schatten, K., Thompson, R., Thomson, A. W. P., White, O. R. Panel achieves consensus prediction of solar cycle 23. *EOS Transactions of the American Geophysical Union*, 78(20):205–205, 1997. doi:10.1029/97EO00136

Kahler, S. W. Radio burst characteristics of solar proton flares. *Astrophysical Journal*, 261:710–719, 1982. doi:10.1086/160381

Kahler, S. W. Solar flares and coronal mass ejections. *Annual Review of Astronomy and Astrophysics*, 30:113–141, 1992. doi:10.1146/annurev.aa.30.090192.000553

Kahler, S. W., Hildner, E., Van Hollebeke, M. A. I. Promt solar proton events and coronal mass ejections. *Solar Physics*, 57(2):429–443, 1978. doi:10.1007/BF00160116

Kahler, S. W., Lin, R. P., Reames, D. V., Stone, R. G., Liggett, M. Characteristics of solar coronal source regions producing ^{3}He-rich particle events. *Solar Physics*, 107(2):385–394, 1987. doi:10.1007/BF00152032

Kahler, S. W., Reames, D. V., Sheeley, J., N. R. Coronal Mass Ejections Associated with Impulsive Solar Energetic Particle Events. *Astrophysical Journal*, 562(1):558–565, 2001. doi:10.1086/323847

Kahler, S. W., Sheeley, J., N. R., Howard, R. A., Michels, D. J., Koomen, M. J., McGuire, R. E., von Rosenvinge, T. T., Reames, D. V. Associations beteen coronal mass ejections and solar energetic proton events. *Journal of Geophysical Research*, 89(A11):9683–9694, 1984. doi:10.1029/JA089iA11p09683

Kaiser, M. L., Kucera, T. A., Davila, J. M., St. Cyr, O. C., Guhathakurta, M., Christian, E. The STEREO Mission: An Introduction. *Space Science Reviews*, 136:5–16, 2008. doi:10.1007/s11214-007-9277-0

Kakad, B., Kakad, A., Ramesh, D. S., Lakhina, G. S. Diminishing activity of recent solar cycles (22-24) and their impact on geospace. *Journal of Space Weather and Space Climate*, 9:A1, 2019. doi:10.1051/swsc/2018048

Käpylä, M. J., Käpylä, P. J., Olspert, N., Brandenburg, A., Warnecke, J., Karak, B. B., Pelt, J. Multiple dynamo modes as a mechanism for long-term solar activity variations. *Astronomy & Astrophysics*, 589:A56, 2016. doi:10.1051/0004-6361/201527002

Kennedy, A. R. Biological effects of space radiation and development of effective countermeasures. *Life Sciences in Space Research*, 1:10–43, 2014. doi:10.1016/j.lssr.2014.02.004

Kieda, D., Salamon, M., Dingus, B., (editors). *Proceedings of the 26th International Cosmic Ray Conference*. Salt Lake City, Utah, USA, 1999

Kilpua, E. K. J., Balogh, A., von Steiger, R., Liu, Y. D. Geoeffective Properties of Solar Transients and Stream Interaction Regions. *Space Science Reviews*, 212(3-4):1271–1314, 2017. doi:10.1007/s11214-017-0411-3

Kimura, H. Sun-Spots and Faculæ, On the harmonic analysis of sun-spot relative numbers. *Monthly Notices of the Royal Astronomical Society*, 73:543, 1913. doi:10.1093/mnras/73.7.543

King, J. H. Solar Proton Fluences for 1977-1983 Space Missions. *Journal of Spacecraft and Rockets*, 11:401, 1974. doi:10.2514/3.62088

Kintner, P. M., Ledvina, B. M., de Paula, E. R. GPS and ionospheric scintillations. *Space Weather*, 5(9):09003, 2007. doi:10.1029/2006SW000260

Kitiashvili, I. N. Application of Synoptic Magnetograms to Global Solar Activity Forecast. *Astrophysical Journal*, 890(1):36, 2020. doi:10.3847/1538-4357/ab64e7

Klecker, B., Hovestadt, D., Scholer, M., Gloeckler, G., Ipavich, F. M., Fan, C. Y., Fisk, L. A. Direct determination of the ionic charge distribution of helium and iron in He-3-rich solar energetic particle events. *Astrophysical Journal*, 281:458–462, 1984. doi:10.1086/162117

Klein, K.-L., Dalla, S. Acceleration and Propagation of Solar Energetic Particles. *Space Science Reviews*, 212(3):1107–1136, 2017. ISSN 1572-9672. doi:10.1007/s11214-017-0382-4

Knipp, D. J., Ramsay, A. C., Beard, E. D., Boright, A. L., Cade, W. B., Hewins, I. M., McFadden, R. H., Denig, W. F., Kilcommons, L. M., Shea, M. A., Smart, D. F. The May 1967 great storm and radio disruption event: Extreme space weather and extraordinary responses. *Space Weather*, 14(9):614–633, 2016. doi:10.1002/2016SW001423

Knizhnik, K., Swisdak, M., Drake, J. F. The Acceleration of Ions in Solar Flares during Magnetic Reconnection. *Astrophysical Journal, Letters*, 743(2):L35, 2011. doi:10.1088/2041-8205/743/2/L35

Kocharov, L., Torsti, J. Hybrid Solar Energetic Particle Events Observed on Board Soho. *Solar Physics*, 207:149–157, 2002. doi:10.1023/A:1015540311183

Koskinen, H. E. J. *Physics of Space Storms: From the Solar Surface to the Earth*. Springer Berlin Heidelberg, Berlin, Germany, 2011. ISBN 978-3-642-00310-3

Koskinen, H. E. J., Baker, D. N., Balogh, A., Gombosi, T., Veronig, A., von Steiger, R. Achievements and Challenges in the Science of Space Weather. *Space Science Reviews*, 212(3-4):1137–1157, 2017. doi:10.1007/s11214-017-0390-4

Koskinen, H. E. J., Huttunen, K. E. J. Geoeffectivity of Coronal Mass Ejections. *Space Science Reviews*, 124(1-4):169–181, 2006. doi:10.1007/s11214-006-9103-0

Kreplin, R. W., Chubb, T. A., Friedmann, H. X-Ray and Lyman-Alpha Emission from the Sun as Measured from the NRL SR-1 Satellite. *Journal of Geophysical Research*, 67(6):2231–2253, 1962. doi:10.1029/JZ067i006p02231

Kuznetsov, N. V., Nymmik, R. A., Panasyuk, M. I. Models of solar energetic particle fluxes: The main requirements and the development prospects. *Advances in Space Research*, 36(10):2003–2011, 2005. doi:10.1016/j.asr.2004.09.021

Labonville, F., Charbonneau, P., Lemerle, A. A Dynamo-based Forecast of Solar Cycle 25. *Solar Physics*, 294(6):82, 2019. doi:10.1007/s11207-019-1480-0

Lai, S. T., Cahoy, K., Lohmeyer, W., Carlton, A., Aniceto, R., Minow, J. Chapter 16 - deep dielectric charging and spacecraft anomalies. In N. Buzulukova (editor), *Extreme Events in Geospace*, pages 419–432. Elsevier, 2018. ISBN 978-0-12-812700-1. doi:10.1016/B978-0-12-812700-1.00016-9

Lamy, P. L., Floyd, O., Boclet, B., Wojak, J., Gilardy, H., Barlyaeva, T. Coronal Mass Ejections over Solar Cycles 23 and 24. *Space Science Reviews*, 215(5):39, 2019. doi:10.1007/s11214-019-0605-y

Lanzerotti, L. J. *Space weather effects on technologies*, pages 11–22. In Song et al. (2001), 2001

Lanzerotti, L. J. *Space weather effects on communications*, pages 247–268. In Bothmer and Daglis (2007), 2007

Lanzerotti, L. J. Space Weather: Historical and Contemporary Perspectives. *Space Science Reviews*, 212(3-4):1253–1270, 2017. doi:10.1007/s11214-017-0408-y

Lee, C. O., Luhmann, J. G., Zhao, X. P., Liu, Y., Riley, P., Arge, C. N., Russell, C. T., de Pater, I. Effects of the Weak Polar Fields of Solar Cycle 23: Investigation Using OMNI for the STEREO Mission Period. *Solar Physics*, 256(1-2):345–363, 2009. doi:10.1007/s11207-009-9345-6

Lee, M. A. Coupled hydromagnetic wave excitation and ion acceleration at interplanetary traveling shocks. *Journal of Geophysical Research*, 88(A8):6109–6120, 1983. doi:10.1029/JA088iA08p06109

Lee, M. A. Coupled Hydromagnetic Wave Excitation and Ion Acceleration at an Evolving Coronal/Interplanetary Shock. *Astrophysical Journal, Supplement Series*, 158(1):38–67, 2005. doi:10.1086/428753

Lee, M. A., Mewaldt, R. A., Giacalone, J. Shock Acceleration of Ions in the Heliosphere. *Space Science Reviews*, 173(1-4):247–281, 2012. doi:10.1007/s11214-012-9932-y

Leske, R. A., Cummings, J. R., Mewaldt, R. A., Stone, E. C., von Rosenvinge, T. T. Measurements of the Ionic Charge States of Solar Energetic Particles Using the Geomagnetic Field. *Astrophysical Journal, Letters*, 452:L149, 1995. doi:10.1086/309718

Lett, J. T., Lee, A. C., Cox, A. B. Risks of radiation cataracts from interplanetary space missions. *Acta Astronautica*, 32(11):739–748, 1994. doi:10.1016/0094-5765(94)90169-4

Leussu, R., Usoskin, I. G., Arlt, R., Mursula, K. Inconsistency of the Wolf sunspot number series around 1848. *Astronomy & Astrophysics*, 559:A28, 2013. doi:10.1051/0004-6361/201322373

Liu, S., Petrosian, V., Mason, G. M. Stochastic Acceleration of ^{3}He and ^{4}He by Parallel Propagating Plasma Waves. *Astrophysical Journal, Letters*, 613:L81–L84, 2004. doi:10.1086/425070

Liu, S., Petrosian, V., Mason, G. M. Stochastic Acceleration of ^{3}He and ^{4}He in Solar Flares by Parallel-propagating Plasma Waves: General Results. *Astrophysical Journal*, 636:462–474, 2006. doi:10.1086/497883

Lovell, B. The Emergence of Radio Astronomy in the U.K. after World-War. *Quarterly Journal of the Royal Astronomical Society*, 28:1, 1987

Lu, E. T., Hamilton, R. J. Avalanches and the Distribution of Solar Flares. *Astrophysical Journal, Letters*, 380:L89, 1991. doi:10.1086/186180

Luhn, A., Klecker, B., Hovestadt, D., Möbius, E. The mean ionic charge of silicon in He-3-rich solar flares. *Astrophysical Journal*, 317:951–955, 1987. doi:10.1086/165343

Luntama, J., Glover, A., Hilgers, A. M. ESA SSA Programme in support of Space Weather forecasting. In *AGU Fall Meeting Abstracts*, volume 2010, pages SM53B–05. 2010

Mann, I. R., Di Pippo, S., Opgenoorth, H. J., Kuznetsova, M., Kendall, D. J. International Collaboration Within the United Nations Committee on the Peaceful Uses of Outer Space: Framework for International Space Weather Services (2018-2030). *Space Weather*, 16(5):428–433, 2018. doi:10.1029/2018SW001815

Marconi, G. Radio Communication. *Proceedings of the Institute of Radio Engineers*, 16(1):40–69, 1928. doi:10.1109/JRPROC.1928.221288

Mason, G. M., Mazur, J. E., Dwyer, J. R. ^{3}He Enhancements in Large Solar Energetic Particle Events. *Astrophysical Journal, Letters*, 525:L133–L136, 1999. doi:10.1086/312349

Mason, G. M., Mazur, J. E., Dwyer, J. R., Jokipii, J. R., Gold, R. E., Krimigis, S. M. Abundances of Heavy and Ultraheavy Ions in ^{3}He-rich Solar Flares. *Astrophysical Journal*, 606:555–564, 2004. doi:10.1086/382864

Mason, G. M., Reames, D. V., Klecker, B., Hovestadt, D., von Rosenvinge, T. T. The Heavy-Ion Compositional Signature in ^{3}He-rich Solar Particle Events. *Astrophysical Journal*, 303:849, 1986. doi:10.1086/164133

Matthiä, D., Berger, T., Mrigakshi, A. I., Reitz, G. A ready-to-use galactic cosmic ray model. *Advances in Space Research*, 51(3):329–338, 2013. doi:10.1016/j.asr.2012.09.022

Maunder, E. W. Prof. Spoerer's researches on Sun-spots. *Monthly Notices of the Royal Astronomical Society*, 50:251, 1890. doi:10.1093/mnras/50.4.251

Mavromichalaki, H., Papaioannou, A., Plainaki, C., Sarlanis, C., Souvatzoglou, G., Gerontidou, M., Papailiou, M., Eroshenko, E., Belov, A., Yanke, V., Flückiger, E. O., Bütikofer, R., Parisi, M., Storini, M., Klein, K. L., Fuller, N., Steigies, C. T., Rother, O. M., Heber, B., Wimmer-Schweingruber, R. F., Kudela, K., Strharsky, I., Langer, R., Usoskin, I., Ibragimov, A., Chilingaryan, A., Hovsepyan, G., Reymers, A., Yeghikyan, A., Kryakunova, O., Dryn, E., Nikolayevskiy, N., Dorman, L., Pustil'Nik, L. Applications and usage of the real-time Neutron Monitor Database. *Advances in Space Research*, 47(12):2210–2222, 2011. doi:10.1016/j.asr.2010.02.019

Mayaud, P.-N. The aa indices: A 100-year series characterizing the magnetic activity. *Journal of Geophysical Research*, 77(34):6870, 1972. doi:10.1029/JA077i034p06870

Mazur, J. E., Mason, G. M., Klecker, B., McGuire, R. E. The Energy Spectra of Solar Flare Hydrogen, Helium, Oxygen, and Iron: Evidence for Stochastic Acceleration. *Astrophysical Journal*, 401:398, 1992. doi:10.1086/172071

Mazur, J. E., Mason, G. M., Klecker, B., McGuire, R. E. The Abundances of Hydrogen, Helium, Oxygen, and Iron Accelerated in Large Solar Particle Events. *Astrophysical Journal*, 404:810, 1993. doi:10.1086/172336

McComas, D. J., Angold, N., Elliott, H. A., Livadiotis, G., Schwadron, N. A., Skoug, R. M., Smith, C. W. Weakest Solar Wind of the Space Age and the Current "Mini" Solar Maximum. *Astrophysical Journal*, 779(1):2, 2013. doi:10.1088/0004-637X/779/1/2

McComas, D. J., Ebert, R. W., Elliott, H. A., Goldstein, B. E., Gosling, J. T., Schwadron, N. A., Skoug, R. M. Weaker solar wind from the polar coronal holes and the whole Sun. *Geophysical Research Letters*, 35(18):L18103, 2008. doi:10.1029/2008GL034896

McCracken, K. G., Dreschhoff, G. A. M., Zeller, E. J., Smart, D. F., Shea, M. A. Solar cosmic ray events for the period 1561-1994: 1. Identification in polar ice, 1561-1950. *Journal of Geophysical Research*, 106(A10):21585–21598, 2001. doi:10.1029/2000JA000237

McCracken, K. G., Moraal, H., Shea, M. A. The high-energy impulsive ground-level enhancement. *Astrophysical Journal*, 761(2):101, 2012. doi:10.1088/0004-637X/761/2/101

McCracken, K. G., Moraal, H., Stoker, P. H. Investigation of the multiple-component structure of the 20 January 2005 cosmic ray ground level enhancement. *Journal of Geophysical Research*, 113(A12):A12101, 2008. doi:10.1029/2007JA012829

McGuire, R. E., von Rosenvinge, T. T., McDonald, F. B. The composition of solar energetic particles. *Astrophysical Journal*, 301:938–961, 1986. doi:10.1086/163958

McIlwain, C. E. Coordinates for Mapping the Distribution of Magnetically Trapped Particles. *Journal of Geophysical Research*, 66(11):3681–3691, 1961. doi:10.1029/JZ066i011p03681

McIntosh, S. W., Chapman, S., Leamon, R. J., Egeland, R., Watkins, N. W. Overlapping Magnetic Activity Cycles and the Sunspot Number: Forecasting Sunspot Cycle 25 Amplitude. *Solar Physics*, 295(12):163, 2020. doi:10.1007/s11207-020-01723-y

McNish, A. G. The magnetic storm of March 24, 1940. *Terrestrial Magnetism and Atmospheric Electricity*, 45(3):359, 1940. doi:10.1029/TE045i003p00359

McNish, A. G., Lincoln, J. V. Prediction of sunspot numbers. *Transactions, American Geophysical Union*, 30(5):673–685, 1949. doi:10.1029/TR030i005p00673

McNulty, P. J. Single-event effects experienced by astronauts and microelectronic circuits flown in space. *IEEE Transactions on Nuclear Science*, 43(2):475–482, 1996. doi:10.1109/23.490894

Meloni, A., Lanzerotti, L. J., Gregori, G. P. Induction of Currents in Long Submarine Cables by Natural Phenomena (Paper 2R1945). *Reviews of Geophysics and Space Physics*, 21:795, 1983. doi:10.1029/RG021i004p00795

Mewaldt, R. A., Cohen, C. M. S., Labrador, A. W., Leske, R. A., Mason, G. M., Desai, M. I., Looper, M. D., Mazur, J. E., Selesnick, R. S., Haggerty, D. K. Proton, helium, and electron spectra during the large solar particle events of October-November 2003. *Journal of Geophysical Research*, 110:A09S18, 2005. doi:10.1029/2005JA011038

Mewaldt, R. A., Cohen, C. M. S., Mason, G. M., von Rosenvinge, T. T., Li, G., Smith, C. W., Vourlidas, A. Investigating the Causes of Solar-Cycle Variations in Solar Energetic Particle Fluences and Composition. In *Proceedings of the 34th International Cosmic Ray Conference*. The Hague, The Netherlands, 2015

Mewaldt, R. A., Davis, A. J., Lave, K. A., Leske, R. A., Stone, E. C., Wiedenbeck, M. E., Binns, W. R., Christian, E. R., Cummings, A. C., de Nolfo, G. A., Israel, M. H., Labrador, A. W., von Rosenvinge, T. T. Record-setting Cosmic-ray Intensities in 2009 and 2010. *Astrophysical Journal, Letters*, 723(1):L1–L6, 2010. doi:10.1088/2041-8205/723/1/L1

Mewaldt, R. A., Li, G., Hu, J., Cohen, C. M. S. What is Causing the Deficit of High-Energy Solar Particles in Solar Cycle 24. In *Proceedings of the 35th International Cosmic Ray Conference*. Bexco, Busan, Korea, 2017

Mewaldt, R. A., Looper, M. D., Cohen, C. M. S., Haggerty, D. K., Labrador, A. W., Leske, R. A., Mason, G. M., Mazur, J. E., von Rosenvinge, T. T. Energy Spectra, Composition, and Other Properties of Ground-Level Events During Solar Cycle 23. *Space Science Reviews*, 171:97–120, 2012. doi:10.1007/s11214-012-9884-2

Meyer, J.-P. The baseline composition of solar energetic particles. *Astrophysical Journal, Supplement Series*, 57:151–171, 1985. doi:10.1086/191000

Michalek, G., Gopalswamy, N., Yashiro, S. On the Coronal Mass Ejection Detection Rate during Solar Cycles 23 and 24. *Astrophysical Journal*, 880(1):51, 2019. doi:10.3847/1538-4357/ab26a7

Millan, R. M., Baker, D. N. Acceleration of Particles to High Energies in Earth's Radiation Belts. *Space Science Reviews*, 173(1-4):103–131, 2012. doi:10.1007/s11214-012-9941-x

Miller, J. A. Particle Acceleration in Impulsive Solar Flares. *Space Science Reviews*, 86:79–105, 1998. doi:10.1023/A:1005066209536

Mironova, I. A., Aplin, K. L., Arnold, F., Bazilevskaya, G. A., Harrison, R. G., Krivolutsky, A. A., Nicoll, K. A., Rozanov, E. V., Turunen, E., Usoskin, I. G. Energetic Particle Influence on the Earth's Atmosphere. *Space Science Reviews*, 194(1-4):1–96, 2015. doi:10.1007/s11214-015-0185-4

Miroshnichenko, L. I. Retrospective analysis of GLEs and estimates of radiation risks. *Journal of Space Weather and Space Climate*, 8:A52, 2018. doi:10.1051/swsc/2018042

Mishev, A., Usoskin, I., Raukunen, O., Paassilta, M., Valtonen, E., Kocharov, L., Vainio, R. First Analysis of Ground-Level Enhancement (GLE) 72 on 10 September 2017: Spectral and Anisotropy Characteristics. *Solar Physics*, 293(10):136, 2018. doi:10.1007/s11207-018-1354-x

Morrison, P. Solar Origin of Cosmic-Ray Time Variations. *Physical Review*, 101(4):1397–1404, 1956. doi:10.1103/PhysRev.101.1397

Muñoz-Jaramillo, A., Balmaceda, L. A., DeLuca, E. E. Using the Dipolar and Quadrupolar Moments to Improve Solar-Cycle Predictions Based on the Polar Magnetic Fields. *Physical Review Letters*, 111(4):041106, 2013. doi:10.1103/PhysRevLett.111.041106

Mursula, K., Manoharan, P., Nandy, D., Tanskanen, E., Verronen, P. Long-term solar activity and its implications to the heliosphere, geomagnetic activity, and the Earth's climate. Preface to the Special Issue on Space Climate. *Journal of Space Weather and Space Climate*, 3:A21, 2013. doi:10.1051/swsc/2013043

Mursula, K., Usoskin, I. G., Kovaltsov, G. A. Persistent 22-year cycle in sunspot activity: Evidence for a relic solar magnetic field. *Solar Physics*, 198(1):51–56, 2001. doi:10.1023/A:1005218414790

Mursula, K., Usoskin, I. G., Maris, G. Introduction to Space Climate. *Advances in Space Research*, 40(7):885–887, 2007. doi:10.1016/j.asr.2007.07.046

Nagovitsyn, Y. A., Nagovitsyna, E. Y., Makarova, V. V. The Gnevyshev-Ohl rule for physical parameters of the solar magnetic field: The 400-year interval. *Astronomy Letters*, 35(8):564–571, 2009. doi:10.1134/S1063773709080064

Neugebauer, M. Pioneers of space physics: A career in the solar wind. *Journal of Geophysical Research*, 102(A12):26887–26894, 1997. doi:10.1029/97JA02444

Neugebauer, M., Snyder, C. W. Solar Plasma Experiment. *Science*, 138(3545):1095–1097, 1962. doi:10.1126/science.138.3545.1095-a

Ng, C. K., Reames, D. V. Shock Acceleration of Solar Energetic Protons: The First 10 Minutes. *Astrophysical Journal, Letters*, 686(2):L123, 2008. doi:10.1086/592996

Nymmik, R. A. Radiation environment induced by cosmic ray particle fluxes in the international space station orbit according to recent galactic and solar cosmic ray models. *Advances in Space Research*, 21:1689–1698, 1998. doi:10.1016/S0273-1177(98)00015-5

Nymmik, R. A. Probabilistic model for fluences and peak fluxes of solar energetic particles. *Radiation Measurements*, 30(3):287–296, 1999a. ISSN 1350-4487. doi:10.1016/S1350-4487(99)00065-7

Nymmik, R. A. Relationships among solar activity SEP occurrence frequency, and solar energetic particle event distribution function. In Kieda et al. (1999)

Nymmik, R. A. SEP Event Distribution Function as Inferred from Spaceborne Measurements and Lunar Rock Isotopic Data. In Kieda et al. (1999)

Nymmik, R. A. Improved environment radiation models. *Advances in Space Research*, 40(3):313–320, 2007. doi:10.1016/j.asr.2006.12.028

Nymmik, R. A., Panasyuk, M. I., Suslov, A. A. Galactic cosmic ray flux simulation and prediction. *Advances in Space Research*, 17(2):19–30, 1996. doi:10.1016/0273-1177(95)00508-C

Oh, S., Bieber, J. W., Evenson, P., Clem, J., Yi, Y., Kim, Y. Record neutron monitor counting rates from galactic cosmic rays. *Journal of Geophysical Research*, 118(9):5431–5436, 2013. doi:10.1002/jgra.50544

Ohl, A. I. Wolf's number prediction for the maximum of the cycle 20. *Byulletin Solnechnye Dannye Akademie Nauk*, 12:84, 1966

Ohl, A. I., Ohl, G. I. A new method of very long-term prediction of solar activity. In R. Donnelly (editor), *Solar-Terrestrial Predictions Proceedings*, pages 258–263. Boulder, Colorado, USA, 1979

O'Neill, P. M. Badhwar - O'Neill galactic cosmic ray model update based on advanced composition explorer (ACE) energy spectra from 1997 to present. *Advances in Space Research*, 37(9):1727–1733, 2006. doi:10.1016/j.asr.2005.02.001

O'Neill, P. M., Golge, S., Slaba, T. C. Badhwar - O'Neill 2014 Galactic Cosmic Ray Flux Model Description. Technical Report NASA/TP-2015-218569, NASA Johnson Space Center, Houston, Texas, USA, 2015

Onsager, T., Grubb, R., Kunches, J., Matheson, L., Speich, D., Zwickl, R., Sauer, H. Operational uses of the GOES energetic particle detectors. In E. R. Washwell (editor), *GOES-8 and Beyond*, Proceedings of SPIE, pages 281–290. Denver, Colorado, USA, 1996. doi:10.1117/12.254075

Ossendrijver, M. The solar dynamo. *The Astronomy and Astrophysics Review*, 11(4):287–367, 2003. doi:10.1007/s00159-003-0019-3

Paassilta, M., Raukunen, O., Vainio, R., Valtonen, E., Papaioannou, A., Siipola, R., Riihonen, E., Dierckxsens, M., Crosby, N., Malandraki, O., Heber, B., Klein, K.-L. Catalogue of 55-80 MeV solar proton events extending through solar cycles 23 and 24. *Journal of Space Weather and Space Climate*, 7:A14, 2017. doi:10.1051/swsc/2017013

Pallavicini, R., Serio, S., Vaiana, G. S. A survey of soft X-ray limb flare images: the relation between their structure in the corona and other physical parameters. *Astrophysical Journal*, 216:108–122, 1977. doi:10.1086/155452

Papaioannou, A., Sandberg, I., Anastasiadis, A., Kouloumvakos, A., Georgoulis, M. K., Tziotziou, K., Tsiropoula, G., Jiggens, P., Hilgers, A. Solar flares, coronal mass ejections and solar energetic particle event characteristics. *Journal of Space Weather and Space Climate*, 6(27):A42, 2016. doi:10.1051/swsc/2016035

Parker, E. N. The Gross Dynamics of a Hydromagnetic Gas Cloud. *Astrophysical Journal, Supplement Series*, 3:51, 1957. doi:10.1086/190032

Parker, E. N. Dynamics of the Interplanetary Gas and Magnetic Fields. *Astrophysical Journal*, 128:664, 1958. doi:10.1086/146579

Parker, E. N. The passage of energetic charged particles through interplanetary space. *Planetary and Space Science*, 13(1):9–49, 1965. doi:10.1016/0032-0633(65)90131-5

Pease, R. L. Total-dose issues for microelectronics in space systems. *IEEE Transactions on Nuclear Science*, 3(2):442–452, 1996. doi:10.1109/23.490892

Pesnell, W. D. Predictions of Solar Cycle 24. *Solar Physics*, 252(1):209–220, 2008. doi:10.1007/s11207-008-9252-2

Pesnell, W. D. Solar Cycle Predictions (Invited Review). *Solar Physics*, 281(1):507–532, 2012. doi:10.1007/s11207-012-9997-5

Pesnell, W. D., Schatten, K. H. An Early Prediction of the Amplitude of Solar Cycle 25. *Solar Physics*, 293(7):112, 2018. doi:10.1007/s11207-018-1330-5

Pesnell, W. D., Thompson, B. J., Chamberlin, P. C. The Solar Dynamics Observatory (SDO). *Solar Physics*, 275(1-2):3–15, 2012. doi:10.1007/s11207-011-9841-3

Petrie, G. J. D. Solar Magnetic Activity Cycles, Coronal Potential Field Models and Eruption Rates. *Astrophysical Journal*, 768(2):162, 2013. doi:10.1088/0004-637X/768/2/162

Petrie, G. J. D. Solar Magnetism in the Polar Regions. *Living Reviews in Solar Physics*, 12(1):5, 2015. doi:10.1007/lrsp-2015-5

Petrie, G. J. D., Petrovay, K., Schatten, K. Solar Polar Fields and the 22-Year Activity Cycle: Observations and Models. *Space Science Reviews*, 186(1-4):325–357, 2014. doi:10.1007/s11214-014-0064-4

Petrosian, V. Stochastic Acceleration by Turbulence. *Space Science Reviews*, 173(1-4):535–556, 2012. doi:10.1007/s11214-012-9900-6

Petrovay, K. Solar cycle prediction. *Living Reviews in Solar Physics*, 17(1):2, 2020. doi:10.1007/s41116-020-0022-z

Pevtsov, A. A., Tlatova, K. A., Pevtsov, A. A., Heikkinen, E., Virtanen, I., Karachik, N. V., Bertello, L., Tlatov, A. G., Ulrich, R., Mursula, K. Reconstructing solar magnetic fields from historical observations. V. Sunspot magnetic field measurements at Mount Wilson Observatory. *Astronomy & Astrophysics*, 628:A103, 2019. doi:10.1051/0004-6361/201834985

Pirjola, R. Geomagnetically induced currents during magnetic storms. *IEEE Transactions on Plasma Science*, 28(6):1867–1873, 2000. doi:10.1109/27.902215

Poluianov, S. V., Usoskin, I. G., Mishev, A. L., Shea, M. A., Smart, D. F. GLE and Sub-GLE Redefinition in the Light of High-Altitude Polar Neutron Monitors. *Solar Physics*, 292(11):176, 2017. doi:10.1007/s11207-017-1202-4

Potgieter, M. S. Solar Modulation of Cosmic Rays. *Living Reviews in Solar Physics*, 10:3, 2013. doi:10.12942/lrsp-2013-3

Priest, E. R., Forbes, T. G. The magnetic nature of solar flares. *The Astronomy and Astrophysics Review*, 10(4):313–377, 2002. doi:10.1007/s001590100013

Rawat, R., Echer, E., Gonzalez, W. D. How Different Are the Solar Wind-Interplanetary Conditions and the Consequent Geomagnetic Activity During the Ascending and Early Descending Phases of the Solar Cycles 23 and 24? *Journal of Geophysical Research*, 123(8):6621–6638, 2018. doi:10.1029/2018JA025683

Reames, D. V. Bimodal abundances in the energetic particles of solar and interplanetary origin. *Astrophysical Journal, Letters*, 330:L71–L75, 1988. doi:10.1086/185207

Reames, D. V. Coronal abundances determined from energetic particles. *Advances in Space Research*, 15:41–51, 1995

Reames, D. V. The Two Sources of Solar Energetic Particles. *Space Science Reviews*, 175:53–92, 2013. doi:10.1007/s11214-013-9958-9

Reames, D. V., Dennis, B. R., Stone, R. G., Lin, R. P. X-Ray and Radio Properties of Solar 3He-rich Events. *Astrophysical Journal*, 327:998, 1988. doi:10.1086/166257

Reames, D. V., Meyer, J. P., von Rosenvinge, T. T. Energetic-particle abundances in impulsive solar flare events. *Astrophysical Journal, Supplement Series*, 90:649–667, 1994. doi:10.1086/191887

Reames, D. V., Stone, R. G. The Identification of Solar 3He-rich Events and the Study of Particle Acceleration at the Sun. *Astrophysical Journal*, 308:902, 1986. doi:10.1086/164560

Reames, D. V., von Rosenvinge, T. T., Lin, R. P. Solar He-3-rich events and nonrelativistic electron events - A new association. *Astrophysical Journal*, 292:716–724, 1985. doi:10.1086/163203

Reber, G. Cosmic Static. *Astrophysical Journal*, 100:279, 1944. doi:10.1086/144668

Reeves, G. D., Friedel, R. H. W., Belian, R. D., Meier, M. M., Henderson, M. G., Onsager, T., Singer, H. J., Baker, D. N., Li, X., Blake, J. B. The relativistic electron response at geosynchronous orbit during the January 1997 magnetic storm. *Journal of Geophysical Research*, 103(A8):17559–17570, 1998. doi:10.1029/97JA03236

Richardson, I. G. Geomagnetic activity during the rising phase of solar cycle 24. *Journal of Space Weather and Space Climate*, 3:A08, 2013. doi:10.1051/swsc/2013031

Richardson, I. G., Cane, H. V. Solar wind drivers of geomagnetic storms during more than four solar cycles. *Journal of Space Weather and Space Climate*, 2:A01, 2012. doi:10.1051/swsc/2012001

Richardson, I. G., Cliver, E. W., Cane, H. V. Sources of geomagnetic storms for solar minimum and maximum conditions during 1972-2000. *Geophysical Research Letters*, 28(13):2569–2572, 2001. doi:10.1029/2001GL013052

Richardson, I. G., von Rosenvinge, T. T., Cane, H. V. 25 MeV solar proton events in Cycle 24 and previous cycles. *Advances in Space Research*, 60(4):755–767, 2017. doi:10.1016/j.asr.2016.07.035

Robinson, Z. D., Adams, J. H., Fisher, J. H., Nonnast, J. H., Terry, D. C. Mission Specific Solar Radiation Environment Model (MSSREM): Peak Flux Model. *Space Weather*, 18(8):e02361, 2020. doi:10.1029/2019SW002361

Ron, E. Ionizing Radiation and Cancer Risk: Evidence from Epidemiology. *Radiation Research*, 150(5):30, 1998. doi:10.2307/3579806

Root, H. G. Earth-current effects on communication-cable power subsystems. *IEEE Transactions on Electromagnetic Compatibility*, EMC-21(2):87–92, 1979. doi:10.1109/TEMC.1979.303750

Rosenqvist, L., Hilgers, A., Evans, H., Daly, E., Hapgood, M., Stamper, R., Zwickl, R., Bourdarie, S., Boscher, D. Toolkit for Updating Interplanetary Proton Cumulated Fluence Models. *Journal of Spacecraft and Rockets*, 42:1077–1090, 2005. doi:10.2514/1.8211

Roth, I., Temerin, M. Enrichment of ^{3}He and Heavy Ions in Impulsive Solar Flares. *Astrophysical Journal*, 477(2):940–957, 1997. doi:10.1086/303731

Sandberg, I., Daglis, I. A., Heynderickx, D., Truscott, P., Hands, A., Evans, H., Nieminen, P. Development and Validation of the Electron Slot Region Radiation Environment Model. *IEEE Transactions on Nuclear Science*, 61(4):1656–1662, 2014. doi:10.1109/TNS.2014.2304982

Sandroos, A., Vainio, R. Simulation Results for Heavy Ion Spectral Variability in Large Gradual Solar Energetic Particle Events. *Astrophysical Journal, Letters*, 662:L127–L130, 2007. doi:10.1086/519378

Sandroos, A., Vainio, R. Reacceleration of Flare Ions in Coronal and Interplanetary Shock Waves. *Astrophysical Journal, Supplement Series*, 181:183–196, 2009. doi:10.1088/0067-0049/181/1/183

Sargent, H. H. A prediction for the next sunspot cycle. In *28th IEEE Vehicular Technology Conference*, pages 490–496. Denver, Colorado, USA, 1978. doi:10.1109/VTC.1978.1622589

Schatten, K. H., Hedin, A. E. A dynamo theory prediction for solar cycle 22: Sunspot number, radio flux, exospheric temperature, and total density at 400 km. *Geophysical Research Letters*, 11(9):873–876, 1984. doi:10.1029/GL011i009p00873

Schatten, K. H., Scherrer, P. H., Svalgaard, L., Wilcox, J. M. Using Dynamo Theory to predict the sunspot number during Solar Cycle 21. *Geophysical Research Letters*, 5(5):411–414, 1978. doi:10.1029/GL005i005p00411

Scherrer, P. H., Wilcox, J. M., Svalgaard, L., Duvall, J., T. L., Dittmer, P. H., Gustafson, E. K. The mean magnetic field of the Sun: observations at Stanford. *Solar Physics*, 54(2):353–361, 1977. doi:10.1007/BF00159925

Schrijver, C. J., Kauristie, K., Aylward, A. D., Denardini, C. M., Gibson, S. E., Glover, A., Gopalswamy, N., Grande, M., Hapgood, M., Heynderickx, D., Jakowski, N., Kalegaev, V. V., Lapenta, G., Linker, J. A., Liu, S., Mandrini, C. H., Mann, I. R., Nagatsuma, T., Nandy, D., Obara, T., O'Brien, T. P., Onsager, T., Opgenoorth, H. J., Terkildsen, M., Valladares, C. E., Vilmer, N. Understanding space weather to shield society: A global road map for 2015-2025 commissioned by COSPAR and ILWS. *Advances in Space Research*, 55(12):2745–2807, 2015. doi:10.1016/j.asr.2015.03.023

Schwabe, H. Sonnenbeobachtungen im Jahre 1843. Von Herrn Hofrath Schwabe in Dessau. *Astronomische Nachrichten*, 21:233, 1844. doi:10.1002/asna.18440211505

Schwadron, N. A., Cooper, J. F., Desai, M., Downs, C., Gorby, M., Jordan, A. P., Joyce, C. J., Kozarev, K., Linker, J. A., Mikíc, Z., Riley, P., Spence, H. E., Török, T., Townsend, L. W., Wilson, J. K., Zeitlin, C. Particle Radiation Sources, Propagation and Interactions in Deep Space, at Earth, the Moon, Mars, and Beyond: Examples of Radiation Interactions and Effects. *Space Science Reviews*, 212(3-4):1069–1106, 2017. doi:10.1007/s11214-017-0381-5

Selesnick, R. S., Looper, M. D., Mewaldt, R. A. A theoretical model of the inner proton radiation belt. *Space Weather*, 5(4):S04003, 2007. doi:10.1029/2006SW000275

Seppälä, A., Verronen, P. T., Sofieva, V. F., Tamminen, J., Kyrölä, E., Rodger, C. J., Clilverd, M. A. Destruction of the tertiary ozone maximum during a solar proton event. *Geophysical Research Letters*, 33(7):L07804, 2006. doi:10.1029/2005GL025571

Serlemitsos, A. T., Balasubrahmanyan, V. K. Solar particle events with anomalously large relative abundance of ^{3}He. *Astrophysical Journal*, 198:195–204, 1975. doi:10.1086/153592

Sexton, F. W. Destructive single-event effects in semiconductor devices and ICs. *IEEE Transactions on Nuclear Science*, 50(3):603–621, 2003. ISSN 0018-9499. doi:10.1109/TNS.2003.813137

Shea, M. A., Smart, D. F. A Summary of Major Solar Proton Events. *Solar Physics*, 127(2):297–320, 1990. doi:10.1007/BF00152170

Shea, M. A., Smart, D. F. Fifty Years of Cosmic Radiation Data. *Space Science Reviews*, 93:229–262, 2000. doi:10.1023/A:1026500713452

Shea, M. A., Smart, D. F. Compendium of the eight articles on the "Carrington Event" attributed to or written by Elias Loomis in the American Journal of Science, 1859 1861. *Advances in Space Research*, 38(2):313–385, 2006. doi:10.1016/j.asr.2006.07.005

Shea, M. A., Smart, D. F., McCracken, K. G., Dreschhoff, G. A. M., Spence, H. E. Solar proton events for 450 years: The Carrington event in perspective. *Advances in Space Research*, 38(2):232–238, 2006. doi:10.1016/j.asr.2005.02.100

Sheeley, J., N. R., Bohlin, J. D., Brueckner, G. E., Purcell, J. D., Scherrer, V. E., Tousey, R., Smith, J., J. B., Speich, D. M., Tandberg Hanssen, E., Wilson, R. M., de Loach, A. C., Hoover, R. B., McGuire, J. P. Coronal Changes Associated with a Disappearing Filament. *Solar Physics*, 45(2):377–392, 1975. doi:10.1007/BF00158457

Shibata, K., Magara, T. Solar Flares: Magnetohydrodynamic Processes. *Living Reviews in Solar Physics*, 8(1):6, 2011. doi:10.12942/lrsp-2011-6

Sicard-Piet, A., Bourdarie, S., Boscher, D., Friedel, R. H. W. A model for the geostationary electron environment: Pole, from 30 kev to 5.2 mev. In *2005 8th European Conference on Radiation and Its Effects on Components and Systems*, pages D2–1–D2–6. 2005. doi:10.1109/RADECS.2005.4365580

Sicard-Piet, A., Bourdarie, S., Boscher, D., Friedel, R. H. W., Thomsen, M., Goka, T., Matsumoto, H., Koshiishi, H. A new international geostationary electron model: IGE-2006, from 1 keV to 5.2 MeV. *Space Weather*, 6(7):07003, 2008. doi:10.1029/2007SW000368

Simpson, J. A. The Cosmic Ray Nucleonic Component: The Invention and Scientific Uses of the Neutron Monitor - (Keynote Lecture). *Space Science Reviews*, 93:11–32, 2000. doi:10.1023/A:1026567706183

Simpson, J. A., Fonger, W., Treiman, S. B. Cosmic Radiation Intensity-Time Variations and Their Origin. I. Neutron Intensity Variation Method and Meteorological Factors. *Physical Review*, 90:934–950, 1953. doi:10.1103/PhysRev.90.934

Singer, S. F. "Radiation Belt" and Trapped Cosmic-Ray Albedo. *Physical Review Letters*, 1(5):171–173, 1958. doi:10.1103/PhysRevLett.1.171

Slaba, T. C., Whitman, K. The Badhwar-O'Neill 2020 GCR Model. *Space Weather*, 18(6):e02456, 2020. doi:10.1029/2020SW002456

Smith, E. J., Balogh, A. Decrease in heliospheric magnetic flux in this solar minimum: Recent Ulysses magnetic field observations. *Geophysical Research Letters*, 35(22):L22103, 2008. doi:10.1029/2008GL035345

Solanki, S. K., Krivova, N. A., Haigh, J. D. Solar Irradiance Variability and Climate. *Annual Review of Astronomy and Astrophysics*, 51(1):311–351, 2013. doi:10.1146/annurev-astro-082812-141007

Sonett, C. P., Finney, S. A. The Spectrum of Radiocarbon. *Philosophical Transactions of the Royal Society of London Series A*, 330(1615):413–425, 1990. doi:10.1098/rsta.1990.0022

Song, P., Singer, H. J., Siscoe, G. L. *Space Weather*. American Geophysical Union, Washington DC, USA, 2001. ISBN 978-0875909844

Southworth, G. C. Microwave radiation from the sun. *Journal of the Franklin Institute*, 239(4):285–297, 1945. ISSN 0016-0032. doi:10.1016/0016-0032(45)90163-3

Spörer, G. Ueber die Periodicität der Sonnenflecken seit Jahre 1618. *Verhandlungen der Kaiserlich Leopoldinisch-Carolinischen Deutschen Akademie der Naturforscher*, 53(2), 1889

Stewart, B. On the Great Magnetic Disturbance Which Extended from August 28 to September 7, 1859, as Recorded by Photography at the Kew Observatory. *Philosophical Transactions of the Royal Society of London Series I*, 151:423–430, 1861

Stewart, J. Q., Eggleston, F. C. A Prediction of the Remaining Course of the Present Sunspot Cycle. *Physical Review*, 55(11):1102–1102, 1939. doi:10.1103/PhysRev.55.1102

Stoker, P. H., Dorman, L. I., Clem, J. M. Neutron Monitor Design Improvements. *Space Science Reviews*, 93:361–380, 2000. doi:10.1023/A:1026560932107

Stone, E. C., Frandsen, A. M., Mewaldt, R. A., Christian, E. R., Margolies, D., Ormes, J. F., Snow, F. The Advanced Composition Explorer. *Space Science Reviews*, 86:1–22, 1998. doi:10.1023/A:1005082526237

Suess, H. E. The Radiocarbon Record in Tree Rings of the Last 8000 Years. *Radiocarbon*, 22(2):200–209, 1980. doi:10.1017/S0033822200009462

Svalgaard, L. Solar activity – past, present, future. *Journal of Space Weather and Space Climate*, 3:A24, 2013. doi:10.1051/swsc/2013046

Svalgaard, L., Duvall, J., T. L., Scherrer, P. H. The strength of the Sun's polar fields. *Solar Physics*, 58(2):225–239, 1978. doi:10.1007/BF00157268

Švestka, Z. Optical Observations of Solar Flares. *Space Science Reviews*, 5(3):388–418, 1966. doi:10.1007/BF02653250

Tapping, K., Morgan, C. Changing Relationships Between Sunspot Number, Total Sunspot Area and $F_{10.7}$ in Cycles 23 and 24. *Solar Physics*, 292(6):73, 2017. doi:10.1007/s11207-017-1111-6

Tapping, K. F. The 10.7 cm solar radio flux ($F_{10.7}$). *Space Weather*, 11(7):394–406, 2013. doi:10.1002/swe.20064

Tapping, K. F., Detracey, B. The Origin of the 10.7 cm Flux. *Solar Physics*, 127(2):321–332, 1990. doi:10.1007/BF00152171

Taylor, B., Vacanti, G., Maddox, E., Underwood, C. I. The Interplanetary Electron Model (IEM). *IEEE Transactions on Nuclear Science*, 58(6):2785–2792, 2011. ISSN 0018-9499. doi:10.1109/TNS.2011.2171718

Temerin, M., Roth, I. The production of He-3 and heavy ion enrichment in He-3-rich flares by electromagnetic hydrogen cyclotron waves. *Astrophysical Journal, Letters*, 391:L105–L108, 1992. doi:10.1086/186408

Thompson, R. J. A Technique for Predicting the Amplitude of the Solar Cycle. *Solar Physics*, 148(2):383–388, 1993. doi:10.1007/BF00645097

Thorne, R. M. Energetic radiation belt electron precipitation: a natural depletion mechanism for stratospheric ozone. *Science*, 195:287–289, 1977. doi:10.1126/science.195.4275.287

Toriumi, S., Wang, H. Flare-productive active regions. *Living Reviews in Solar Physics*, 16(1):3, 2019. doi:10.1007/s41116-019-0019-7

Torsti, J., Valtonen, E., Lumme, M., Peltonen, P., Eronen, T., Louhola, M., Riihonen, E., Schultz, G., Teittinen, M., Ahola, K., Holmlund, C., Kelhä, V., Leppälä, K., Ruuska, P., Strömmer, E. Energetic Particle Experiment ERNE. *Solar Physics*, 162:505–531, 1995. doi:10.1007/BF00733438

Tousey, R. The Solar Corona. In M. J. Rycroft, S. K. Runcorn (editors), *Space Research XIII*. Akademie-Verlag, Berlin, Germany, 1973

Tylka, A. J., Adams, J. H., Boberg, P. R., Brownstein, B., Dietrich, W. F., Flueckiger, E. O., Petersen, E. L., Shea, M. A., Smart, D. F., Smith, E. C. CREME96: A Revision of the Cosmic Ray Effects on Micro-Electronics Code. *IEEE Transactions on Nuclear Science*, 44(6):2150–2160, 1997. ISSN 0018-9499. doi:10.1109/23.659030

Tylka, A. J., Cohen, C. M. S., Dietrich, W. F., Lee, M. A., Maclennan, C. G., Mewaldt, R. A., Ng, C. K., Reames, D. V. Shock Geometry, Seed Populations, and the Origin of Variable Elemental Composition at High Energies in Large Gradual Solar Particle Events. *Astrophysical Journal*, 625:474–495, 2005. doi:10.1086/429384

Tylka, A. J., Cohen, C. M. S., Dietrich, W. F., Lee, M. A., Maclennan, C. G., Mewaldt, R. A., Ng, C. K., Reames, D. V. A Comparative Study of Ion Characteristics in the Large Gradual Solar Energetic Particle Events of 2002 April 21 and 2002 August 24. *Astrophysical Journal, Supplement Series*, 164(2):536–551, 2006. doi:10.1086/503203

Tylka, A. J., Dietrich, W. F. A New and Comprehensive Analysis of Proton Spectra in Ground-Level Enhanced (GLE) Solar Particle Events. In M. Giller, J. Szabelski (editors), *Proceedings of the 31st International Cosmic Ray Conference*. Łódź, Poland, 2009

Tylka, A. J., Lee, M. A. A Model for Spectral and Compositional Variability at High Energies in Large, Gradual Solar Particle Events. *Astrophysical Journal*, 646:1319–1334, 2006. doi:10.1086/505106

Upton, L. A., Hathaway, D. H. An Updated Solar Cycle 25 Prediction With AFT: The Modern Minimum. *Geophysical Research Letters*, 45(16):8091–8095, 2018. doi:10.1029/2018GL078387

Usoskin, I. G. A history of solar activity over millennia. *Living Reviews in Solar Physics*, 14(1):3, 2017. doi:10.1007/s41116-017-0006-9

Usoskin, I. G., Mursula, K., Kananen, H., Kovaltsov, G. A. Dependence of cosmic rays on solar activity for odd and even solar cycles. *Advances in Space Research*, 27(3):571–576, 2001. doi:10.1016/S0273-1177(01)00084-9

Usoskin, I. G., Solanki, S. K., Kovaltsov, G. A. Grand minima and maxima of solar activity: new observational constraints. *Astronomy & Astrophysics*, 471(1):301–309, 2007. doi:10.1051/0004-6361:20077704

Vainio, R., Desorgher, L., Heynderickx, D., Storini, M., Flückiger, E., Horne, R. B., Kovaltsov, G. A., Kudela, K., Laurenza, M., McKenna-Lawlor, S., Rothkaehl, H., Usoskin, I. G. Dynamics of the Earth's Particle Radiation Environment. *Space Science Reviews*, 147:187–231, 2009. doi:10.1007/s11214-009-9496-7

Vainio, R., Valtonen, E., Heber, B., Malandraki, O. E., Papaioannou, A., Klein, K.-L., Afanasiev, A., Agueda, N., Aurass, H., Battarbee, M., Braune, S., Dröge, W., Ganse, U., Hamadache, C., Heynderickx, D., Huttunen-Heikinmaa, K., Kiener, J., Kilian, P., Kopp, A., Kouloumvakos, A., Maisala, S., Mishev, A., Miteva, R., Nindos, A., Oittinen, T., Raukunen, O., Riihonen, E., Rodríguez-Gasén, R., Saloniemi, O., Sanahuja, B., Scherer, R., Spanier, F., Tatischeff, V., Tziotziou, K., Usoskin, I. G., Vilmer, N. The first SEPServer event catalogue ˜68-MeV solar proton events observed at 1 AU in 1996-2010. *Journal of Space Weather and Space Climate*, 3(27):A12, 2013. doi:10.1051/swsc/2013030

van Allen, J. A. The Geomagnetically Trapped Corpuscular Radiation. *Journal of Geophysical Research*, 64(11):1683–1689, 1959. doi:10.1029/JZ064i011p01683

Van Allen, J. A. On the modulation of galactic cosmic ray intensity during solar activity cycles 19, 20, 21, 22 and early 23. *Geophysical Research Letters*, 27(16):2453–2456, 2000. doi:10.1029/2000GL003792

Van Allen, J. A., Baker, D. N., Randall, B. A., Sentman, D. D. The magnetosphere of Jupiter as observed with Pioneer 10: 1. Instrument and principal findings. *Journal of Geophysical Research*, 79(25):3559, 1974. doi:10.1029/JA079i025p03559

van Allen, J. A., Krimigis, S. M. Impulsive Emission of 40-kev Electrons from the Sun. *Journal of Geophysical Research*, 70(23):5737–5751, 1965. doi:10.1029/JZ070i023p05737

van Driel-Gesztelyi, L., Green, L. M. Evolution of Active Regions. *Living Reviews in Solar Physics*, 12(1):1, 2015. doi:10.1007/lrsp-2015-1

Vaquero, J. M., Gallego, M. C., Usoskin, I. G., Kovaltsov, G. A. Revisited Sunspot Data: A New Scenario for the Onset of the Maunder Minimum. *Astrophysical Journal, Letters*, 731(2):L24, 2011. doi:10.1088/2041-8205/731/2/L24

Vaquero, J. M., Svalgaard, L., Carrasco, V. M. S., Clette, F., Lefèvre, L., Gallego, M. C., Arlt, R., Aparicio, A. J. P., Richard, J. G., Howe, R. A Revised Collection of Sunspot Group Numbers. *Solar Physics*, 291(9-10):3061–3074, 2016. doi:10.1007/s11207-016-0982-2

Vaquero, J. M., Trigo, R. M., Gallego, M. C., Moreno-Corral, M. A. Two Early Sunspots Observers: Teodoro de Almeida and José Antonio Alzate. *Solar Physics*, 240(1):165–175, 2007. doi:10.1007/s11207-006-0264-5

Verronen, P. T., Seppälä, A., Kyrölä, E., Tamminen, J., Pickett, H. M., Turunen, E. Production of odd hydrogen in the mesosphere during the January 2005 solar proton event. *Geophysical Research Letters*, 33(24):L24811, 2006. doi:10.1029/2006GL028115

Vette, J. I. The NASA/National Space Science Data Center Trapped Radiation Environment Model Program (1946-1991). Technical Report NSSDC/WDC-A-R/S-91-29, National Space Science Data Center, 1991

Viljanen, A., Pulkkinen, A., Pirjola, R., Pajunpää, K., Posio, P., Koistinen, A. Recordings of geomagnetically induced currents and a nowcasting service of the Finnish natural gas pipeline system. *Space Weather*, 4(10):S10004, 2006. doi:10.1029/2006SW000234

Waldmeier, M. Neue Eigenschaften der Sonnenfleckenkurve. *Astronomische Mitteilungen der Eidgenössischen Sternwarte Zürich*, 14:105–136, 1935

Waldmeier, M. Prognose für das nächste Sonnenfleckenmaximum. *Astronomische Nachrichten*, 259:267, 1936

Wang, Y.-M., Colaninno, R. Is Solar Cycle 24 Producing More Coronal Mass Ejections Than Cycle 23? *Astrophysical Journal, Letters*, 784(2):L27, 2014. doi:10.1088/2041-8205/784/2/L27

Wang, Y.-M., Robbrecht, E., Sheeley, J., N. R. On the Weakening of the Polar Magnetic Fields during Solar Cycle 23. *Astrophysical Journal*, 707(2):1372–1386, 2009. doi:10.1088/0004-637X/707/2/1372

Wang, Y.-M., Sheeley, N. R. Understanding the Geomagnetic Precursor of the Solar Cycle. *Astrophysical Journal, Letters*, 694(1):L11–L15, 2009. doi:10.1088/0004-637X/694/1/L11

Webb, D. F., Howard, R. A. The solar cycle variation of coronal mass ejections and the solar wind mass flux. *Journal of Geophysical Research*, 99(A3):4201–4220, 1994. doi:10.1029/93JA02742

Webber, W. R., Lockwood, J. A. Characteristics of the 22-year modulation of cosmic rays as seen by neutron monitors. *Journal of Geophysical Research*, 93(A8):8735–8740, 1988. doi:10.1029/JA093iA08p08735

Wild, J. P., Smerd, S. F., Weiss, A. A. Solar Bursts. *Annual Review of Astronomy and Astrophysics*, 1:291, 1963. doi:10.1146/annurev.aa.01.090163.001451

Willson, R. C. Total solar irradiance trend during solar cycles 21 and 22. *Science*, 277(5334):1963–1965, 1997. doi:10.1126/science.277.5334.1963

Wilson, J. W., Cucinotta, F. A., Shinn, J. L., Simonsen, L. C., Dubey, R. R., Jordan, W. R., Jones, T. D., Chang, C. K., Kim, M. Y. Shielding from solar particle event exposures in deep space. *Radiation Measurements*, 30(3):361–382, 1999. doi:10.1016/S1350-4487(99)00063-3

Wilson, P. R., Altrocki, R. C., Harvey, K. L., Martin, S. F., Snodgrass, H. B. The extended solar activity cycle. *Nature*, 333(6175):748–750, 1988. doi:10.1038/333748a0

Withbroe, G. L. Solar activity cycle - History and predictions. *Journal of Spacecraft and Rockets*, 26:394–402, 1989. doi:10.2514/3.26085

Withbroe, G. L., Guhathakurta, M., Hoeksema, J. T. Origins of the International Living With a Star program. *Advances in Space Research*, 35(1):40–43, 2005. doi:10.1016/j.asr.2004.09.012

Xapsos, M. A., Stauffer, C., Barth, J. L., Burke, E. A. Solar Particle Events and Self-Organized Criticality: Are Deterministic Predictions of Events Possible? *IEEE Transactions on Nuclear Science*, 53(4):1839–1843, 2006. doi:10.1109/TNS.2006.880576

Xapsos, M. A., Stauffer, C., Gee, G. B., Barth, J. L., Stassinopoulos, E. G., McGuire, R. E. Model for solar proton risk assessment. *IEEE Transactions on Nuclear Science*, 51(6):3394–3398, 2004. ISSN 0018-9499. doi:10.1109/TNS.2004.839159

Xapsos, M. A., Stauffer, C., Jordan, T., Barth, J. L., Mewaldt, R. A. Model for Cumulative Solar Heavy Ion Energy and Linear Energy Transfer Spectra. *IEEE Transactions on Nuclear Science*, 54(6):1985–1989, 2007. ISSN 0018-9499. doi:10.1109/TNS.2007.910850

Xapsos, M. A., Summers, G. P., Barth, J. L., Stassinopoulos, E. G., Burke, E. A. Probability model for worst case solar proton event fluences. *IEEE Transactions on Nuclear Science*, 46(6):1481–1485, 1999. doi:10.1109/23.819111

Xapsos, M. A., Summers, G. P., Barth, J. L., Stassinopoulos, E. G., Burke, E. A. Probability model for cumulative solar proton event fluences. *IEEE Transactions on Nuclear Science*, 47(3):486–490, 2000. ISSN 0018-9499. doi:10.1109/23.856469

Xapsos, M. A., Summers, G. P., Burke, E. A. Extreme Value Analysis of Solar Energetic Proton Peak Fluxes. *Solar Physics*, 183(1):157–164, 1998a. doi:10.1023/A:1005075421711

Xapsos, M. A., Summers, G. P., Burke, E. A. Probability model for peak fluxes of solar proton events. *IEEE Transactions on Nuclear Science*, 45(6):2948–2953, 1998b. doi:10.1109/23.736551

Yeates, A. R., Muñoz-Jaramillo, A. Kinematic active region formation in a three-dimensional solar dynamo model. *Monthly Notices of the Royal Astronomical Society*, 436(4):3366–3379, 2013. doi:10.1093/mnras/stt1818

Yeh, K. C., Liu, C. H. Radio wave scintillations in the ionosphere. *Proceedings of the IEEE*, 70:324–360, 1982

Zerbo, J. L., Richardson, J. D. The solar wind during current and past solar minima and maxima. *Journal of Geophysical Research*, 120(12):10,250–10,256, 2015. doi:10.1002/2015JA021407

Zhao, L., Zhang, M., Rassoul, H. K. Double Power Laws in the Event-integrated Solar Energetic Particle Spectrum. *Astrophysical Journal*, 821(1):62, 2016. doi:10.3847/0004-637X/821/1/62

Zolotova, N. V., Ponyavin, D. I. Is the new Grand minimum in progress? *Journal of Geophysical Research*, 119(5):3281–3285, 2014. doi:10.1002/2013JA019751

TURUN
YLIOPISTO
UNIVERSITY
OF TURKU

Painosalama Oy, Turku, Finland 2021

ISBN 978-951-29-8490-9 (PRINT)
ISBN 978-951-29-8491-6 (PDF)
ISSN 0082-7002 (PRINT)
ISSN 2343-3175 (ONLINE)